Axisymmetric Spacetimes in Relativity

S. P. Drake
Department of Physics and Mathematical Physics
University of Adelaide
Adelaide, S. A. 5005
Australia

22 July 1998

DECLARATION

This work contains no material which has been accepted for the award of any other degree or diploma in any university or other tertiary institution and, to the best of my knowledge and belief, contains no material previously published or written by another person, except where due reference has been made in the text.

I give consent to this copy of my thesis, when deposited in the University Library, being available for loan and photocopying.

ACKNOWLEDGEMENTS

It is an unfortunate fact that only my name goes on this thesis. This is not the work of one person, it is an accumulation of the labor of many. All those who have helped me in ways that none of us could image should be acknowledged, but how.

None of this would have been possible were it not for the wisdom and guidance of my supervisor Peter Szekeres. I have often pondered over the difficulty of supervising students. It must be heart-breaking to watch as students make necessary mistakes. Patience I'm sure must be the key. So for his wisdom, patience and kindness I am deeply indebted to Peter Szekeres.

Without the love and support of my family this thesis would never have begun, much less been completed, to them I owe my life, and all that comes with it.

It would take too long to write the names of all those I wish to thank. Those who are special to me, have helped me through so much over the years will receive the thanks in person.

I would like to the department of physics here at Adelaide where most of my thesis work was done. I would like to thank the department of physics at Melbourne university, where I did my undergraduate degree and began my PhD. I would like to thank the university of Padova for there hospitality during my stay there. I am greatly appreciative of the government of Australia for providing me with a scholarship.

To all my friends (who I will thank individually) and to those whom I care about.

Contents

List of Figures

Chapter 1

Introduction

1.1 Stationary axisymmetric spacetimes

The high degree of symmetry for static spherically symmetric spacetimes makes it possible to examine their geometry in detail. If one degree of symmetry is broken so that the spacetime is axisymmetric an examination of the geometry and its physical implications is much more difficult. As an example of the unusual behaviour of axisymmetric spacetimes consider the results of Scott and Szekeres [1]. This work demonstrates how one particular static axisymmetric vacuum metric, known as the Curzon solution, has a directional singularity. Unexpectedly, the geodesic motion of spacetimes with directional singularities may avoid the singularity altogether and pass through into a flat spacetime. Though directional singularities are not studied in this work, they provide evidence of the unpredictable properties of axisymmetric spacetimes. Directional singularities by definition only occur in axisymmetric spacetimes. Consider also for example "frame-dragging", an effect which does not occur in the static or Newtonian limits. Frame-dragging is the process where by particles in a stationary spacetime are dragged along gaining angular velocity, according to some observer at infinity. Recent experimental results [2] suggest that this frame-dragging effect has been measured and can be considered to be further confirmation of the general theory of relativity.

Stationary axisymmetric spacetimes both interior and exterior to rotating perfect fluids is still a relatively unexplored field.

The literature review in the next section, gives a detailed account of research done in the area of stationary axisymmetric (SAS) spacetimes. A subset of stationary spacetimes are static ones. Recent results [3]-[7] have shown that the geodesic motion in Majumdar-Papapetrou spacetimes is in general chaotic but has isolated regions of stability, one of which is the Newtonian region.

In general relativity there is no preferred reference frame. Hence a description of the symmetries of a spacetime must be done in a coordinate independent way. The symmetries of a particular field, whether it be the Newtonian gravitational potential V or $g_{\mu\nu}$, are determined in the same way; If the potential difference between two spacetime points x^μ and $x^\mu + \epsilon K^\mu$ is zero then K^μ is a Killing vector, satisfying Killing's equation $K_{(\mu;\nu)} \equiv K_{\mu;\nu} + K_{\nu;\mu} = 0$. The symmetries of a spacetime are expressed by the algebra and surface of transitivity generated its Killing vectors. Axisymmetric spacetimes are those for which there is only one spacelike Killing vector K_ϕ corresponding to an angular coordinate ϕ. Spherically symmetric spacetimes have three killing vectors whose commutators form a Lie algebra $O(3)$, and having two dimensional surfaces of transitivity described by angular coordinates θ and ϕ. Similarly the terms stationary and static can be defined in a coordinate independent way. A gravitational field $g_{\mu\nu}$ is called "stationary" if at every point it has a timelike Killing vector K_τ. A distinction between static and stationary spacetimes is made in relativity though there is none in Newtonian gravity. Static spacetimes are stationary spacetimes for which a coordinate transformation exist so that $g_{ti} = 0$, t is a timelike coordinate and i is one of three spacelike coordinates. A coordinate independent way of determining whether a spacetime is static or stationary is to examine the timelike Killing vector K_τ. If the timelike Killing vector K_τ is orthogonal to a hypersurface $f(x^\tau) = 0$, i.e., $K_\tau \propto f(x^\tau), \tau$ the spacetime is static. It is possible to visualize this difference by imagining an observer filming a rotating star. If the film is played in reverse then the rotating star will appear to be rotating in the opposite direction. This situation is deemed stationary but not static. On the other hand if the star where to stop rotating it would be deemed static as no distinction could made as to whether the film was being played in the forward or reverse direction.

The first of the two problems studied in this thesis is a geometrical description for

the interior of a rotating star. Exact solutions for Einstein's field equations for stationary axisymmetric spacetimes are notoriously difficult to solve. Only stationary axisymmetric (SAS) metric tensors which generate the Einstein tensor describing the physical properties of a rotating perfect fluid are studied. Except for few special cases, such as rotating dust and discs of matter the geometrical structure interior to a perfect fluid has not be found. Before entering into the details of the attempts made in thesis to solve the problem we give a review of the literature which already exists on the topic.

1.2 Literature review

1.2.1 Vacuum stationary axisymmetric spacetimes

Kerr in 1963 found a stationary axisymmetric vacuum solution to Einstein's equations. This solution now known as the Kerr metric describes the spacetime of a rotating blackhole. Following Kerr's discovery a great number of publications were produced describing its spacetime properties. It is not feasible nor necessary to cite these publications as most modern text books on the general theory of relativity devote a chapter or at least part of one to a description of the Kerr geometry. The uniqueness theorems of Robinson and Carter [8, 9] established that: [10]

> *The only stationary axisymmetric solution of Einstein's equation for the vacuum, which has a smooth convex event-horizon, is asymptotically flat, and is non-singular outside the event-horizon, is the Kerr metric.*

The Kerr metric [11], which can be shown to be a solution of the Ernst equation [12, 13], belongs to a particular class of spacetimes known as Kerr-Schild (KS) metrics,

$$g_{\mu\nu} = \eta_{\mu\nu} + H l_\mu l_\nu \quad , \tag{1.2.1}$$

where H is some scalar function and l_μ is a null vector. The KS spacetimes are limited to representing the vacuum, electromagnetic field and pure radiation, as the vector field l_μ used to transform Minkowski space is null. A generalization of KS spacetimes has been

considered as possible sources of perfect fluid spacetimes, [14]-[18]. The results of [14] proved that the energy momentum tensor of the generalized KS spacetime,

$$g_{\mu\nu} = \tilde{g}_{\mu\nu} + H l_\mu l_\nu, \tag{1.2.2}$$

has a null eigenvector if and only if l_μ is an eigenvector of the energy-momentum tensor for the seed metric $\tilde{g}_{\mu\nu}$. References [14]-[18] demonstrate the success of this technique in generating inhomogeneous cosmologies and static and stationary spacetimes.

Following the discovery of the Kerr metric Newman and Janis [19], [20] developed a "trick" by which the Kerr metric could be generated by making a complex transformation of the exterior Schwarzschild solution. At the time of writing the papers conceded that

...there is no simple, clear reason for the series of operations performed ...

other than it worked. Despite this, the technique know as the Newman-Janis algorithm (NJA) was successfully used to derive a previously undiscovered solution now known as the Kerr-Newman metric.

A more rigorous account of the NJA was given by Schiffer et. al in 1973 [21]. They provided an elegant proof as to how both Schwarzschild and Kerr metrics were both solutions of the same complex potential equation. It was shown that the Kerr solution is simply the complex solution shifted by an amount ia in the z direction. Also in 1973 Newman [22] showed that the essential reason for the success of the NJA was that the Einstein-Maxwell equations are invariant under complex Poincare transformations, $z'^\mu = a^\mu_\nu z^\nu + b^\mu$. Newman [23] tried to give a more detailed account of the NJA as being a real slice of a complex space,

$$ds^2 = n_{\mu\nu} dz^\mu dz^\nu + \lambda (l_\mu dz^\mu)^2 \quad , \tag{1.2.3}$$

where z^μ are complex coordinates $z^\mu = x^\mu + iy^\mu$. This is not particularly useful, as once again, it relies on knowing results before obtaining them. Gurses and Gursey [24] proved that, if the pseudo energy-momentum tensor vanishes, or Einstein's equations are linear, then complex transformations are allowed in General Relativity.

Demianski et. al. [25] proceeded to modify the NJA slightly and applied it to a generalization of the exterior Schwarzschild solution. This new solution (Kerr-NUT) represents

a gravitational monopole solution. The metric is described as having a monopole solution because the only non-vanishing component of the Weyl tensor is

$$\Psi_2 = \frac{m_0 - ib}{[r - i(a\cos\theta + b)]^3} \quad , \tag{1.2.4}$$

which is analogus to the case for magnetic monopoles where the field invariant is

$$\Psi_1 = \frac{e + ic}{r^2} \quad . \tag{1.2.5}$$

A Kerr-like spacetime was found by Demianski [26] by using a more general complex transformation than that originally used in the NJA. The Kerr-like solution can not be considered as the exterior gravitational field of a bound distribution of matter as it contains a singularity on the axis of rotation $\theta = 0$ and $\theta = \pi$.

Not until 1982 an attempt made to obtain interior solutions to the Kerr metric using the NJA. Herrera and Jimenez [27] used the NJA to obtain a stationary axisymmetric spacetime which could be matched smoothly to the Kerr metric on an oblate spheroid. A study of the static limit of their results revealed that the solution was not a perfect fluid as the radial and tangential pressures where different. The debate as to whether the NJA could be used to generate non perfect fluid spacetimes was not resolved until 1998. The work of Drake and Szekeres [28] clarified exactly what the NJA was and proved that the only perfect fluid generated by the NJA was the vacuum. Drake and Turolla generalized the NJA to include non-vacuum spacetimes which match smoothly to the Kerr metric and are perfect fluids in the static limit.

Another well studied class of stationary axisymmetric spacetimes are the Tomimatsu-Sato solutions [29]. Unfortunately though these solutions can not be considered as viable candidates for the exterior of rotating stars as in the static limit they are axisymmetric Weyl solutions of $\delta = 2$ [30]. It is well accepted, though still defies rigorous proof, that the interior of a static perfect fluid is spherically symmetric. The Scwarzschild solution in Weyl coordinates is $\delta = 1$, hence the Tomimatsu-Sato solutions do not represent the Schwarzschild metric in the static limit.

While there are other stationary axisymmetric solutions to Einstein's field equations most of them are not asymptotically flat. Asymptotic flatness is the property that the

curvature tensor tends to zero at large distances. It is an expected property for the exterior of stars. A review of asymptotically flat rotating solutions to Einstein's equations is found in Islam's article [30].

1.2.2 Non-vacuum stationary axisymmetric spacetimes

Mars et. al [31] have recently shown the uniqueness of exterior solutions of Einstein's field equations matching smoothly to an interior. That is to say the exterior spacetime is matched uniquely to a given interior.

The uniqueness of the Kerr metric tells us nothing of the interior stationary axisymmetric (SAS) spacetimes. The work of Geroch [32], [33] provides a means for obtaining new SAS metrics from known ones. Unfortunately, many of the solutions resulting from this method have no obvious physical interpretation. Solutions up to quadrature where found by Winicour [34] and they represent the complete class of rotating dust solutions. An solution for rigidly rotating dust was determined up to an arbitrary solution of the Laplace equation by van Stockum [35]. The only other well known exact analytic solution is that of Neugenbauer et. al. [36] It represents a rotating dust solution which in some limit appears to represent an extreme Kerr solution. The general properties of rotating dust solutions have been examined by Krasinski [37]- [39].

It was noted [40]that the Kerr solution could be interpretated as arising from a thin rigidly rotating disk with a regular interior and a singular ring. Rotating disks of matter are not the only structure which may be matched smoothly to the Kerr metric but they are the most studied analytically. The inverse scattering method is a powerful technique for generating exterior axisymmetric stationary spacetimes. Unfortunately this method is not suitable for obtaining interior solutions, unless the interior is described by an infinitesimal thin disk [41]. Rigidly rotating dust is the $P/\varrho \to 0$ limit (P = pressure, ϱ = density) of rigidly rotating perfect fluids. Such solutions are interesting as they represent the simplest model of self-gravitating rotating bodies. They also describe crude models of galaxies. Normal galaxies are sufficiently well described by Newtonian gravitating but a relativistic model may be relevant to quasars. The first example of an exactly solvable of rigidly rotating disk of dust seems to have been provided by Neugenbauer [36] et. al. It represents

the only known exact solution to rigidly rotating perfect fluid in general relativity.

Non-disk solutions to the Einstein equations have been found which match the Kerr metric in the first junction condition by fail in the second. Failure to match the second junction condition means that the interior and exterior are separated by a thin shell of matter with finite mass. Thin shells have been considered as sources of the Kerr metric [42] and Magli [43], [44] has considered rotating neutron stars with elastic properties. The situation at this stage is that no perfect fluid source of the Kerr metric has been found.

1.2.3 Numerical methods

The difficulties in obtaining exact solutions to Einstein's field equations for stationary axisymmetric (SAS) fields naturally leads to numerical investigations. Various schemes for numerical integration of the field equations describing rotating perfect fluids are reviewed by Stergioulas [45]. The general technique for numerical integration is to begin with an SAS metric of the form

$$ds^2 = e^{2\nu}dt^2 + e^{\varphi}(d\phi - \omega dt)^2 + e^{2\alpha}(dr^2 + r^2 d\theta^2) \quad , \tag{1.2.6}$$

where ν, φ, ω and α are dependent on r and θ. It is generally assumed that the stress-energy tensor is that of a perfect fluid stress-energy tensor

$$T^{\mu\nu} = (\rho + p)u^{\mu}u^{\nu} + Pg^{\mu\nu} \quad , \tag{1.2.7}$$

with a four velocity

$$u^{\mu} = \frac{e^{-\nu}}{1 - v^2}\left(\delta^{\mu}_{t} + \Omega\delta^{\mu}_{\phi}\right) \quad , \tag{1.2.8}$$

and three velocity

$$v = (\Omega - \omega)e^{\varphi - \nu} \quad . \tag{1.2.9}$$

For a given equation of state numerical means have been used to calculate the geometry of rotating stars [46]- [51]. More recently the interior of hot rotating disks in general relativity has been solved numerically [52]. These results represent a relativistic generalization of the class of Newtonian disks, known as Kalnajs disks [53], which are completely described by simple analytic expressions.

1.3 Current status

Fascination with the Kerr metric not only stems from its simple analytic representation but also from its uniqueness as the final state of a collapsed rotating star [8], [9]. Birkhoff's theorem tells us that the exterior of a static spherically symmetric star must be the Schwarzschild blackhole solution. However no such uniqueness theorem exist for rotating stars. This is not surprising as one would expect that the shape of a rotating star would depend on the equation of state describing its interior. Highly compact objects would have equipotential surfaces which are very close to spheroidal. At the other extreme a pressureless non-interacting gas (dust) is confined to a disc whose equipotential surfaces are highly ellipsoidal. There is still debate as to whether or not the Kerr metric corresponds to the exterior of a self-gravitating massive body, other than a disk. Thus far no conclusive remarks have been made on this topic. There are solutions which can be matched smoothly to the Kerr metric [34], [40], [42], [43], [44] but the problem with these is that they are composed of matter confined to plane, or imperfect fluids.

Simple analytic procedures for the generation new solutions to Einstein's field equations, such as KS spacetimes and the Newman-Janis algorithm, have been shown to be unsuccessful in obtain in perfect fluid solutions. However, the KS spacetimes can be generalized to general KS (GKS) spacetimes which may generate rotating perfect fluid interior spacetimes. Likewise the Newman-Janis algorithm may be generalized (GNJA), to include the possibility of obtaining perfect fluid interior solutions. There are still open questions for SAS spacetimes such as : *Is there a perfect fluid source for the Kerr metric ? and what is the exterior of a rigidly rotating star?*

1.4 Chaotic dynamics in the Hill's reduced model

The second problem considered in this thesis is the study of the chaotic behaviour of an infinitesimal charged particle in motion about two fixed charged centers. The motivation of the problem comes from trying to understand how systems change from regular to chaotic. The fixed two centers problem, known as the Hill's reduced model, is an ideal situation for studying the transition from regular behaviour to chaos in deterministic systems. It is the

simplest three body problem and one of the very few exactly solvable ones. Hill's reduced model has the unusual property of being solvable in Newtonian mechanics and chaotic in relativistic mechanics [54].

The history of the Hill's reduced model is a long and rich one. The Newtonian version of this problem has been treated by a number of authors for example [55]. In this reference it is treated as a gravitational problem but the results are exactly the same for a coulomb potential. In elliptic coordinates particle trajectories are expressed in terms of elliptic integrals. Although these functions are not particularly simple they still enable one to describe trajectories exactly, depending only on initial conditions.

In more recent times the general relativistic version of this problem consisting of two fixed charged black holes which are orbited by an infinitesimal uncharged particle has been shown to be chaotic [3]- [7]. The two fixed blackholes are charged so that the gravitational attraction is balanced by the electrostatic repulsion. Unlike the Newtonian version the technique of changing to elliptic coordinates does not allow the particle trajectories to be described by analytic functions. This suggest, but my no means proves, that the motion is chaotic. The chaotic nature of the motion is found by numerical integration of its trajectories. The singular nature of the spacetimes comprising of two charged blackholes means that a large number of trajectories are captured. Capture makes it difficult to determine the chaotic behaviour. Dettmann et.al [3], [4] demonstrated that the capture condition was actually a help, not a hindrance to examining the chaotic nature. A review of this work is given in chapter 6.

The Hydrogen molecule ion is a good approximation to the fixed two centers problem in quantum mechanics. In 1913 Bohr derived the energy spectrum for the Hydrogen atom. Sommerfield generalized these rules so that they could be applied to other atoms and molecules. Bohr set the task of using these rules to obtain the energy levels for H_2^+ to his PhD student Pauli in 1919. At that time it was not known whether or not the H_2^+ ion existed. This semi-classical approach was designed to resolve this debate. Pauli found that the lowest energy level was positive, concluding that the H_2^+ ion could not exist as a stable configuration. Contrary to this Schroedinger's solved the problem correctly and concluded that the H_2^+ could exist, as is now known by experiment. Semiclassical quantization was

later carried out using improved quantization rules [56]. This new semiclassical approach found stable solutions for the hydrogen molecule ion. The special relativistic version for full quantum model of the H_2^+ ion has never been study. Hopefully future studies will determine whether or not it is chaotic.

Classical special relativistic dynamics allows us to examine whether the chaos of the fixed two center problem arises solely from the non-linear effects of general relativity. The model for this is two fixed positively charged particles and infinitesimal negatively charged one whose motion is describe by special relativistic dynamics. The coulomb potentials for each charge may be added linearly to find the overall potential at any point. The only differences between this model and its Newtonian counterpart is that the kinetic energy of the infinitesimal particle of mass m_0 with velocity $\vec{v}$ is $m_0/\sqrt{1-v^2} - m_0$ and not $mv^2/2$. Is this difference enough to give rise to chaos? The studies of part 2 demonstrate that it is.

1.5 Outline of chapters

The first chapter after the introduction introduces a technique for generating stationary axisymmetric metrics from static spherically symmetric ones. The procedure, known as the Newman-Janis algorithm, was originally proposed as a means of deriving the Kerr solution from the Schwarzschild metric. The original work by Newman et.al was considered by some authors to be a "fluke" and not worthy of further investigation. Chapter 2 outlines precisely what the Newman-Janis algorithm (NJA) is, why it is successful in generating the Kerr-Newman metric and why it is unsuccessful for generating perfect solutions.

Chapter 3 generalizes the Newman-Janis algorithm (GNJA) to include possible rotating perfect fluids as sources of the Kerr metric. It is found that while solutions can be found which join smoothly to the Kerr metric on a static axisymmetric hypersurface, it is not possible to examine their physical properties in detail. It is however possible to calculate the pressure and density profiles of such rotating fluids in the static limit, $a \to 0$. Even for such simplified cases the investigation requires numerical integration in order to obtain any results at all. Chapter 3 concludes by establishing that the GNJA can be used to

generate solutions which match smoothly to the Kerr metric and whose static limit is a perfect fluid.

Following on from attempts to obtain exact solutions chapter 4 looks at *all* stationary axisymmetric metric which describe a rigidly rotating perfect fluid. While it is not possible to find a specific metric for any such spacetime, it is possible to examine some of their general properties. This chapter is devoted to presenting the simplest form perfect fluid spacetimes with rigid rotation and whose vorticity vector is aligned in the $\hat{z}$ direction. This approach leads naturally to a relativistic definition of centrifugal force, which is also explained in this chapter.

A completely new direction in the study of axisymmetric spacetimes is studied in chapters 5 and 6. These chapters introduce the concept of deterministic chaos in relativistic systems. The specific model of two fixed centers is studied as it addresses the question of whether chaos in general relativity is due to the non-linear nature of its structure. The detailed calculations of chapter 6 show that the special relativistic version of the fixed to center problem is chaotic while the Newtonian version is not.

The two studies are tied together in the conclusion with reference to the fact the point out the differences between axisymmetric spacetimes in relativity from there Newtonian counter parts.

Chapter 2

An Explanation of the Newman-Janis algorithm

2.1 Introduction.

Since the discovery of the Kerr metric [11] many attempts have been made to find a physically reasonable interior matter distribution that may be considered as its source. For a review of some of these approaches the reader is referred to the introductions of [57] and [58]. Though much progress has been made results have been generally disappointing. Thus far nobody has obtained a physically satisfactory interior solution. This may seem surprising given the success of matching internal spherical symmetric solutions to the Schwarzschild metric. The problem is not simply that the loss of one degree of symmetry makes the derivation of analytic results that much more difficult. Severe restrictions are placed on an interior metric if one maintains that it must be joined smoothly to the Kerr metric, whereas for spherically symmetric solutions the juncture conditions are less limiting. Further restrictions are placed on interior solutions to ensure that they correspond to physical objects. As the Kerr metric has no radiation field associated with it its source metric must also be non-radiating. This places even further constraints on the structure of the interior metric [59]. Given the strenuous nature of these limiting conditions, it is not surprising to learn that as yet nobody has obtained a truly satisfactory solution to the problem of finding sources for the Kerr metric. In general the failure is due to an internal structure that has unphysical properties, or a failure to satisfactorily match the boundary

conditions.

Axisymmetric solutions to Einstein's field equations are notoriously difficult to find. The unique class of charged rotating black hole (Kerr-Newman spacetimes) can be generated by a technique known as the Newman-Janis algorithm (NJA) [19] [20]. While this algorithm is particularly successful in "deriving" the Kerr metric and its electromagnetic generalization, the Kerr-Newman metric, it has often been criticized [60] on the grounds that (a) the procedure is not a general method of generating vacuum from vacuum metrics, and (b) there is a certain arbitrariness in the choice of complexification of terms in the original seed metric (Schwarzschild or Reissner-Nordström).

The main purpose of this chapter is (a) to specify precisely what the Newman-Janis algorithm is, (b) to understand under what circumstances and with what choice of complexifications it will be successful in generating one solution of Einstein's equations from another, and (c) to explore the possibility of extending the algorithm to arbitrary seed metrics with the view to generating perfect fluid interior solutions of Einstein's equations.

Section 2.2 describes the Newman-Janis Algorithm as a five-step procedure. This may appear to be somewhat overspecific, but these steps constitute the most general algorithm of this kind which has actually been found to work. In Section 2.3 the algorithm is applied to a general spherically symmetric spacetime. Section 2.4 presents the main results, that non-vacuum perfect fluids can never be generated by the NJA, while the Kerr-Newman solution is the most general algebraically special spacetime which can be so generated. The conclusion drawn in Section 2.5 that the particular choice of complexification used in the standard NJA to generate the Kerr-Newman solution is not arbitrary, but in fact could not be chosen in any other way in order for the NJA to be successful. This provides, in a sense, an "explanation" of the algorithm.

2.2 The Newman-Janis algorithm.

Despite the work by Newman and Janis and the work by Herrera and Jiménez and some further papers on the subject, the NJA is not a well known area of general relativity. For this reason we believe it is necessary to give a detailed outline as to what it actually

is. This section describes the Newman-Janis algorithm in a form generalized from the original version used to generate the Kerr-Newman metric (rotating charged black hole) from the Reissner-Nordström solution. The NJA is treated as a five-step procedure for generating new solutions of Einstein's equations from known static spherically symmetric ones. Whether a similar process can apply to original seed metrics which are not spherically symmetric is not known.

The five steps of the Newman-Janis algorithm are as follows:

1. Write a static spherically symmetric seed line element in advanced null coordinates $\{u, r, \theta, \phi\}$

$$ds^2 = e^{2\Phi(r)}du^2 + 2e^{\Phi(r)+\lambda(r)}dudr - r^2\left(d\theta^2 + \sin^2\theta d\phi^2\right) \quad . \tag{2.2.1}$$

In the Newman-Janis algorithm the seed was the Reissner-Nordström metric which in advanced Eddington-Finkelstein coordinates is

$$ds^2 = \left(1 - \frac{2m}{r} - \frac{Q^2}{r^2}\right)du^2 + 2dudr - r^2\left(d\theta^2 + \sin^2\theta d\phi^2\right) \quad . \tag{2.2.2}$$

2. Express the contravariant form of the seed metric in terms of a null tetrad,

$$g^{\mu\nu} = l^\mu n^\nu + l^\nu n^\mu - m^\mu \bar{m}^\nu - m^\nu \bar{m}^\mu \quad , \tag{2.2.3}$$

See Appendix B for relevant details of the Newman-Penrose formalism. For the spacetime 2.2.1 the null tetrad vectors are

$$\begin{aligned} l^\mu &= \delta^\mu_1 \quad , \\ n^\mu &= e^{-\lambda(r)-\Phi(r)}\delta^\mu_0 - \frac{1}{2}e^{-2\lambda(r)}\delta^\mu_1 \quad , \\ m^\mu &= \frac{1}{\sqrt{2}r}\left(\delta^\mu_2 + \frac{i}{\sin\theta}\delta^\mu_3\right) \quad . \end{aligned}$$

It is convenient to use the tetrad notation introduced by Newman and Penrose [61]

$$Z^\mu_a = (l^\mu, n^\mu, m^\mu, \bar{m}^\mu) \quad , \qquad a = 1, 2, 3, 4 \quad .$$

The null tetrad vectors for the Reissner-Nordström metric are

$$l^\mu = \delta^\mu_1 \quad ,$$

$$n^\mu = \delta_0^\mu - \frac{1}{2}\left(1 - \frac{2m}{r} - \frac{Q^2}{r^2}\right)\delta_1^\mu \quad ,$$
$$m^\mu = \frac{1}{\sqrt{2}r}\left(\delta_2^\mu + \frac{i}{\sin\theta}\delta_3^\mu\right) \quad .$$

3. Extend the coordinates x^ρ to a new set of complex coordinates $\tilde{x}^\rho$

$$x^\rho \to \tilde{x}^\rho = x^\rho + iy^\rho(x^\sigma) \quad ,$$

where $y^\rho(x^\sigma)$ are analytic functions of the real coordinates x^σ, and simultaneously let the null tetrad vectors Z_a^μ undergo a transformation

$$Z_a^\mu(x^\rho) \to \tilde{Z}_a^\mu(\tilde{x}^\rho) \quad . \tag{2.2.4}$$

An additional requirement is that the transformation recovers the old tetrad and metric when $\tilde{x}^\rho = \bar{\tilde{x}}^\rho$. In summary the effect of this "tilde transformation" is the creation of a new metric whose components are (real) functions of complex variables,

$$g_{\mu\nu} \to \tilde{g}_{\mu\nu} : \tilde{\mathbf{x}} \times \tilde{\mathbf{x}} \mapsto \mathbb{R} \quad , \tag{2.2.5}$$

with

$$\tilde{Z}_a^\mu(\tilde{x}^\rho)|_{\tilde{\mathbf{x}}=\bar{\tilde{\mathbf{x}}}} = Z_a^\mu(x^\rho) \quad . \tag{2.2.6}$$

The tilde transformation is clearly not unique as there are many different choices of the null tetrad vector coefficients satisfying the conditions 2.2.5 and 2.2.6.

In the original NJA, the tilde transformation on the Reissner-Nordström null tetrad vectors is

$$l^\mu \to \tilde{l}^\mu = \delta_1^\mu \quad , \tag{2.2.7}$$
$$n^\mu \to \tilde{n}^\mu = \delta_0^\mu - \frac{1}{2}\left(1 - m\left(\frac{1}{\tilde{r}} + \frac{1}{\bar{\tilde{r}}}\right) - \frac{Q^2}{\tilde{r}\bar{\tilde{r}}}\right)\delta_1^\mu \quad , \tag{2.2.8}$$
$$m^\mu \to \tilde{m}^\mu = \frac{1}{\sqrt{2}\tilde{r}}\left(\delta_2^\mu + \frac{i}{\sin\tilde{\theta}}\delta_3^\mu\right) \quad . \tag{2.2.9}$$

A quick check shows that the above null tetrad vectors are those corresponding to the Reissner-Nordström metric when $\tilde{x}^\rho = \bar{\tilde{x}}^\rho$. However it is precisely here that a certain arbitrariness crept into the process, since the method of complexifying the term $2m/r$ is quite different to the complexification of the Q^2/r^2 term. It is our aim to provide some rationale for this part of the NJ procedure.

4. A new metric is obtained by making a complex coordinate transformation

$$\tilde{x}^\rho = x^\rho + i\gamma^\rho(x^\sigma) \quad , \tag{2.2.10}$$

to the null tetrad vectors $\tilde{Z}_a^\mu$. The null tetrad vectors transform in the usual way

$$Z_a^\mu = \tilde{Z}_a^\nu \frac{\partial x^\mu}{\partial \tilde{x}^\nu} \quad .$$

The particular choice of complex transformations chosen by Newman and Janis to generate the Kerr-Newman metric were

$$\tilde{x}^\rho = x^\rho + ia\cos\theta\,(\delta_0^\rho - \delta_1^\rho) \quad . \tag{2.2.11}$$

Explicitly

$$\tilde{u} = u + ia\cos\theta, \;\; \tilde{r} = r - ia\cos\theta, \;\; \tilde{\theta} = \theta, \;\; \tilde{\phi} = \phi \quad . \tag{2.2.12}$$

From the transformed null tetrad vectors a new metric is recovered using 2.2.3.

The null tetrad vectors of the Kerr metric are generated from the complexified Schwarzschild metric, (equations 2.2.7 to 2.2.9) by making the complex coordinate transformatin 2.2.11,

$$\begin{aligned}
\tilde{l}^\mu &= \delta_1^\mu \\
\tilde{n}^\mu &= \delta_0^\mu - \frac{1}{2}\left(1 - \frac{2mr}{\rho^2} - \frac{Q^2}{\rho^2}\right)\delta_1^\mu \\
\tilde{m}^\mu &= \frac{1}{\sqrt{2}(r + ia\cos\theta)}\left(ia\sin\theta(\delta_0^\mu - \delta_1^\mu) + \delta_2^\mu + \frac{i}{\sin\theta}\delta_3^\mu\right) \quad .
\end{aligned}$$

The Kerr-Newman metric generated from these null tetrad vectors, in covariant form is

$$g_{\mu\nu} = \begin{pmatrix} 1 - \frac{2mr-Q^2}{\rho^2} & 1 & 0 & a\sin^2\theta\frac{2mr-Q^2}{\rho^2} \\ . & 0 & 0 & -a\sin^2\theta \\ . & . & -\rho^2 & 0 \\ . & . & . & -\sin^2\theta\left(r^2 + a^2 - a^2\sin^2\theta\frac{2mr-Q^2}{\rho^2}\right) \end{pmatrix} \quad , \tag{2.2.13}$$

where

$$\rho^2 \equiv r^2 + a^2\cos\theta^2.$$

As the metric is symmetric the "." is used to indicate $g_{\mu\nu} = g_{\nu\mu}$, This is not the usually Boyer-Lindquist form of the Kerr-Newman metric.

5. Finally it is assumed that a simple coordinate transformation of the form $u = t+F(r)$, $\phi = \psi + G(r)$ will transform the metric to *Boyer-Lindquist coordinates.* For our purposes a set of coordinates in which the metric has only one off-diagonal term $g_{t\phi}$ will be termed "Boyer-Lindquist".

   To obtain the usual representation of the Kerr-Newman metric in Boyer-Lindquist coordinates, it is necessary to make a transformation on the null coordinate u and the angle coordinate ϕ

$$u = t - \int \frac{a}{r^2 + a^2 + Q^2 - 2mr} dr \quad , \tag{2.2.14}$$

$$\phi = \psi - \int \frac{r^2 + a^2}{r^2 + a^2 + Q^2 - 2mr} dr \quad . \tag{2.2.15}$$

2.3 Application of the Newman-Janis algorithm.

In the various stages of the NJA described above the only ambiguous point was the tilde transformation in step 3. Applying this step to a general static spherically symmetric seed metric 2.2.1, the tilde operation produces the null tetrad vectors

$$\begin{aligned} \tilde{l}^\mu &= \delta_1^\mu \quad , \\ \tilde{n}^\mu &= e^{-\lambda(\tilde{r},\bar{\tilde{r}})-\phi(\tilde{r},\bar{\tilde{r}})}\delta_0^\mu - \frac{1}{2}e^{-2\lambda(\tilde{r},\bar{\tilde{r}})}\delta_1^\mu \quad , \\ \tilde{m}^\mu &= \frac{1}{\sqrt{2}\tilde{r}}\left(\delta_2^\mu + \frac{i}{\sin\tilde{\theta}}\delta_3^\mu\right) \quad . \end{aligned}$$

A new set of null tetrad vectors, and hence a new metric, results after the transformation 2.2.11. These new null tetrad vectors are

$$l^\mu = \delta_1^\mu \quad , \tag{2.3.1}$$

$$n^\mu = e^{-\lambda(r,\theta)-\phi(r,\theta)}\delta_0^\mu - \frac{1}{2}e^{-2\lambda(r,\theta)}\delta_1^\mu \quad , \tag{2.3.2}$$

$$m^\mu = \frac{1}{\sqrt{2}(r + ia\cos\theta)}\left(ia\sin\theta(\delta_0^\mu - \delta_1^\mu) + \delta_2^\mu + \frac{i}{\sin\theta}\delta_3^\mu\right) \quad . \tag{2.3.3}$$

The coordinates $x^\rho = \{u, r, \theta, \phi\}$ are all real. By equation 2.2.3 the metric obtained from the null tetrad vectors 2.3.1, 2.3.2 and 2.3.3 is, in covariant form,

$$g_{\mu\nu} = \begin{pmatrix} e^{2\Phi(r,\theta)} & e^{\lambda(r,\theta)+\Phi(r,\theta)} & 0 & a\sin^2\theta e^{\Phi(r,\theta)}(e^{\lambda(r,\theta)} - e^{\Phi(r,\theta)}) \\ . & 0 & 0 & -ae^{\Phi(r,\theta)+\lambda(r,\theta)}\sin^2\theta \\ . & . & -\rho^2 & 0 \\ . & . & . & -\sin^2\theta(\rho^2 + a^2\sin^2\theta e^{\Phi(r,\theta)}(2e^{\lambda(r,\theta)} - e^{\Phi(r,\theta)})) \end{pmatrix} \tag{2.3.4}$$

This completes steps 3 and 4, the application of the NJA to static spherically symmetric seed metrics without guessing the tilde transformation 2.2.4. At this stage the metric contains two unknown functions $\exp(\Phi)$ and $\exp(\lambda)$ of two variables r, θ. The only constraints on these functions are given by 2.2.5 and 2.2.6.

Step 5 is the transformation of the new metric into Boyer-Lindquist coordinates. To express the metric 2.3.4 in Boyer-Lindquist coordinates the following transformations are made,

$$u = t + \int g(r)dr; \quad \phi = \phi' + \int h(r)dr; \quad r = r'; \quad \theta = \theta'. \tag{2.3.5}$$

These particular transformations are made because as the functions $\exp\Phi, \exp\lambda$ and ρ are functions of r and θ only they are unaffected by 2.3.5. The functions $g(r)$ and $h(r)$ ensuring that the new metric $g'_{\mu\nu}$ has only one off diagonal term, $g'_{t\phi}$,

$$\begin{aligned}
g'_{tt} &= \frac{\partial x^\mu}{\partial t}\frac{\partial x^\nu}{\partial t}g_{\mu\nu} = g_{uu} \\
g'_{tr} &= \frac{\partial x^\mu}{\partial t}\frac{\partial x^\nu}{\partial r}g_{\mu\nu} = \frac{\partial x^\nu}{\partial r}g_{u\nu} = g(r)g_{uu} + g_{ur} + h(r)g_{u\phi} = 0 \qquad (2.3.6) \\
g'_{t\theta} &= 0 \\
g'_{t\psi} &= g_{t\phi} \\
g'_{rr} &= \frac{\partial x^\mu}{\partial r}\frac{\partial x^\nu}{\partial r}g_{\mu\nu} \\
&= g(r)^2 g_{uu} + 2g(r)g_{ur} + 2g(r)h(r)g_{u\phi} + 2h(r)g_{r\phi} + g_{rr} + h(r)g_{\phi\phi} \qquad (2.3.7) \\
g'_{r\theta} &= 0 \\
g'_{r\psi} &= \frac{\partial x^\mu}{\partial r}\frac{\partial x^\nu}{\partial \phi}g_{\mu\nu} \\
&= g(r)g_{u\phi} + g_{r\phi} + h(r)g_{\phi\phi} = 0 \qquad (2.3.8) \\
g'_{\theta\theta} &= g_{\theta\theta} \\
g'_{\psi\psi} &= g_{\phi\phi}.
\end{aligned}$$

The expression for $g(r)$ and $h(r)$ are found by solving 2.3.6 and 2.3.8 simultaneously,

$$g(r) = -\frac{e^{\lambda(r,\theta)}(\rho^2 + a^2\sin^2\theta e^{\lambda(r,\theta)+\Phi(r,\theta)})}{e^{\Phi(r,\theta)}(\rho^2 + a^2\sin^2\theta e^{2\lambda(r,\theta)})} \quad , \tag{2.3.9}$$

$$h(r) = -\frac{ae^{2\lambda(r,\theta)}}{\rho^2 + a^2\sin^2\theta e^{2\lambda(r,\theta)}} \quad . \tag{2.3.10}$$

Substituting the above expressions for $g(r)$ and $h(r)$ into equation 2.3.7 one finds that in these coordinates $\{t, r, \theta, \psi\}$ the metric is

$$g_{\mu\nu} = \begin{pmatrix} e^{2\Phi(r,\theta)} & 0 & 0 & a\sin^2\theta e^{\Phi(r,\theta)}(e^{\lambda(r,\theta)} - e^{\Phi(r,\theta)}) \\ . & -\rho^2/(\rho^2 e^{-2\lambda(r,\theta)} + a^2\sin^2\theta) & 0 & 0 \\ . & . & -\rho^2 & 0 \\ . & . & . & -\sin^2\theta(\rho^2 + a^2\sin^2\theta e^{\Phi(r,\theta)}(2e^{\lambda(r,\theta)} - e^{\Phi(r,\theta)})) \end{pmatrix} . \tag{2.3.11}$$

Recalling that $\rho^2 \equiv r^2 + a^2\cos^2\theta$, by rearrangement of equation 2.3.10 we find

$$e^{2\lambda(r,\theta)} = \frac{-h(r)\rho^2}{a^2h(r)\sin^2\theta + a} = \frac{\rho^2}{j(r) + a^2\cos^2\theta} .$$

where $j(r) \equiv -a/h(r) - a^2$.

In a similar manner equation 2.3.10 may be used to express $\exp\Phi(r,\theta)$ in terms of the single variable functions $g(r)$ and $j(r)$,

$$e^{\Phi(r,\theta)} = \frac{\sqrt{\rho^2(j(r) + a^2\cos^2\theta)}}{k(r) + a^2\cos^2\theta}$$

where $k(r) \equiv -g(r)(j(r) + a^2) - a^2$. The Boyer-Lindquist form of 2.3.4 is then

$$g_{\mu\nu} = \begin{pmatrix} \frac{\rho^2\left(j(r)+a^2\chi^2\right)}{\left(k(r)+a^2\chi^2\right)^2} & 0 & 0 & -\frac{a\left(1-\chi^2\right)(j(r)-k(r))\rho^2}{\left(k(r)+a^2\chi^2\right)^2} \\ . & -\frac{\rho^2}{j(r)+a^2} & 0 & 0 \\ . & . & -\frac{\rho^2}{1-\chi^2} & 0 \\ . & . & . & -\left(1-\chi^2\right)\rho^2\frac{\left(k(r)+a^2\right)^2 - a^2\left(1-\chi^2\right)\left(j(r)+a^2\right)}{\left(k(r)+a^2\chi^2\right)^2} \end{pmatrix} . \tag{2.3.12}$$

Where $\chi \equiv \cos\theta$ so that

$$\rho^2 \equiv r^2 + a^2\chi^2 \quad .$$

In order to calculate properties of the metric tensor 2.3.12 the packages *Tensor* and *Debever* where used inside *Maple V*. It is well known that while humans often prefer to work with trigonometric functions computers do not, the reason being that there is unique way to simplify trigonometric functions. The safest way to remove this problem is to avoid using trigonometric functions altogether in computer aided calculations. It is for this reason that the substitution $\chi \equiv \cos\theta$ was made.

2.4 Properties of metrics generated by the Newman-Janis algorithm

The package *Tensor* in *Maple V* enables the calculation of the Einstein tensor from any metric tensor. *Debever* calculates the Newman-Penrose spin coefficients. Below some theorems are provided for spacetimes generated using the above mentioned packages. The algebraic expressions of the Einstein tensor and the spin coefficients tend to be rather lengthy, fortunately all those of interest to us can be expressed in the form $\sum_m H_m \chi^{2m}$ where H_m is a function of r only. For reasons of compactification all the curvature expressions will be written in this way and the specific forms for H_m will be shown only when required. The interested reader is encouraged to check these expressions with *Maple*, *Mathematica* or their favorite algebraic manipulation program.

Theorem 1 : *The only perfect fluid generated by the Newman-Janis Algorithm is the vacuum.*

Proof: Generation of the Einstein tensor from the metric 2.3.12 reveals that $G_{tA} \equiv 0$ if $A = r$ or $A = \chi$. If the Einstein tensor is equivalent to the stress energy tensor of a perfect fluid then

$$G_{\mu\nu} = (P + \varrho)U_\mu U_\nu - P g_{\mu\nu} \quad . \tag{2.4.1}$$

As the four velocity is timelike ($U_t \neq 0$). The vanishing of G_{tr} and $G_{t\chi}$ is assured if and only if $U_r = U_\chi = 0$, as $g_{t\chi} = g_{tr} = 0$. Given that $U_r = U_\chi = 0$ then from 2.4.1 $G_{r\chi} = 0$. The $G_{r\chi}$ component of the Einstein tensor generated by *Tensor* in *Maple V* is

$$-3\chi a^2 \frac{(2r - k'(r))\, a^4\chi^4 + (2k(r) - k'(r)r)\, 2ar\chi^2 - k'(r)r^4 + 2rk(r)^2}{\rho^4 \left(k(r) + a^2\chi^2\right)^2} \quad ,$$

where " ′ " denotes the derivative with respect to r. This expression vanishes if and only if

$$k(r) = r^2 \quad . \tag{2.4.2}$$

To resolve $j(r)$ with this definition of $k(r)$ we look at the isotropic pressure condition,

$$G_{rr}/g_{rr} - G_{\chi\chi}/g_{\chi\chi} = 0 \quad ,$$

which for metric 2.3.12 reads

$$\frac{-1}{2}\frac{(j''(r)-2)a^2\chi^2}{r^2+a^2\chi^2} - \frac{1}{2}\frac{2r^2+r^2j''(r)-4rj'(r)+4j(r)}{r^2+a^2\chi^2} = 0 \quad . \tag{2.4.3}$$

As χ is an independent variable the isotropic pressure condition 2.4.3 is satisfied if and only if

$$\begin{aligned} j''(r) \quad &- \quad 2 = 0 \quad , \\ (j''(r)-2)\,a^2\chi^2 + 2r^2 + r^2j''(r) \quad &- \quad 4rj'(r) + 4j(r) = 0 \quad . \end{aligned}$$

The unique solution to this pair of equations is

$$j(r) = r^2 + d_1 r \quad , \tag{2.4.4}$$

where d_1 is a constant of integration.

Substituting equations 2.4.4 and 2.4.2 into the metric 2.3.12 generated by the NJA, and setting the constant of integration d_1 to equal twice the mass we get the Kerr metric in Boyer-Lindquist coordinates. □

Theorem 2 : *The only algebraically special spacetimes generated by the Newman-Janis algorithm are Petrov type D.*

Proof: It was shown in section 2.3 that since the metric 2.3.4 can be transformed to Boyer-Lindquist coordinates the functions $\exp\Phi(r,\theta)$ and $\exp\lambda(r,\theta)$ can be expressed in the form

$$e^{\lambda(r,\chi)} = \frac{\sqrt{\rho^2}}{\sqrt{j(r)+a^2\chi^2}} \quad , \tag{2.4.5}$$

$$e^{\Phi(r,\chi)} = \frac{\sqrt{\rho^2\,(j(r)+a^2\chi^2)}}{k(r)+a^2\chi^2} \quad , \tag{2.4.6}$$

$$\rho^2 \equiv r^2 + a^2\chi^2 \quad , \tag{2.4.7}$$

$$\chi \equiv \cos\theta \quad . \tag{2.4.8}$$

The resulting null tetrad vectors are

$$l^\mu = \delta^\mu_1 \quad , \tag{2.4.9}$$

$$n^\mu = \frac{k(r)+a^2\chi^2}{\rho^2}\delta^\mu_1 - \frac{1}{2}\frac{j(r)+a^2\chi^2}{\rho^2}\delta^\mu_0 \quad , \tag{2.4.10}$$

$$m^\mu = \frac{1}{\sqrt{2}(r+ia\chi)}\left(ia\sqrt{1-\chi^2}(\delta^\mu_0-\delta^\mu_1)+\delta^\mu_2+\frac{i}{\sqrt{1-\chi^2}}\delta^\mu_3\right) \quad , \tag{2.4.11}$$

Using the package *Debever* in *Maple V* it is possible to compute the Newman-Penrose coefficients [61] from the null tetrad vectors 2.4.9, 2.4.10 and 2.4.11. It is found that Ψ_0 is identically zero. A spacetime is said to be algebraically special [62] if $\Psi_0 = \Psi_1 = 0$. Ψ_1 is a rather long expression which can however be expressed as

$$\Psi_1 = \frac{\sum_{m=0}^{4} iK_m\chi^{2m}}{\rho^4(r-ia\chi)(k(r)+a^2\chi^2)\sqrt{1-\chi^2}} \quad , \tag{2.4.12}$$

where K_m are functions of $k(r)$ only. That is, the vanishing of Ψ_1 is independent of $j(r)$. As r and χ are independent variables, $\Psi_1 = 0$ if and only if $K_m = 0$ for $m = 0,1,2,3,4$. In particular

$$K_4 = k''(r) - 2 \quad ,$$

which equals zero if and only if $k(r) = r^2 + c_1 r + c_0$. Substituting this expression for $k(r)$ into K_3 it is found that $K_3 = a^4(4c_0 - c_1^2)$ which equals zero for $a \neq 0$ if and only if $c_1^2 - 4c_0 = 0$ so that

$$k(r) = r^2 + c_1(r + c_1/4) \quad . \tag{2.4.13}$$

Furthermore with $k(r)$ given by equation 2.4.13 it is easy to show by direct substitution that $K_m = 0$ for all allowed values of m.

Hence all spacetimes generated by the Newman-Janis Algorithm which are algebraically special uniquely satisfy equation 2.4.13. The proof that they are also Petrov type D involves substituting the expression for $k(r)$ into the expressions for the Newman-Penrose spin coefficients Ψ_i, where $i = 1 \ldots 4$, and showing that they satisfy the relation

$$\Psi_2\Psi_4 - 2\Psi_3^2/3 = 0 \quad .$$

This can be checked checked with the *Debever* package in *Maple V*. □

Theorem 3 : *The only Petrov type D spacetime generated by the Newman-Janis algorithm with a vanishing Ricci scalar is the Kerr-Newman spacetime.*

Proof: Solutions to the Einstein-Maxwell field equations have a vanishing Ricci scalar. Once again using *Tensor* within *Maple V* it is possible to calculate the Ricci scalar from the metric 2.3.12 with the definition 2.4.13. By grouping the Ricci scalar R into powers of χ

$$R = \frac{\sum_{m=0}^{4} J_m \chi^{2m}}{\rho^6 \left(r^2 + c_1(r + c_1/4)\right)^2} \quad ,$$

J_m are functions of $j(r)$ only. As r and χ are independent variables $R = 0$ if and only if $J_m = 0$ for all allowed values of m. In particular

$$J_4 = j''(r) - 2 \quad ,$$

which equals zero if and only if $j(r) = r^2 + d_1 r + d_0$. Substituting this expression for $j(r)$ along with 2.4.2 into R it is found that

$$R = c_1 \frac{\sum_{m=0}^{3} I_m \chi^{2m}}{\rho^6 \left(r^2 + c_1(r + c_1/4)\right)^2} \quad ,$$

where I_m depends on the constants c_1, d_1, d_0 and the variable r. It is not difficult, though tiresome, to show that if you do not assume that $c_1 = 0$ then $c_1 = -2d_1$ and $d_1 = d_0 = 0$. Hence $R = 0$ if and only if $c_1 = 0$. In which case the functions $j(r)$ and $k(r)$ are

$$\begin{aligned} j(r) &= r^2 + d_1 r + d_0 \quad , \\ k(r) &= r^2 \quad , \end{aligned}$$

Setting the constants of integration d_1 and d_0 to be twice the mass and the square of the charge of the black hole respectively one obtains the Kerr-Newman metric. □

2.5 Conclusion

Previously all work on the Newman-Janis algorithm has involved some guess work. It was noticed that the Kerr-Newman metric could be obtained if a complex extension to the metric coefficients of the Reissner-Nordström seed metric was made

$$ds^2 = \left(1 - m\left(\frac{1}{r} + \frac{1}{\bar{r}}\right) + \frac{Q^2}{r\bar{r}}\right) dt^2 - \left(\frac{r\bar{r}}{r\bar{r} - m(r + \bar{r}) + Q^2}\right) dr^2 - r\bar{r} d^2\theta - r\bar{r} \sin^2\theta d^2\phi$$

before applying the NJA, where the bar denotes the complex conjugate of a particular variable. The only reason given for doing this was that it was successful. Our analysis does not rely on any such guess work and gives an unambiguous explanation of the success of the NJA in generating the Kerr-Newman metric.

In this chapter the following has been proven: 1) The only perfect fluid spacetime generated by applying the Newman-Janis algorithm to a static spherically symmetric seed metric which may be written in Boyer-Lindquist form is the Kerr metric. 2) The only algebraically special spacetimes generated by applying the Newman-Janis algorithm to static spherically symmetric seed metrics which may be written in Boyer-Lindquist form are Petrov-type D. 3) The only algebraically special spacetime generated by applying the Newman-Janis algorithm to a static spherically symmetric seed metric which may be written in Boyer-Lindquist form and which has vanishing Ricci scalar (e.g. is a solution of the Einstein-Maxwell equations) is the Kerr-Newman metric.

Chapter 3

Generalization of the Newman-Janis algorithm.

3.1 Introduction

The previous chapter proved that no perfect fluids (other than the trivial case $P = \varrho = 0$) could be generated by the Newman-Janis Algorithm (NJA). The Newman-Janis algorithm was put forward as a very specific 5 step process. It was also mentioned that the most ambiguous step in this process was step 3, the tilde transformation. The tilde transformation converted the null tetrad vector coefficients of n^μ;

$$n^\mu = e^{-\lambda(r)-\Phi(r)}\delta_0^\mu - \frac{1}{2}e^{-2\lambda(r)}\delta_1^\mu \rightarrow \tilde{n}^\mu = e^{-\lambda(\bar{r},\bar{\bar{r}})-\phi(\bar{r},\bar{\bar{r}})}\delta_0^\mu - \frac{1}{2}e^{-2\lambda(\bar{r},\bar{\bar{r}})}\delta_1^\mu \quad .$$

On the other hand the tilde transformation did nothing to m^μ, despite the fact that there is a $1/r$ term. This result seems contradictory as the $1/r$ term in the Schwarzschild metric becomes $(1/2r + 1/2\bar{r})$ under the tilde transformation. One can not help but suspect that the reason m^μ was left unchanged is because it obtained the known result of the Kerr metric. This chapter investigates scenarios for which no assumption is made for the tilde transformation of $1/r$ in m^μ. Since the Kerr metric describes the spacetime of a rotating blackhole, it is naturally of interest to determine whether or not it describes the exterior of an extended axisymmetric rotating massive body. While Birkhoff's theorem [63] tells us that the spacetime exterior to a spherically symmetric body is uniquely defined by the Schwarzschild metric there is no reason to expect that the spacetime exterior to an arbitrary stationary axisymmetric (SAS) perfect fluid body should be the Kerr spacetime.

In fact it remains an open question as to whether the Kerr solution can represent the exterior of any perfect fluid source at all.

The first genuine example of a Kerr interior solution appears to have been provided by Neugebauer and Meinel [36], but it is rather difficult to access analytically, and as it represents a disc of matter, the concept of perfect fluid can only apply in a degenerate sense. It would therefore be particularly attractive to generate interior Kerr solutions by some simple procedure. An obvious candidate appears to be a generalization of the NJA, since that procedure is precisely capable of generating the Kerr metric from the Schwarzschild metric.

There are two main themes that run through this chapter. The first is the generalization of the Newman-Janis algorithm (GNJA) and its application to static spherically symmetric (SSS) seed metrics. The second is the joining of a SAS metric generated by the GNJA to the Kerr metric on a static axisymmetric boundary surface. These two themes are linked together with the aim of finding a physically reasonable source for the Kerr metric.

The rest of the outline of the chapter is as follows. In the second section 3.2 the generalised Newman-Janis algorithm (GNJA) NJA for obtaining SAS metrics from static spherically symmetric (SSS) ones is outlined. The resulting metric is written in terms of three arbitrary functions $(\exp\Phi, \rho, \exp\lambda)$. These functions give the physical properties of the internal structure. Furthermore a coordinate transformation is performed so that the new metric is written in Boyer-Lindquist coordinates. This makes the physical interpretation much clearer and decreases the amount of algebra required in calculating various metric properties. Section 3.3 develops a set of boundary conditions for the joining of any two SAS metrics on an arbitrary static axisymmetric boundary surface. The term boundary surface is used according to Israel's original definition where that the surface separating the two geometries has a vanishing surface stress-energy tensor. Particular emphasis is placed on those SAS metrics that can be generated from SSS metrics via the GNJA. Following on directly from this, section 3.4 examines explicitly the case when the exterior metric corresponds to the Kerr metric. In this section the boundary conditions for matching an interior metric generated by the GNJA to the Kerr metric are presented. Requiring that the interior metric be "physically reasonable" places even further constraints on it. The

meaning of the term "physically reasonable source of the Kerr metric" is discussed. Having established a rigorous formalism in the previous sections, section 3.5 looks for solutions to which the GNJA may be successfully applied. One such solution is examined, the "trial solution". The trial solution is found to match smoothly to the Kerr metric on surfaces of constant r. An examination of the static limit of this solution shows it to have physically reasonable properties. The last section 3.6 is the conclusion and sums up all the results obtained in this chapter.

3.2 Generalizing the Newman-Janis algorithm

Recall that in the previous chapter the tilde operation transformed the null tetrad vectors of a static spherically symmetric seed metric,

$$\begin{aligned} l^\mu &= \delta_1^\mu \quad , \\ n^\mu &= e^{-\lambda(r)-\Phi(r)}\delta_0^\mu - \frac{1}{2}e^{-2\lambda(r)}\delta_1^\mu \quad , \\ m^\mu &= \frac{1}{\sqrt{2}r}\left(\delta_2^\mu + \frac{i}{\sin\theta}\delta_3^\mu\right) \end{aligned}$$

to

$$\tilde{l}^\mu = \delta_1^\mu \quad , \tag{3.2.1}$$

$$\tilde{n}^\mu = e^{-\lambda(\tilde{r},\bar{\tilde{r}})-\Phi(\tilde{r},\bar{\tilde{r}})}\delta_0^\mu - \frac{1}{2}e^{-2\lambda(\tilde{r},\bar{\tilde{r}})}\delta_1^\mu \quad , \tag{3.2.2}$$

$$\tilde{m}^\mu = \frac{1}{\sqrt{2}\tilde{r}}\left(\delta_2^\mu + \frac{i}{\sin\tilde{\theta}}\delta_3^\mu\right) \quad .$$

No justification was given as to why the tilde transformation simply changes the $1/\tilde{r}$ to $1/\bar{\tilde{r}}$ in m^μ. Results of the previous chapter demonstrated that the only perfect fluid generated by the GNJA are vacuum spacetimes. The question examined here is whether non-vacuum perfect fluids may be generated by generalizing the NJA. The Newman-Janis algorithm is generalized by leaving the tilde transformation on the $1/r$ coefficient in front of m^μ unspecified, so that

$$\tilde{m}^\mu = \frac{1}{\sqrt{2}\rho(\tilde{r},\bar{\tilde{r}})}\left(\delta_2^\mu + \frac{i}{\sin\tilde{\theta}}\delta_3^\mu\right) \quad , \tag{3.2.3}$$

where $\rho(\tilde{r},\bar{\tilde{r}})$ is an unknown real valued function of the complex variables $\tilde{r}$ and $\bar{\tilde{r}}$. The metric generated by applying the coordinate transformations 2.2.12 to the null tetrad

vectors 3.2.1, 3.2.2 and 3.2.3 is determined using 2.2.3 to be

$$g^{\mu\nu} = \begin{pmatrix} -\frac{a^2\sin^2\theta}{\rho^2} & e^{-\lambda-\Phi}+\frac{a^2\sin^2\theta}{\rho^2} & 0 & -\frac{a}{\rho^2} \\ . & -e^{-2\lambda}-\frac{a^2\sin^2\theta}{\rho^2} & 0 & -\frac{a^2}{\rho^2} \\ . & . & -\frac{1}{\rho^2} & 0 \\ . & . & . & -\frac{1}{\rho^2\sin^2\theta} \end{pmatrix} . \tag{3.2.4}$$

In the above expression and from now on ρ, Φ and λ are understood to be functions of r and θ. In the covariant form this is

$$g_{\mu\nu} = \begin{pmatrix} e^{2\Phi} & e^{\lambda+\Phi} & 0 & a\sin^2\theta e^{\Phi}(e^{\lambda}-e^{\Phi}) \\ . & 0 & 0 & -ae^{\Phi+\lambda}\sin^2\theta \\ . & . & -\rho^2 & 0 \\ . & . & . & -\sin^2\theta(\rho^2+a^2\sin^2\theta e^{\Phi}(2e^{\lambda}-e^{\Phi})) \end{pmatrix} . \tag{3.2.5}$$

As the metric is symmetric the "." is used to indicate $g_{\mu\nu} = g_{\nu\mu}$. The form of this metric gives the result of applying the generalized Newman-Janis algorithm (GNJA) to the static spherically symmetric seed metric.

The metric given in equation (3.2.5), though relatively simple, is still hard to calculate with. To eradicate this problem one can make a gauge transformation so that the only off-diagonal component is $g_{t\phi}$. This makes it easier to compare with the more usual Boyer-Lindquist form of the Kerr metric [64] and to interpret the physical properties such as frame dragging. The Boyer-Lindquist form is also an aid to the calculation and evaluation of the Einstein tensor as there are five independent components of $g_{\mu\nu}$ instead of the six in 3.2.5. To express the metric 3.2.5 in Boyer-Lindquist coordinates the following transformations are made,

$$u = t + \int b(r)dr; \quad \phi = \phi' + \int c(r)dr; \quad r = r'; \quad \theta = \theta' \quad . \tag{3.2.6}$$

These particular transformations are made because as the functions $\exp\Phi, \exp\lambda$ and ρ are functions of r and θ only they are unaffected by 3.2.6. The functions $b(r)$ and $c(r)$ ensuring

that the new metric $g'_{\mu\nu}$ has only one off diagonal term, $g'_{t\phi}$, and

$$\begin{aligned}
g'_{tt} &= \frac{\partial x^\mu}{\partial t}\frac{\partial x^\nu}{\partial t}g_{\mu\nu} = g_{uu} \quad , \\
g'_{tr} &= \frac{\partial x^\mu}{\partial t}\frac{\partial x^\nu}{\partial r}g_{\mu\nu} = \frac{\partial x^\nu}{\partial r}g_{u\nu} = b(r)g_{uu} + g_{ur} + c(r)g_{u\phi} = 0 \quad , \\
g'_{t\theta} &= 0 \quad , \\
g'_{t\phi} &= g_{t\phi} \quad , \\
g'_{rr} &= \frac{\partial x^\mu}{\partial r}\frac{\partial x^\nu}{\partial r}g_{\mu\nu} \quad , \\
&= b(r)^2 g_{uu} + 2b(r)g_{ur} + 2b(r)c(r)g_{u\phi} + 2c(r)g_{r\phi} + g_{rr} + c(r)g_{\phi\phi} \quad , \\
g'_{r\theta} &= 0 \quad , \\
g'_{r\phi} &= \frac{\partial x^\mu}{\partial r}\frac{\partial x^\nu}{\partial \phi}g_{\mu\nu} \quad , \\
&= b(r)g_{u\phi} + g_{r\phi} + c(r)g_{\phi\phi} = 0 \quad , \\
g'_{\theta\theta} &= g'_{\theta\theta} \quad , \\
g'_{\phi\phi} &= g'_{\phi\phi} \quad .
\end{aligned} \tag{3.2.7}$$

$$\tag{3.2.8}$$

The expression for $b(r)$ and $c(r)$ are found by solving 3.2.7 and 3.2.8 simultaneously,

$$b(r) = -\frac{e^\lambda(\rho^2 + a^2\sin^2\theta e^{\lambda+\phi})}{e^\phi(\rho^2 + a^2\sin^2\theta e^{2\lambda})} \quad , \tag{3.2.9}$$

$$c(r) = -\frac{ae^{2\lambda}}{\rho^2 + a^2\sin^2\theta e^{2\lambda}} \quad . \tag{3.2.10}$$

Substituting these expressions for $b(r)$ and $c(r)$ into g_{rr} it is found that

$$g_{\mu\nu} = \begin{pmatrix} e^{2\Phi} & 0 & 0 & a\sin^2\theta e^\Phi(e^\lambda - e^\Phi) \\ . & -\rho^2/(\rho^2 e^{-2\lambda} + a^2\sin^2\theta) & 0 & 0 \\ . & . & -\rho^2 & 0 \\ . & . & . & a\sin^2\theta\,(\rho^2 + e^\Phi(2e^{2\lambda} - e^\Phi)) - \rho^2 \end{pmatrix} \quad . \tag{3.2.11}$$

In the same manner as the previous chapter, equation 3.2.10 may be rearranged so that

$$e^{2\lambda} = \frac{-c(r)\rho^2}{a^2 c(r)\sin^2\theta + a} = \frac{\rho^2}{d(r) + a^2\cos^2\theta} \quad . \tag{3.2.12}$$

Where $d(r) \equiv -a/c(r) - a^2$. Rearrangement of 3.2.10 with the use of 3.2.12 leads to

$$e^\Phi = \frac{\sqrt{\rho^2(d(r) + a^2\cos^2\theta)}}{e(r) + a^2\cos^2\theta} \quad , \tag{3.2.13}$$

where $e(r) \equiv -b(r)(d(r) + a^2) - a^2$. The metric 3.2.11 with the definitions of $\exp\lambda$ and $\exp\Phi$ given by equations 3.2.12 and 3.2.13 respectively represent the complete family of metrics that may be obtained by generalizing the NJA (GNJA) and applying it to a static spherical symmetric seed metric. The validity of these transformations requires that $\rho^2 + a^2 \sin^2\theta e^{2\lambda} \neq 0$, which is always the case since $e^{2\lambda} > 0$ and the signature of the metric is such that $g_{\theta\theta} = -\rho^2 < 0$. Note that the choice of $e^{2\Phi} = e^{-2\lambda} = 1 + (Q^2 - 2mr)/(r^2 + a^2\cos^2\theta)$ and $\rho^2 = r^2 + a^2\cos^2\theta$ corresponds to the Kerr-Newman solution, where Q and m are the charge and mass of the body respectively.

3.3 Matching interior solutions to an exterior Kerr

The boundary surface separating a stationary rotating star from the vacuum is a static axisymmetric hypersurface. Having obtained a class of metrics generated by the GNJA the next question is whether or not they can be considered as sources of the Kerr metric. In order to be sources of the Kerr metric they should join smoothly to the Kerr metric on some hypersurface Σ. Appendix A reviews the juncture conditions for the matching two 4 dimensional spacetime manifolds on a common 3 dimensional hypersurface Σ. This section looks at the more specific example of matching interior solutions generated by the GNJA smoothly to the Kerr metric on static axisymmetric spacetime hypersurface Σ.

The metrics generated by the GNJA are in terms of Boyer-Lindquist coordinates $x^\alpha = \{t, r, \theta, \phi\}$. This coordinate system is common to both the interior M^- and the exterior Kerr M^+. On static axisymmetric hypersurfaces the coordinates r and θ are related by some function

$$F(r, \theta) = 0 \quad . \tag{3.3.1}$$

It is always possible to express this surface condition for Σ as

$$F = r - R(\theta) = 0 \quad , \tag{3.3.2}$$

where $R(\theta)$ is some unknown function of θ. Components of the normal vector to this surface are

$$N_\gamma = \pm\frac{\partial_\gamma F}{\sqrt{\partial_\beta F \partial^\beta F}} = \pm\frac{r - \partial_\theta R(\theta)}{\sqrt{g^{rr}r^2 + g^{\theta\theta}\partial_\theta R(\theta)^2}} \quad . \tag{3.3.3}$$

The $\pm$ is used to indicate that any surface has two normal vectors, one pointing in, and the other out. The direction of N_γ is not important in our calculations, so for convenience the positive value is chosen. On Σ the coordinates r and θ are related by a single coordinate σ, i.e., $r = r(\sigma)$ and $\theta = \theta(\sigma)$. A Gaussian coordinate system $y^\mu = \{n, \xi^i\}$ can be chosen so that on the hypersurface separating the two spacetimes $n = 0$ and $\xi^i = \{t, \sigma, \Phi\}$. In Gaussian coordinates the metric tensor may be expressed as $g_{\mu\nu} = {}^4g_{\mu\nu}(n, \xi^i)$. The first fundamental form is ${}^3g_{ij}(n = 0, \xi^i)$. In Appendix A it is shown that the first juncture condition for the smooth matching of two spacetimes M^+ and M^- on a hypersurface Σ is

$$\left[{}^3g_{ij}\right] = 0 \quad .$$

The square bracket [X] is used to denote that

$$[X] = X^+_\Sigma - X^-_\Sigma \quad ,$$

where the notation X^+_Σ indicates that the quantity X is calculated in M^+ and evaluated on Σ. Hence

$$\left[{}^3g_{ij}\right] = \frac{\partial x^{\alpha+}}{\partial \xi^{i+}} \frac{\partial x^{\beta+}}{\partial \xi^{j+}} g^+_{\Sigma\alpha\beta} - \frac{\partial x^{\alpha-}}{\partial \xi^{i-}} \frac{\partial x^{\beta-}}{\partial \xi^{j-}} g^-_{\Sigma\alpha\beta} \quad .$$

If the two spacetimes have a common set of coordinates $x^{\alpha+} = x^{\alpha-} = \{t, r, \theta, \phi\}, \xi^{i+} = \xi^{i-} = \{t, \sigma, \phi\}$ and the metrics are stationary and axisymmetric then,

$$ds^{2\pm} = g_{tt}\, dt^2 + 2\, g_{t\phi}\, dt d\phi + g_{rr}\, dr^2 + g_{\theta\theta}\, d\theta^2 + g_{\phi\phi}\, d\phi^2 \quad , \tag{3.3.4}$$

where the metric coefficients depend on r and θ only. The first junction condition for metrics of the form 3.3.4, with a common coordinate system, separated by a static axisymmetric hypersurface Σ is

$$\left[{}^3g_{tt}\right] = \frac{\partial x^\mu}{\partial t} \frac{\partial x^\nu}{\partial t} \left[{}^4g_{\mu\nu}\right] = \delta^\mu_t \delta^\nu_t \left[{}^4g_{\mu\nu}\right] = \left[{}^4g_{tt}\right] = 0 \quad , \tag{3.3.5}$$

$$\left[{}^3g_{t\phi}\right] = \frac{\partial x^\mu}{\partial t} \frac{\partial x^\nu}{\partial \phi} \left[{}^4g_{\mu\nu}\right] = \delta^\mu_t \delta^\nu_\phi \left[{}^4g_{\mu\nu}\right] = \left[{}^4g_{t\phi}\right] = 0 \quad , \tag{3.3.6}$$

$$\left[{}^3g_{\phi\phi}\right] = \frac{\partial x^\mu}{\partial \phi} \frac{\partial x^\nu}{\partial \phi} \left[{}^4g_{\mu\nu}\right] = \delta^\mu_\phi \delta^\nu_\phi \left[{}^4g_{\mu\nu}\right] = \left[{}^4g_{\phi\phi}\right] = 0 \quad , \tag{3.3.7}$$

$$\left[{}^3g_{\sigma\sigma}\right] = \frac{\partial x^\mu}{\partial \sigma} \frac{\partial x^\nu}{\partial \sigma} \left[{}^4g_{\mu\nu}\right] = \left(\frac{\partial r}{\partial \sigma}\right)^2 \left[{}^4g_{rr}\right] + \left(\frac{\partial \theta}{\partial \sigma}\right)^2 \left[{}^4g_{\theta\theta}\right] = 0 \quad . \tag{3.3.8}$$

The last equation may be simplified using $r - R(\theta) = 0$ and $r = r(\sigma), \theta = \theta(\sigma)$,

$$\begin{aligned} \frac{\partial r}{\partial \sigma} &- \frac{\partial R(\theta)}{\partial \sigma} = 0 \quad , \\ \frac{\partial r}{\partial \sigma} &- \frac{\partial R(\theta)}{\partial \theta}\frac{\partial \theta}{\partial \sigma} = 0 \quad , \\ \frac{\partial r}{\partial \sigma} &= \partial_\theta R(\theta)\frac{\partial \theta}{\partial \sigma} \quad , \end{aligned} \tag{3.3.9}$$

so that

$$\left[{}^3g_{\sigma\sigma}\right] = \left(\frac{\partial \theta}{\partial \sigma}\right)^2 \left((\partial_\theta R(\theta))^2 \left[{}^4g_{rr}\right] + \left[{}^4g_{\theta\theta}\right]\right) = 0 \quad . \tag{3.3.10}$$

Metrics generated by the GNJA have coefficients given by (3.2.11). The continuity of the first fundamental for two SAS metrics generated by the GNJA can be found using equations (3.3.5) to (3.3.10),

$$[g_{tt}] = \left[e^{2\Phi}\right] = 0 \quad , \tag{3.3.11}$$

$$\begin{aligned} [g_{t\phi}] &= \left[-a\sin^2\theta e^{\Phi}\left(e^{\lambda} - e^{\Phi}\right)\right] \quad , \\ &= -a\sin^2\theta e^{\Phi}\left[e^{\lambda}\right] = 0 \quad \text{using } e^{\Phi+} = e^{\Phi-} = e^{\Phi} \text{ from 3.3.11} \quad . \end{aligned} \tag{3.3.12}$$

If $a \neq 0$ then 3.3.12 becomes $[\exp\lambda] = 0$. If $a = 0$ then $g_{t\phi} = 0$ identically and $\exp\lambda$ need not be continuous. Similarly

$$\begin{aligned} [g_{\Phi\Phi}] &= \left[-\sin^2\theta(\rho^2 + a^2\sin^2\theta e^{\Phi}(2e^{\lambda} - e^{\Phi}))\right] \quad , \\ &= -\sin^2\theta\left[\rho^2\right] + 2a^2\sin^4\theta e^{\Phi}\left[e^{\lambda}\right] = 0 \quad . \end{aligned} \tag{3.3.13}$$

If the metric is stationary ($a \neq 0$) then $[\exp\lambda] = 0$ and hence equation 3.3.13 vanishes if and only if $[\rho^2] = 0$. These boundary conditions can be summarized as follows:
Two metrics generated by applying the GNJA to two different static spherically symmetric seed metrics have a continuous first fundamental form when $a \neq 0$ if

$$[e^{\Phi}] = [e^{\lambda}] = [\rho] = 0 \quad . \tag{3.3.14}$$

As the metric coefficients g_{rr} and $g_{\theta\theta}$ can be expressed in terms of $\exp\lambda$ and ρ the smoothness of these two functions are guaranteed by equation 3.3.14. In the static limit ($a = 0$) the above conditions reduce to

$$[e^{\Phi}] = [\rho] = 0 \quad .$$

If it can be assumed that n in the static limit $\partial_\theta R(\theta) = 0$, then $g_{\sigma\sigma}$ vanishes identically. The importance of this result comes from examining solutions like the Schwarzschild interior solution. The Schwarzschild interior solution describes the interior of a static spherically symmetric uniform density star. It is matched smoothly to the Schwarzschild exterior despite the fact that $\exp\lambda$ is not continuous on the boundary. The above results demonstrate that the Schwarzschild interior can not be generalized to the rotating case as from Eq. 3.3.14 $\exp\lambda$ must be matched to the exterior.

Appendix A demonstrated that if the stress energy tensor contains no jump discontinuities on the hypersurface Σ then the second fundamental form (extrinsic curvature) must be continuous. The matching of the first fundamental form for SAS metrics generated by the GNJA were summarized in equation 3.3.14. Let us examine what constraints are placed by the smooth matching of the second fundamental form.

Appendix A shows that the extrinsic curvature is given the equation

$$K_{ij} = -N_\gamma \left(\frac{\partial^2 x^\gamma}{\partial\zeta^i \partial\zeta^j} + \Gamma^\gamma_{\alpha\beta} \frac{\partial x^\alpha}{\partial\zeta^i} \frac{\partial x^\beta}{\partial\zeta^j} \right) \quad .$$

where N_γ are components of the normalised normal vector, x^μ are the coordinates in M^+ and M^-, and ξ^i coordinates on the hypersurface Σ. For SAS spacetimes on hypersurfaces described by 3.3.2 the extrinsic curvature is

$$K_{ij} = -\frac{1}{N} \left(\frac{\partial^2 x^r}{\partial\zeta^i \partial\zeta^j} + \Gamma^r_{\alpha\beta} \frac{\partial x^\alpha}{\partial\xi^i} \frac{\partial x^\beta}{\partial\xi^j} \right) + \frac{\partial_\theta R(\theta)}{N} \left(\frac{\partial^2 x^\theta}{\partial\zeta^i \partial\zeta^j} + \Gamma^\theta_{\alpha\beta} \frac{\partial x^\alpha}{\partial\xi^i} \frac{\partial x^\beta}{\partial\xi^j} \right) \quad .$$

The non-zero Christoffel symbols are

$$\begin{aligned}
\Gamma^r_{rr} &= \frac{1}{2} g^{rr} g_{rr,r} \quad \Gamma^\theta_{\theta\theta} = \frac{1}{2} g^{\theta\theta} g_{\theta\theta,\theta} \quad , \\
\Gamma^r_{r\theta} &= \frac{1}{2} g^{rr} \left(g_{rr,\theta} + g_{\theta r,r} - g_{r\theta,r} \right) = \frac{1}{2} g^{rr} g_{rr,\theta} \quad \Gamma^\theta_{\theta r} = \frac{1}{2} g^{\theta\theta} g_{\theta\theta,r} \quad , \\
\Gamma^r_{\theta\theta} &= \frac{1}{2} g^{rr} \left(g_{r\theta,\theta} + g_{\theta r,\theta} - g_{\theta\theta,r} \right) = -\frac{1}{2} g^{rr} g_{\theta\theta,r} \quad \Gamma^\theta_{rr} = -\frac{1}{2} g^{\theta\theta} g_{rr,\theta} \quad .
\end{aligned}$$

Evaluating the non-zero components of the $[K_{ij}]$ one finds

$$[\mathrm{K_{tt}}] = -\frac{1}{2N} \left([g^{rr} g_{tt,r}] - \partial_\theta R(\theta) \left[g^{\theta\theta} g_{tt,\theta} \right] \right) = 0 \quad , \tag{3.3.15}$$

$$[K_{t\phi}] = -\frac{1}{2N} \left([g^{rr} g_{t\phi,r}] - \left[g^{\theta\theta} \partial_\theta R(\theta) g_{t\phi,\theta} \right] \right) = 0 \quad , \tag{3.3.16}$$

$$[K_{\phi\phi}] = -\frac{1}{2N}\left([g^{rr}g_{\phi\phi,r}] - \left[g^{\theta\theta}\partial_\theta R(\theta) g_{\phi\phi,\theta}\right]\right) = 0 \quad , \tag{3.3.17}$$

$$[K_{\sigma\sigma}] = -\frac{1}{N}\left(\left[\frac{\partial^2 r}{\partial\sigma^2} + \frac{1}{2}\left(g^{rr}g_{rr,r}\left(\frac{\partial r}{\partial\sigma}\right)^2 + 2g^{rr}g_{rr,\theta}\frac{\partial r}{\partial\sigma}\frac{\partial\theta}{\partial\sigma} - \left(\frac{\partial\theta}{\partial\sigma}\right)^2 g^{rr}g_{\theta\theta,r}\right)\right]\right.$$
$$\left. - \partial_\theta R(\theta)\left[\frac{\partial^2\theta}{\partial\sigma^2} + \frac{1}{2}\left(-g^{\theta\theta}g_{rr,\theta}\left(\frac{\partial\theta}{\partial\sigma}\right)^2 + 2g^{\theta\theta}g_{\theta\theta,r}\frac{\partial r}{\partial\sigma}\frac{\partial\theta}{\partial\sigma} + \left(\frac{\partial r}{\partial\sigma}\right)^2 g^{\theta\theta}g_{\theta\theta,\theta}\right)\right]\right) = 0 \tag{3.3.18}$$

The first junction condition established that $[g^{rr}] = [g^{\theta\theta}]$, this can be used along with 3.3.14 and the definitions

$$\begin{aligned} \Lambda &\equiv -g^{\theta\theta}/(2N), \quad , \\ \Delta &\equiv g^{rr}/g^{\theta\theta}, \quad , \\ D &\equiv \Delta\frac{\partial}{\partial r} + \partial_\theta R\frac{\partial}{\partial\theta} \quad , \end{aligned}$$

to simplify equations 3.3.15 to 3.3.18,

$$[K_{tt}] = \Lambda\,[D\,g_{tt}] = 0 \quad , \tag{3.3.19}$$

$$[K_{t\phi}] = \Lambda\,[D\,g_{t\phi}] = 0 \quad , \tag{3.3.20}$$

$$[K_{\phi\phi}] = \Lambda\,[D\,g_{\phi\phi}] = 0 \quad , \tag{3.3.21}$$

$$[K_{\sigma\sigma}] = \Lambda\left(\frac{\partial\theta}{\partial\sigma}\right)^2\left[(\Delta g_{rr,r} + \partial_\theta R(\theta))\,(\partial_\theta R(\theta))^2\right.$$
$$\left. - 2\,(\Delta g_{rr,\theta} - \partial_\theta R(\theta) g_{\theta\theta,r})\,\partial_\theta R(\theta) - (\Delta g_{\theta\theta,r} + \partial_\theta R(\theta) g_{\theta\theta,\theta})\right] \quad . \tag{3.3.22}$$

The above junction conditions simplify further if the SAS metrics are generated by the GNJA. When the metric components are those of equation 3.2.11 then

$$[K_{tt}] = \Lambda\left[De^{\Phi}\right] = 0 \quad , \tag{3.3.23}$$

$$[K_{t\phi}] = \Lambda\, a\sin^2\theta e^{\Phi}\left[De^{\lambda}\right] = 0 \quad \text{using 3.3.23} \quad , \tag{3.3.24}$$

$$[K_{\phi\phi}] = -\sin^2\theta\left[D\rho^2\right] + 2a^2\sin^4\theta e^{\Phi}\left[De^{\lambda}\right] \quad . \tag{3.3.25}$$

The term $[K_{\sigma\sigma}]$ is somewhat more complicated and as it will not be used for later calculations it will not be expressed here. Equations 3.3.22-3.3.25 and 3.3.14 represent the complete set of boundary conditions for the joining of any two metrics generated by the GNJA on a static axially symmetric hypersurface. The next section examines these continuity conditions when the exterior metric is the Kerr metric.

3.4 Possible sources for the Kerr metric

The ultimate goal of this chapter is to find new static axisymmetric solutions to Einstein's field equations which may be considered as sources for the Kerr metric. With this in mind equations 3.3.22-3.3.25 and 3.3.14 are evaluated for the exterior Kerr metric. The subscript $_\Sigma$ is used for terms evaluated on a hypersurface Σ, the superscript $^-$ indicates functions defined in the interior. The continuity conditions for interior metrics generated by the GNJA separated by the hypersurface $r - R(\theta) = 0$ from the Kerr metric are

$$e_\Sigma^{2\phi^-} = 1 - \frac{2MR(\theta)}{\rho_\Sigma^2} \quad , \tag{3.4.1}$$

$$e_\Sigma^{2\lambda^-} = \frac{\rho_\Sigma^2}{\rho_\Sigma^2 - 2MR(\theta)} \quad , \tag{3.4.2}$$

$$\rho_\Sigma^2 = R(\theta)^2 + a^2\cos^2\theta \quad , \tag{3.4.3}$$

$$(De^{\Phi})_\Sigma = (D(1 - \frac{2mr}{r^2 + a^2\cos^2\theta}))_\Sigma \quad , \tag{3.4.4}$$

$$(De^{2\lambda^-}{}_{,r})_\Sigma = (D(\frac{r^2 + a^2\cos^2\theta}{r^2 + a^2\cos^2\theta - 2Mr}))_\Sigma \quad , \tag{3.4.5}$$

$$(D\rho^2)_\Sigma = D(r^2 + a^2\cos^2\theta)_\Sigma \quad , \tag{3.4.6}$$

and equation 3.3.22 which will not be written out explicitly. These results have been obtained from a purely geometric point of view. So far the only physical constraint invoked is the continuity of the stress energy tensor on the hypersurface separating the two spacetimes. It is of particular interest to find "physically reasonable" sources of the Kerr metric. Before proceeding further it is necessary to define exactly what is meant by the term "physically reasonable". A SAS metric which matches smoothly to the Kerr metric is termed physically reasonable if the Einstein tensor generated by the metric can be equated to the stress energy tensor of a perfect fluid satisfing the following:

- The strong and weak energy conditions are obeyed, i.e. the density ϱ is always positive and the density is always greater than the pressure P: $\varrho \geq 0$; $\varrho \geq P$.

- P and ϱ are monotonically decreasing out from the center.
- P and ϱ are related by an equation of state.

Another expected property of an interior solution to Kerr is that it corresponds to interior solutions of the Schwarzschild metric in the static limit. The static limit of Kerr is given by $a \to 0$. It is an inherent consequence of the transformations 2.2.6 and 2.2.12 that the seed metric is recovered in the limit $a \to 0$. This means that a necessary (but not sufficient) condition that the GNJA generate a physically reasonable source for the Kerr metric is that the seed metric is physically reasonable. The technique frequently used for obtaining interior seed solutions is to combine Einstein's field equations along with the conservation laws for a given stellar model, such as a perfect fluid with a given equation of state. In the case of SSS perfect fluids this lends to the Oppenheimer-Volkov equation [65]. Even with these simplifications analytic solutions to the Oppenheimer-Volkov equation are difficult to obtain, see [59] for some examples. It is noted in [59] that the few known analytic solutions generally fail on physical grounds. This is a fairly major hurdle in the application of GNJA to interior solutions since exact analytic expressions are required in order for it to be implemented successfully.

3.5 A trial solution

One of the difficulties faced in looking for sources of the Kerr metric is the matching of boundary conditions on appropriate surfaces. The approach taken here is not the usual one of guessing the solution and then seeing if the boundary conditions match. In fact the reverse approach will be taken. Only interior structures that join smoothly to the Kerr metric will be considered. The physical nature of these structures are studied via the generation of the Einstein tensor. If these structures are "physically reasonable" they may be considered possible sources of the Kerr metric.

Although the boundary conditions 3.4.1-3.4.6 and 3.3.22 come in a relatively simple form, they are still rather difficult to work with. The situation is rectifiable if one considers surfaces described by $\partial_\theta R(\theta) = 0$. The justification for choosing such simplified boundary surfaces goes beyond merely making the boundary condition equations more solvable. To

understand this the first thing one must realise is that the Kerr metric written in Boyer-Lindquist coordinates leads to a confusing interpretation of the variable r.

At the beginning of this thesis the importance of relativity as being a coordinate independent description of gravity was emphasized. Despite this the problem of obtaining interior solutions to the Kerr metric lead us into a coordinate based approach. The reason is that an exact solution is being sought after, which means that the metric will be found a particular coordinate system. The tensor relationship allow us to transform form one coordinate system to another.

The interpretation of a particular set of coordinates is a dangerous game to play but it is necessary in order to motivate the argument that the surface separating the interior solution from the Kerr metric is $R(\theta) = constant$. Consider for example the Kerr metric as first written by Kerr in KS coordinates,

$$\begin{aligned} ds^2 &= d\bar{t}^2 - dx^2 - dy^2 - dz^2 \\ &- \frac{2m\varrho^3}{\varrho^4 + a^2z^2}\left[\frac{\varrho(xdx + ydy) - a(xdy - ydx)}{\varrho^2 + a^2} + \frac{z}{\varrho}dz + d\bar{t}\right]^2 \quad , \end{aligned} \tag{3.5.1}$$

where ϱ is determined implicitly, up to a sign, by

$$\varrho^4 - (x^2 + y^2 + z^2 - a^2)\varrho^2 - a^2z^2 = 0 \quad . \tag{3.5.2}$$

Let us assume that the Kerr Schild coordinates x, y, z are Cartesian coordinates. The only justification for doing this is that in the flat space limit $m \to 0$ the Kerr metric 3.5.1 is the Minkowski metric in Cartesian coordinates. The coordinates x, y, z are related to Boyer-Lindquist coordinates r, θ, ϕ in the following way

$$x = r\sin\theta\cos\phi + a\sin\theta\sin\phi;\ y = r\sin\theta\sin\phi - a\sin\theta\cos\phi;\ z = r\cos\theta \quad . \tag{3.5.3}$$

Assuming that x, y, z are cartesian coordinates and taking the magnitude of the radial vector in spherical coordinates ($radius$) to have its usual definition,

$$radius^2 = x^2 + y^2 + z^2 \quad , \tag{3.5.4}$$

then by substitution of (3.5.3) into (3.5.4),

$$radius^2 = r^2 + a^2\sin^2\theta \quad . \tag{3.5.5}$$

Since a surface is described by $r = R(\theta)$ it is apparent why $\partial R(\theta)/\partial\theta = 0$, i.e. $R(\theta) = R =$ constant, is a sensible choice of boundary surface. The surface defined by

$$radius^2 - a^2 \sin^2\theta = R^2 \quad , \tag{3.5.6}$$

is an oblate spheroid. An oblate spheroid is a surface of revolution swept out by an ellipse rotating about its minor axis. An oblate spheroid defined by Eq.(3.5.6) transforms to a sphere in the limit $a \to 0$. These are the types of surfaces one would expect for a rotating star. If, as has been argued, the boundary surface separating the interior and exterior solutions is an oblate spheroid then equations (3.4.1) to (3.4.6) and 3.3.22 simplify to

$$e_\Sigma^{2\Phi-} = 1 - \frac{2MR}{\varrho_\Sigma^2} \quad , \tag{3.5.7}$$

$$e_\Sigma^{2\lambda-} = \frac{\varrho_\Sigma^2}{\varrho_\Sigma^2 - 2MR} \quad , \tag{3.5.8}$$

$$(e^{2\Phi-}{}_{,r})_\Sigma = \frac{2M(R^2 - a^2\cos^2\theta)}{\varrho_\Sigma^4} \quad , \tag{3.5.9}$$

$$(e^{2\lambda-}{}_{,r})_\Sigma = \frac{2M(a^2\cos^2\theta - R^2)}{(\varrho_\Sigma^2 - 2MR(\theta))^2} \quad . \tag{3.5.10}$$

The above equations give the boundary conditions for the joining of a SAS metric generated by the GNJA to the Kerr metric on a static oblate spheroidal boundary surface, $r = R =$ *constant*. With these constraint equations it is possible to look for new sources of the Kerr metric. In the static limit ($a \to 0$) the function $\exp\lambda$ provides information on the density profile of the interior. Assuming that $a = 0$ and that $\partial_\theta R(\theta) = 0$ implies that the first junction condition becomes

$$\left[e^\Phi\right] = [\varrho] = 0 \quad , \tag{3.5.11}$$

and the second

$$\left[e^\Phi{}_{,r}\right] = [\varrho_{,r}] = 0 \quad . \tag{3.5.12}$$

As was discussed previously the continuity of $\exp\lambda$ and its first derivative across the boundary Σ is required only if the spacetime is not static. However, if the a solution generated by the GNJA is to join smoothly to the Kerr metric then the continuity of the $\exp\lambda$ and its first derivative *is* required. For this reason, and the fact that it gives us the density profile in the static limit, let us examine solutions for which $[\exp\lambda] = 0$ first. The

technique used for finding the solutions to 3.5.8 and 3.5.9 is to integrate 3.5.9 with respect to r and add a arbitrary function of θ so that 3.5.8 is satisfied. This procedure gives

$$e^{2\lambda-} = \frac{\varrho_\Sigma^4 - 2M(R^2 r + a^2 \cos\theta(2R - r))}{(\varrho_\Sigma^2 - 2MR(\theta))^2} \quad . \tag{3.5.13}$$

Using this guess it should be possible to obtain a density and pressure profile as well as finding an exact solution for $e^{2\Phi}$ by the use of Einstein's equations. It is shown by the extremely low number of exact solutions of Einstein's equations that such a method, even for SSS metrics, is extremely difficult to work with. The use of algebraic programs such as *Cartan* and *grtensor* [66] [67] cut down most of the algebra; however they do not reduce the problem to a solvable state.

Although it is a complex task to examine the nature of stationary axisymmetric metrics, the examination of the non-rotating case is much simpler. It is always useful to examine the slow or zero rotation limit of such solutions since one would expect that these limits must also represent physical objects. The $a \to 0$ limit of such metrics determines the properties of the seed metric.

The trial solution for $\exp 2\lambda$ given by (3.5.13) obeys the boundary conditions on an oblate spheroid surface. One method for obtaining the interior structure might be to examine various functions of $\exp 2\Phi$ satisfying the boundary conditions (3.5.7) and (3.5.9). Once this has been done $\exp\Phi$ and $\exp\lambda$ could be fed into the general metric (3.2.11), from this ϱ and the stress-energy tensor could be derived by equating it to the Einstein tensor. The author is opposed to such a method as it relies on a great deal of guess work. As such it does not guarantee anything about the physical nature of the spacetime metrics.

A more sensible approach is to examine the properties of the seed metric first. If the seed metric corresponds to a physically sensible object then the hope is that the new metric generated by the GNJA will also represent a physical object. To begin this process the limit $a \to 0$ is taken of the metric (3.2.11) so that the static spherically symmetric seed metric,

$$ds^2 = e^{2\Phi}dt^2 - e^{2\lambda}dr^2 - r^2 d\theta^2 - r^2 \sin^2\theta d\phi^2 \quad , \tag{3.5.14}$$

and (3.5.13) becomes

$$e^{2\lambda(r_*)} = \frac{1 - xr_*}{(1-x)^2} \quad , \tag{3.5.15}$$

where

$$x = 2M/R \quad ,$$
$$r_* = r/R \quad .$$

The theory of radially symmetric distributions of matter is a well explored field. One of the classic papers on this subject is by Wyman [68]. For a static spherically symmetric perfect fluid described by (3.5.14) the pressure P and density ϱ satisfy the relationship

$$P_* = e^{-2\lambda}(2\Phi'/r_* + 1/r_*^2) - 1/r_*^2 \quad , \tag{3.5.16}$$
$$P_* = e^{-2\lambda}(2\Phi''/r_* - \lambda'\Phi' + (\Phi' - \lambda')/r_* + \Phi'^2) \quad , \tag{3.5.17}$$
$$\varrho_* = e^{-2\lambda}(2\lambda'/r_* - 1/r_*^2) + 1/r_*^2 \quad . \tag{3.5.18}$$

The notation used is that λ and Φ are understood to be only functions of r_*, $P_* = PR^2$, $\varrho_* = \varrho R^2$ and the prime denotes derivatives with respect to r_*. From (3.5.18) and (3.5.15) the density profile is

$$\varrho_* = \frac{1}{r_*^2} - \frac{(1-x)^2}{r_*^2(r_*x - 1)^2} \quad . \tag{3.5.19}$$

This density profile corresponds to that of a physically sensible stellar object as it is always positive and monotonically decreasing for all values of x in the range. The fact that ϱ_* diverges at $r_* = 0$ should not concern the reader too much. It would be worrying if the total mass of the star diverged. However a quick check shows that an infinitesimal sphere encapsulating the central singularity has finite mass;

$$M_\epsilon = 4\pi \int_0^\epsilon r_*^2 = 4\pi[2x - x^2]_0^\epsilon = 4\pi(2x - x^2)\epsilon \quad .$$

As the density monotonically decreases and the star has a finite radius the total mass converges. The divergence at $r_* = 0$ may disappear in a full quantum theory of gravity, a discussion of this point is beyond the scope of this material.

Given that the function $\exp\lambda$ is known then the equality of (3.5.16) and (3.5.17) results in a Riccati equation of first order in Φ'. There are various methods for finding solutions to the Riccati equation [69] and if a solution can be found then the pressure profile may be obtained. For the example given the resulting Riccati equation is

$$\Phi'' = \frac{1}{r_*^2} + \frac{r_*x - 1}{r_*(x-1)^2} + \frac{x}{2r_*(1 - r_*x)} + \left[\frac{1}{r_*} + \frac{x}{2(r_*x - 1)}\right]\Phi' - \Phi'^2 \quad . \tag{3.5.20}$$

Since this is a second order differential equation the solution involves two constants of integration. These two constants are determined by making sure that at the surface the pressure is zero and the exterior metric is Schwarzschild. In general solutions to the Riccati equation 3.5.20 are defined by functions more complicated than the elementary transcendental functions. Thus far it has not been possible to obtain analytic solutions to 3.5.20. As a result numerical integration is used to examine the solutions quantitatively.

The integration routine chosen is the ubiquitous fourth-order adaptive step-size Runge-Kutta routine. Using this routine enables us to see how Φ' varies as a function of r_*. This along with the known relation $\exp\lambda$ makes it possible to determine the pressure profile of the stellar object. The pressure and density profiles are shown in figures (3.1) to (3.3) for $x = 0.3$ as typical for neutron stars.

3.6 Conclusion

The previous chapter showed that the NJA was successful only in generating vacuum to vacuum solutions of Einstein's field equations. This chapter commenced by generalizing the NJA (GNJA) to include non-vacuum perfect fluid sources which could be considered as interiors to the Kerr metric. A coordinate transformation was made after applying the GNJA so that the metric could be written in Boyer-Lindquist type form. The metric formed by this algorithm belongs to a special class of metrics which are both stationary and axisymmetric (SAS). The Kerr metric belongs to this class.

The third section 3.3 established the constraints placed by matching smoothly two metrics generated by the GNJA on a static axisymmetric surface. The juncture conditions used were those first developed Dormois and Israel. It was found that for metrics generated by the GNJA the boundaries conditions reduced to a relatively simple set of constraint equations.

In looking for interior solutions to rotating massive bodies one might expect that its exterior is described by the Kerr metric. Section 3.4 was devoted to examining the properties of an interior metric that matches smoothly to the Kerr metric. This section also elaborated on what is meant by the term "physically reasonably" in describing the properties

of stellar objects.

The last section before the conclusion determined what sort of interior metrics could be matched smoothly to the Kerr metric on oblate spheroidal surfaces. One such solution was found and termed the trial solution, the metric coefficient $\exp\lambda$ was determined explicitly. It was argued that although it would be just as simple to find functions of $\exp\Phi$ that matched the boundary conditions on such surfaces, one has no a priori reason to believe that these would correspond to a physically reasonable stellar model. To work around this problem it was decided that one should begin with a physically reasonable seed metric. The seed solution was examined by taking the zero rotation limit ($a = 0$) of $\exp\lambda$. The density profile resulting from procedure was found to be "physical reasonable". The density ϱ as a function of the radius r was always positive, decreased monotonically out from the center and although it was infinite at the center the total mass was still finite.

The pressure profile on the other hand was slightly more difficult to determine. Seed metrics which describe isotropic perfect fluids were considered. Although the assumption of isotropy and perfect fluidity simplify calculations greatly, exact solutions of $\exp\Phi$ still require solving the Riccati equation. The Riccati equation is a non-linear first order equation which has no general solution. The task of finding such solutions is non-trivial as solutions generally can not be expressed as simple transcendental functions. However such equations can be integrated numerically without too much effort.

Once this was done it was possible to determine the pressure profiles for various mass to surface radius ratios ($x \equiv 2M/R$). An examination of one such profile for a typical value x for compact objects, namely $x = 0.3$, showed extremely encouraging results. The pressure P_* profile as a function of the normalised radius r_* satisfied all the specified criteria for being physically reasonable. The pressure was monotonically decreasing, the strong energy condition was obeyed and although the pressure diverged at $r = 0$ the amount of energy within a given volume was still finite.

The results of this chapter suggest that it is possible to find new sources of the Kerr metric by applying the generalized Newman-Janis algorithm (GNJA) to a static spherically symmetric smooth metric. These solutions have continuous boundary conditions on oblate spheroidal surfaces. At present the physically properties of these metrics has not been fully

investigated.

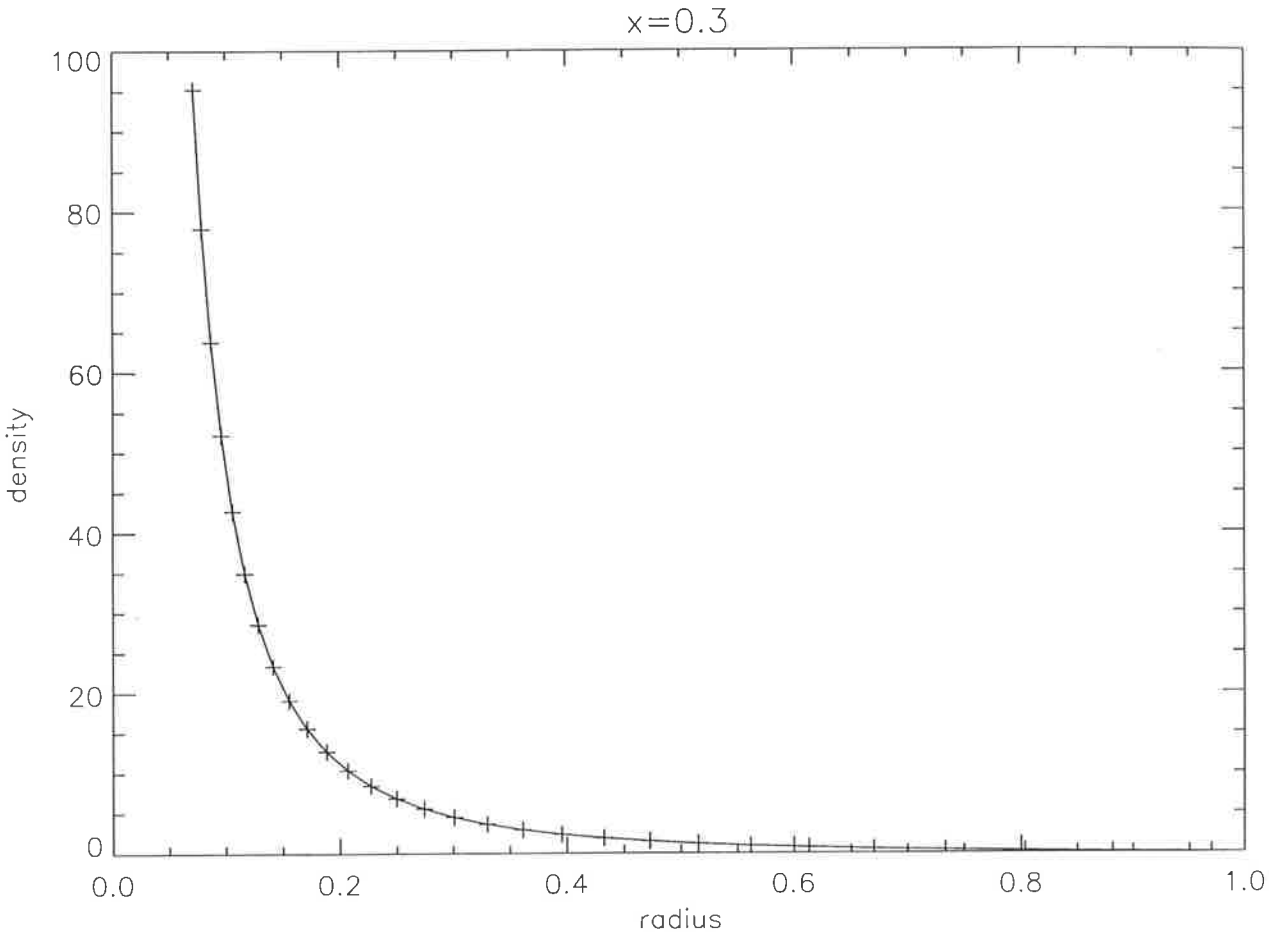

Figure 3.1: The density profile of the trial solution with $a = 0$ and $x = 0.3$

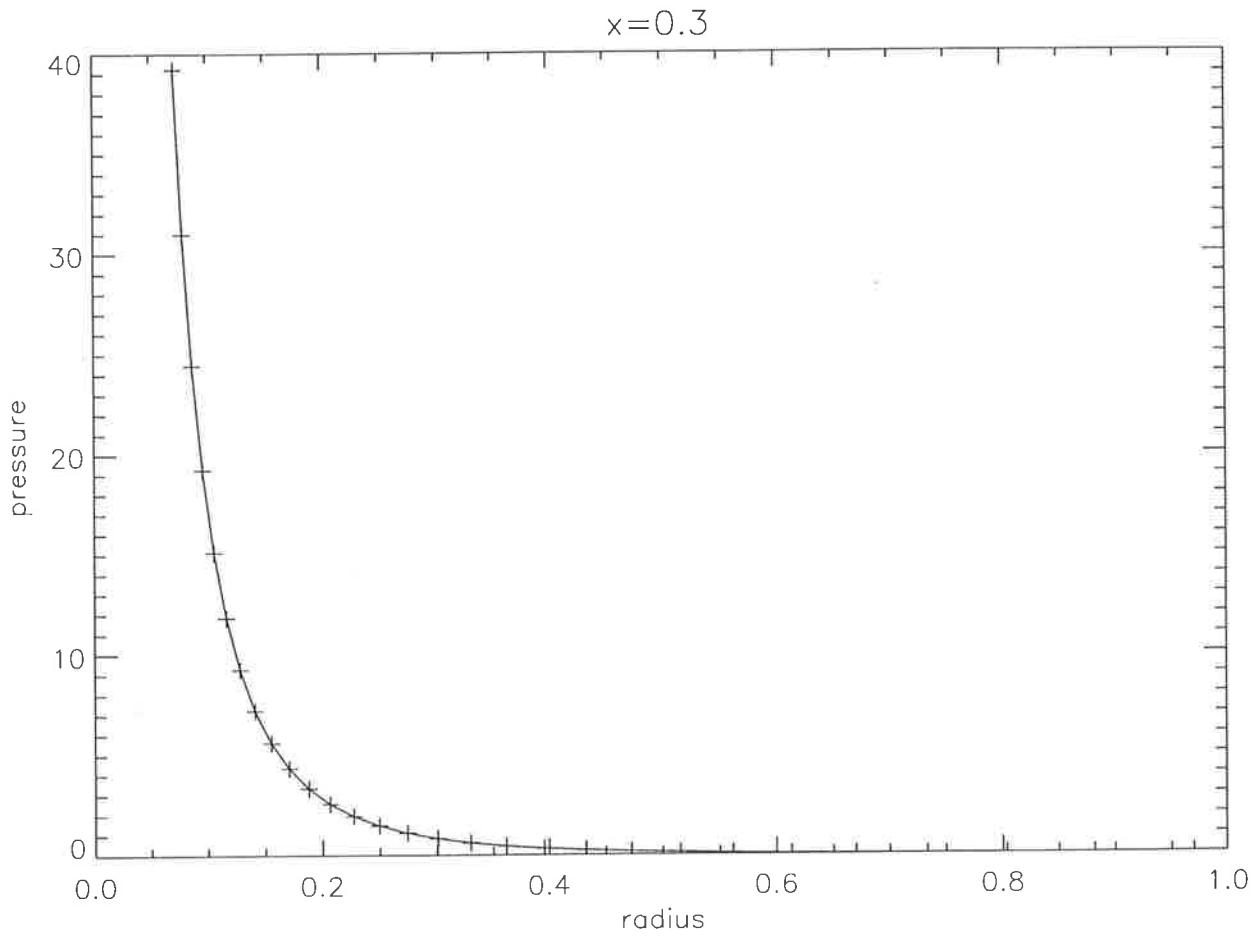

Figure 3.2: The pressure profile of the trial solution with $a = 0$ and $x = 0.3$

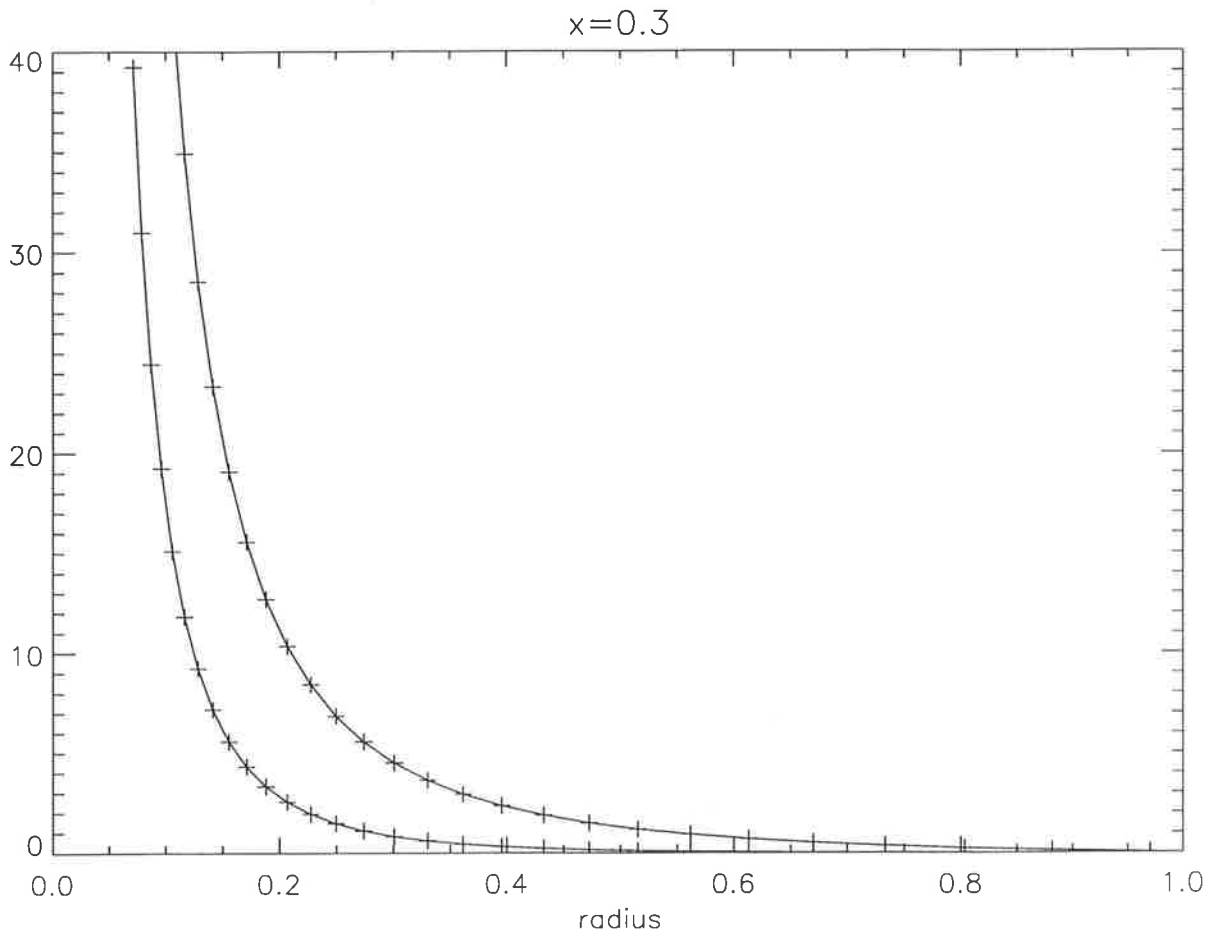

Figure 3.3: Combined density and pressure profiles of the trial solution with $a = 0$ and $x = 0.3$

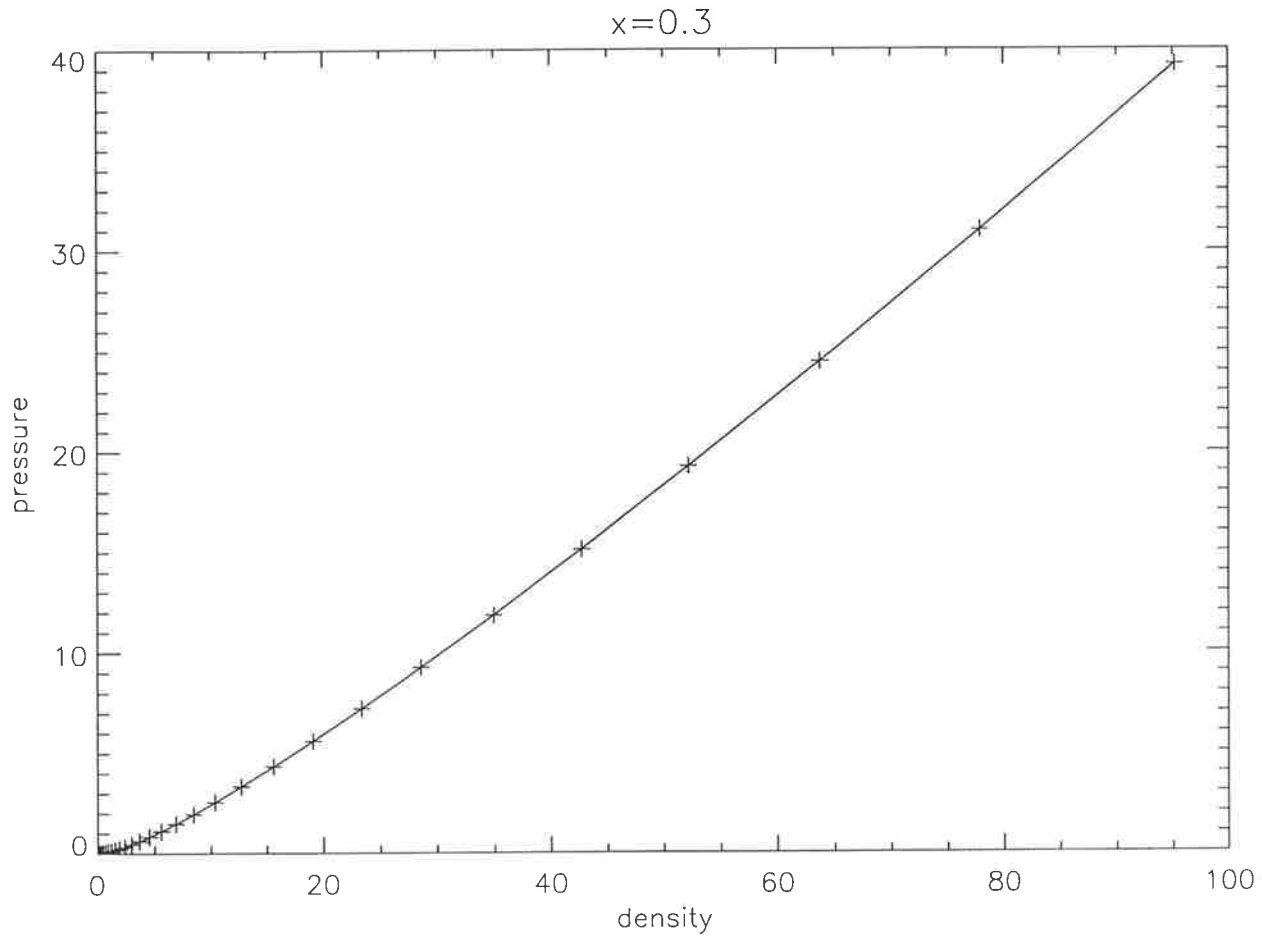

Figure 3.4: Pressure as a function of density for the trial solution with $a = 0$ and $x = 0.3$

Chapter 4

Rigidly rotating perfect fluids

4.1 Introduction

The previous chapters have concentrated on a particular procedure for obtaining stationary axisymmetric solutions to Einstein's field equations. Though the generalized Newman-Janis algorithm is a promising procedure for obtaining "physically reasonable" perfect fluid solutions to Einstein's field equations the results are not conclusive. In this chapter the general properties of stationary axisymmetric spacetimes representing rigidly rotating perfect fluids will be examined in detail, without reference to any "trick" in order to generate them. The disadvantage of this approach is that the resulting metric consists of three unknown functions of two variables ($g_{t\phi}, g_{\phi\phi}$ and $g_{xx} = g_{zz}$) and one unknown single variable function $F(x)$. By comparison the Newman-Janis algorithm generated a stationary axisymmetric metric with two single variable functions, $j(r)$ and $k(r)$. Even the generalized Newman-Janis algorithm simplified matters significantly by producing a stationary axisymmetric metric dependent on a single double variable function $\rho(r, \theta)$ and two single variable functions $d(r)$ and $e(r)$. The disadvantage of the GNJA is that does not necessarily generate a perfect fluid solution to Einstein's field equations even if "seed" solution is a perfect fluid.

In some sense the solving Einstein's field equations is a like a one-way membrane. To Determine the physical properties of a spacetime first the Einstein tensor must be derived from the metric tensor. Physical properties are deduced by equating the Einstein

tensor with the stress-energy tensor. The stress-energy tensor described by any metric is not necessarily physically realizable object. Ideally one hopes to perform the process in reverse, determine the metric from the the stress-energy tensor. Unfortunately except in the highly symmetric cases such as Schwarzschild and interior Schwarzschild solutions the task is extremely difficult. For this reason the relationship between the metric tensor and the Einstein tensor is like a one-way membrane. It is trivial to calculate the Einstein tensor from the metric but it is highly non-trivial to calculate the metric from the Einstein tensor. This phenomenon is not just confined to relativity, it is direct consequence of the fact that while it is a simple to differentiate a function it is in general much more difficult to integrate it.

In this chapter the particular class of stationary axisymmetric (SAS) metrics tensors which describe the geometry of a rigidly rotating perfect fluid are examined. The term rigidly rotating refers to the fact that the fluid is shear-free. Shear-free perfect fluids are studied because they are the ideal case for the interior of astrophysical objects such as a neutron stars.

Following the introduction a definition of stationary axisymmetric spacetimes is given. Using this definition a number of theorems are obtained for rigidly rotating perfect fluids. It is then shown section 4.2 that a rotation may be made which aligns the vorticity vector ω^μ in the $\hat{z}$ direction, simplifying the canonical form of the SAS metric. Section 4.3 suggests how the alignment of the vorticity vector leads naturally to a definition of centrifing force in General Relativity.

4.2 Some theorems

The particular class of spacetimes examined are assumed to have the following property [64]

1. The spacetimes are stationary and axisymmetric, which simply means that their exists a set of coordinates $x^0 = t, x^1, x^2, x^3 = \phi$ for which the metric tensor is independent of t and ϕ. In other words the spacetime admits a global 2-dimensional abelian group of isometries, t trajectories are in the real line $\mathcal{R}$, ϕ trajectories are circles $\mathcal{S}^1$.

A number of theorems can be proven when examining such a class of spacetimes;

Theorem 4 *: The canonical form of non-singular metrics describing stationary axisymmetric spacetimes with a two-surface orthogonal* (Σ_2) *to the group of orbits is*

$$ds^2 = e^{2\nu}dt^2 + e^{2\psi}(d\phi - \omega dt)^2 + e^{2\mu}(dx^2 + dz^2) \quad . \tag{4.2.1}$$

Proof Originally formulated by Lewis [70] and Papapetrou [71] [72], a more modern version can be found in [73]. The essence of the proof is as follows. It was stated at the start of this chapter that stationary axisymmetric metrics would be concentrated on, in which case the line element is given by

$$ds^2 = g_{\mu\nu}(x^1, x^2)dx^\mu dx^\nu \quad . \tag{4.2.2}$$

The coordinates may be labeled as $x^\alpha = \{t, x^1, x^2, \phi\}$ so that each metric coefficient is a function of x^1 and x^2 only. It is well known [74] that any metric in a three dimensional space can be written in a diagonal from. Consequently a time slice $(dt = 0)$ of the above line element may be written as

$$dl^2 = g_{ij}(x^1, x^2)dx^i dx^j \quad , \tag{4.2.3}$$

where $i, j = 1 \ldots 3$ and $g_{ij}(x^1, x^2) = 0$ if $i \neq j$. Furthermore two dimensions the spacetime is conformally flat [74]. That is if $dt = d\phi = 0$ then

$$d\sigma^2 = e^{2\mu}\left((dx^1)^2 + (dx^2)^2\right) \quad . \tag{4.2.4}$$

Hence the combination of equations 4.2.3 and 4.2.4 enable one to express the stationary axisymmetric line element as

$$ds^2 = g_{t\nu}(x^1, x^2)dtdx^\nu + e^{2\mu}\left((dx^1)^2 + (dx^2)^2\right) + g_{\phi\phi}(x^1, x^2)d\phi^2 \quad . \tag{4.2.5}$$

Further simplification may be made if one recognizes the symmetry in the t and ϕ coordinates, the form of the line element should be the same whether $dt = 0$ or $d\phi = 0$. As the three dimensional metric $(d\phi = 0)$ is diagonal,

$$g_{tx^1}(x^1, x^2) = g_{tx^2}(x^1, x^2) = 0 \quad .$$

Which gives the canonical form of a stationary axisymmetric metric as :

$$ds^2 = g_{tt}(x^1, x^2)dt^2 + 2g_{t\phi}(x^1, x^2)dtd\phi + e^{2\mu}\left((dx^1)^2 + (dx^2)^2\right) + g_{\phi\phi}(x^1, x^2)d\phi^2 \quad . \tag{4.2.6}$$

By making the following definitions,

$$g_{tt} \equiv -e^{2\nu} - \omega^2 e^{2\psi}; \quad g_{t\phi} \equiv -\omega e^{\psi}; \quad g_{\phi\phi} \equiv e^{2\psi} \quad , \tag{4.2.7}$$

and assigning the coordinates x^1 and x^2 to be x and z respectively, the metric is that of 4.2.1. □

As the determinate of the two dimensional (t, ϕ) slice of 4.2.6 is always negative

$$g_{tt}g_{\phi\phi} - g_{t\phi}^2 = -y^2 \quad . \tag{4.2.8}$$

The importance of y comes in the vacuum case where on the two dimensional surface Σ_2 the quantity x satisfies the Laplace equation

$$\left(\partial^A y\right);_A = 0 \quad . \tag{4.2.9}$$

Hence y is harmonic in Σ_2, furthermore as y has no saddle points [73] it can be taken as coordinate, $y = x$. Defining $\partial_A z$ to be orthogonal to $\partial_A x$ the z can be taken as another coordinate so

$$ds_\Sigma^2 = e^{2\mu}(dx^2 + dz^2) \quad . \tag{4.2.10}$$

In the vacuum case where x is defined by 4.2.8 then g_{tt} expressed in terms of $g_{t\phi}$ and $g_{\phi\phi}$,

$$g_{tt} = \frac{-x^2 - g_{t\phi}^2}{g_{\phi\phi}} = -x^2 e^{-2\psi} + \omega^2 e^{2\psi} \quad . \tag{4.2.11}$$

Theorem 5 *: The four velocity of a perfect fluid in a stationary axisymmetric metric written in canonical is*

$$u^\alpha = A(x, z)(\delta_t^\alpha + \Omega(x, z)\delta_\phi^\alpha) \qquad u^\alpha u_\alpha = -1 \quad . \tag{4.2.12}$$

Proof: The Einstein tensor generated by 4.2.6 has components $G^{tx} = G^{tz} = 0$. As the Einstein tensor describes a perfect fluid

$$G^{\alpha\beta} = T^{\alpha\beta} = (\varrho + P)u^\alpha u^\beta + Pg^{\alpha\beta} \quad , \tag{4.2.13}$$

and since $g^{tx} = g^{tz} = 0$, the T^{tx} and T^{tz} vanish if and only if $u^x = u^z = 0$ or $P + \varrho = 0$. Only perfect fluids with positive density and pressure are considered, so without loss of generality the four velocity of the fluid is given by equation 4.2.12 □.

Theorem 6 :

$$P_{,\alpha}\, u^\alpha = \varrho_{,\alpha}\, u^\alpha = u_{\beta,\alpha}\, u^\alpha = g_{\alpha\beta,\gamma} u^\gamma = 0 \tag{4.2.14}$$

Proof: Follows directly from Theorems 1 and 2.

In order to describe a congruence of curves it is most useful to examine the expansion, shear, and rotation. These quantities each have a very clear physical meaning. Imagine an observer moving with the fluid draws a sphere around themselves encapsulating part of the fluid and then watches how this sphere evolves with time. The expansion measures how much the volume has expanded, the shear how much it is distorted, and the rotation how much it is twisted, at some later stage $d\tau$. This is represented diagrammatically in figure 4.1.

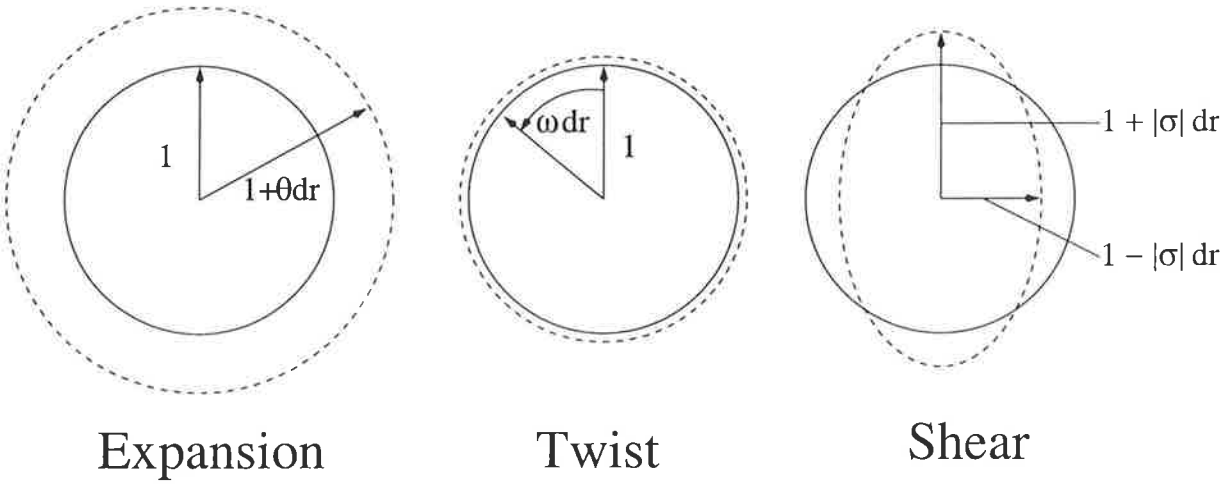

Figure 4.1: The optical scalars

The evaluation of these quantities requires a calculation of the rate of change three orthogonal spacelike vectors. Any vector v^α can be decomposed into its timelike and spacelike components. The time-projection tensor is

$$P_t(v^\alpha) = -u_\alpha u_\beta v^\beta \quad ,$$

the space-projection tensor is

$$P_\Sigma(v^\alpha) = h_{\alpha\beta}v^\beta \quad ,$$

where

$$h_{\alpha\beta} \equiv g_{\alpha\beta} + u_\alpha u_\beta \quad . \tag{4.2.15}$$

With these definitions the spacetime interval can be rewritten as

$$ds^2 = h_{\alpha\beta}dx^\alpha dx^\beta - u_\alpha u_\beta dx^\alpha dx^\beta \quad .$$

Hence an observer comoving with the fluid measure the spatial distance between two events as

$$dl^2 = h_{\alpha\beta}dx^\alpha dx^\beta \quad ,$$

and the time interval as :

$$d\tau^2 = -u_\alpha u_\beta dx^\alpha dx^\beta \quad .$$

Theorem 7 *: The fluid is expansionless.*

Proof: Expansion Θ is a measure of how quickly the volume is expanding and is given by the equation

$$\begin{aligned}
\Theta &\equiv u^\alpha{}_{;\alpha} \quad . \\
\Theta &= u^\alpha{}_{;\alpha} \quad , \\
&= u^\alpha{}_{,\alpha} + \Gamma^\alpha_{\alpha\gamma}u^\gamma \quad , \\
&= u^\alpha{}_{,\alpha} + \frac{1}{2}g^{\alpha\sigma}g_{\alpha\sigma,\gamma}\,u^\gamma \quad , \\
&= 0 \qquad\qquad \Box \quad . \qquad\qquad \text{Theorem 3}
\end{aligned}$$

Theorem 8 *: The fluid is rigidly rotating (shear-free) if and only if Ω is a constant.*

Proof: Shear is a symmetric traceless tensor measuring difference in length of each principle axis minus expansion. It is given by the expression

$$\begin{aligned}
\sigma_{\mu\nu} &\equiv \left[u_{(\alpha;\beta)} - \frac{1}{3}\Theta h_{\alpha\beta}\right] h^\alpha_\mu h^\beta_\nu \quad , \\
&= \left[\frac{1}{2}(u_{\mu;\nu} + u_{\nu;\mu}) - \frac{1}{3}\Theta h_{\alpha\beta}\right] \quad .
\end{aligned}$$

As the fluid is expansionless (Theorem 7)

$$\sigma_{\mu\nu} = u_{(\mu;\nu)} + a_{(\mu}u_{\nu)} \quad ,$$

where a_ν is the acceleration,

$$a_\mu \equiv u_{\mu;\nu}u^\nu \quad . \tag{4.2.16}$$

Aside 1:

$$\begin{aligned} u_{(\mu;\nu)} &= u_{(\mu,\nu)} - \Gamma^\gamma_{\mu\nu}u_\gamma \quad , \\ &= u_{(\mu,\nu)} - \frac{1}{2}g^{\gamma\sigma}\left(g_{\sigma(\mu,\nu)} + g_{\sigma(\nu,\mu)} - g_{(\mu\nu),\sigma}\right)u_\gamma \quad , \\ &= u_{(\mu,\nu)} - u^\sigma g_{\sigma(\mu,\nu)} \qquad \text{From Theorem 3} \quad . \end{aligned}$$

Now

$$\begin{aligned} u_{(\mu,\nu)} &= \left(u^\sigma g_{\sigma(\mu}\right)_{,\nu)} \quad , \\ &= u^\sigma g_{\sigma(\mu,\nu)} + u^\sigma{}_{,(\mu}\, g_{\nu)\sigma} \quad , \\ u_{(\mu,\nu)} - u^\sigma g_{\sigma(\mu,\nu)} &= u^\sigma{}_{,(\mu}\, g_{\nu)\sigma} \quad , \end{aligned}$$

so

$$u_{(\mu;\nu)} = u_{\mu,\nu} - u^\sigma{}_{,(\mu}\, g_{\nu)\sigma} \quad .$$

Aside 2:

$$\begin{aligned} a_\mu &\equiv u_{\mu;\sigma}u^\sigma \quad , \\ &= \left(u_{(\mu,\sigma)} - \Gamma^\gamma_{\mu\sigma}u_\gamma\right)u^\sigma \quad , \\ &= \frac{-1}{2}g_{\chi\sigma,\mu}u^\chi u^\sigma \quad , \end{aligned}$$

note that

$$\left(g_{\chi\sigma}u^\chi u^\sigma\right)_{,\mu} = g_{\chi\sigma,\mu}u^\chi u^\sigma + 2u_\sigma u^\sigma_{,\mu} = 0 \quad ,$$

therefore

$$a_\mu = u_\sigma u^\sigma_{,\mu} \quad . \tag{4.2.17}$$

Hence

$$\begin{aligned} \sigma_{\mu\nu} &= u^\sigma{}_{,(\mu}\, g_{\nu)\sigma} + u_\sigma u^\sigma_{,(\mu}u_{\nu)} \quad , \\ &= u^t{}_{,(\mu}\, g_{\nu)t} + u^\phi{}_{,(\mu}\, g_{\nu)\phi} + u_t u^t_{,(\mu}u_{\nu)} + u_\phi u^\phi_{,(\mu}u_{\nu)} \quad . \end{aligned} \tag{4.2.18}$$

Using the fact the u^μ is a timelike vector, $u_\mu u^\mu = -1$,

$$u_\phi = \frac{-1 - Au_t}{A\Omega} \,. \tag{4.2.19}$$

The only non-vanishing components of the shear tensor are

$$\begin{aligned}
\sigma_{tx} &= u^t{}_{,x}\, g_{tt} + u^\phi{}_{,x}\, g_{t\phi} + u_t u^t_{,x} u_t + u_\phi u^\phi_{,x} u_t \quad , \\
&= A_{,x}\left(g_{tt} + \Omega g_{t\phi} + \Omega u_t u_\phi + u_t^2\right) + A\Omega_{,x}\left(g_{t\phi} + u_t u_\phi\right) \quad , \\
&= A\Omega_{,x}\left(g_{t\phi} + u_t u_\phi\right) \quad . \qquad \text{Using 4.2.19 and } \; u_t = A(g_{tt} + \Omega g_{t\phi})
\end{aligned}$$

In a similar manner it can be shown that

$$\begin{aligned}
\sigma_{tz} &= A\Omega_{,z}\left(g_{t\phi} + u_t u_\phi\right) \quad , \\
\sigma_{x\phi} &= A\Omega_{,x}\left(g_{\phi\phi} + u_\phi u_\phi\right) \quad , \\
\sigma_{z\phi} &= A\Omega_{,z}\left(g_{\phi\phi} + u_\phi u_\phi\right) \quad .
\end{aligned}$$

The signature of the metric was chosen so that $g_{\phi\phi} > 0$, 4.2.6 hence $\sigma_{x\phi} = \sigma_{z\phi} = 0$ if and only if Ω is a constant. If A is a constant then $\sigma_{tx} = \sigma_{tz} = 0$ □.

Theorem 9 *: If the fluid is rigidly rotating then the acceleration (deviation from geodesics motion) depends only on the covariant derivative of A and is given by*

$$a_\mu = \frac{-A_{,\mu}}{A} \tag{4.2.20}$$

Proof:

$$\begin{aligned}
a_\mu &\equiv u_{\mu;\nu} u^\nu \quad , \\
&= u_\nu u^\nu_{,\mu} \qquad \text{using equation 4.2.17} \quad , \\
&= A_{,\alpha}(u_t + \Omega u_\phi) \quad , \\
&= \frac{-A_{,\mu}}{A} \quad . \qquad \text{using equation 4.2.19} \qquad \square
\end{aligned}$$

Theorem 10 *: If their exists an equation of state such that $\varrho = \varrho(P)$ and the fluid is rigidly rotating then*

$$A(x,z) = A(P) = A(0)\exp\int_0^P \frac{dP'}{\varrho'(P') + P'}. \tag{4.2.21}$$

Proof: Original work done by Boyer [64]. From the Bianchi idenities

$$\begin{aligned} T^{\nu}_{\mu};_{\nu} &= \{(P+\varrho)u_\mu u^\nu + \delta^\nu_\mu P\};_\nu = 0 \quad , \\ &= (P+\varrho),_\nu u_\mu u^\nu + (P+\varrho)u_{\mu;\nu}u^\nu + (P+\varrho)u_\mu u^\nu;_\nu + P,_\mu = 0 \quad , \\ &= (P+\varrho)a_\mu + P,_\mu = 0 \quad , \qquad \text{from theorems 3 and 4} \\ &= -(P+\varrho)\frac{A,_\mu}{A} + P,_\mu = 0 \quad . \qquad \text{using equation 4.2.20} \end{aligned}$$

With this equation we begin to understand why the problem of rotation in General Relativity is such a difficult one to solve. In static limit $\Omega = 0$ and $A = g_{tt}$ which is a function of the single coordinate r. Furthermore g_{tt} can be related to the mass of the body by equating G^0_0 and T^0_0. In axisymmetric systems this is not so easily done. With the help of the above equation, A may be written in terms of pressure and density rather than coordinates,

$$\begin{aligned} (P+\varrho)\frac{A,_\mu}{A} &= P,_\mu \quad , \\ \log A &= \int \frac{dP'}{\varrho(P')+P'} + C \quad , \\ A(P) &= A(0)\exp\int_0^P \frac{dP'}{\varrho(P')+P'} \quad . \end{aligned}$$

□

The rotation tensor measures the twist of a vector field. For a congruence of curves u_μ the rotation tensor is

$$\begin{aligned} \omega_{\mu\nu} &= u_{[\alpha;\beta]}h^\alpha_\mu h^\beta_\nu \quad , \\ &= \frac{1}{2}(u_{\mu;\nu} - u_{\nu;\mu}). \end{aligned} \tag{4.2.22}$$

Theorem 11 *: If the fluid is shear-free then the rotation is proportion to the antisymmetric derivative of a Killing vector* $k_\mu = \delta^\mu_t + \Omega\,\delta^m u_\Phi$,

$$\omega_{\alpha\nu} = Ak_{[\mu,\nu]} \quad . \tag{4.2.23}$$

Proof: In the same manner as the proof of Theorem 8 we find that

$$\omega_{\mu\nu} = u_{[\mu;\nu]} - a_{[\mu}u_{\nu]}.$$

The four velocity of the fluid is $u^\mu = A\left(k^\mu_t + \Omega k^m_\phi u\right)$, where k^μ_t and k^μ_ϕ are the time like and spacelike Killing vectors respectively. As fluid is shear-free Ω is constant, which means

that u^μ is proportional to the Killing vector $k^\mu = k_t^\mu + \Omega k_\phi^\mu$. The above equation becomes,

$$\begin{aligned} &= \left(Ak_{[\mu}\right)_{;\nu]} + \frac{A_{,[\mu}Ak_{\nu]}}{A} \quad , \\ &= A_{,[\nu}k_{\mu]} + Ak_{[\mu;\nu]} + A_{,[\mu}k_{\nu]} \quad , \\ &= Ak_{[\mu;\nu]} \quad , \\ &= Ak_{[\mu,\nu]} \quad . \qquad \square \end{aligned}$$

The vorticity pseudo-vector is the antisymmetric contraction of the rotation tensor with the fluid 4-velocity

$$\omega^\alpha \equiv \frac{1}{2}\eta^{\alpha\nu\mu\nu}u_\beta\omega_{\mu\nu} \quad .$$

The Levi-Cevita pseudo-tensor is

$$\eta^{\alpha\beta\mu\nu} \equiv -\frac{1}{\sqrt{g}}\epsilon^{\alpha\beta\mu\nu} \quad ,$$

where $\epsilon^{\alpha\beta\mu\nu}$ equals $+1$ for even permutations of $(0,1,2,3)$ -1 for odd ones, and $\epsilon^{\alpha\beta\mu\nu} \equiv 0$ if an index is repeated.

4.3 Spin allignment

It was shown in the previous section that the vorticity tensor is given by equation 4.2.23. For the a stationary axisymmetric metric this corresponds to

$$\omega_{\mu\nu} = A\begin{pmatrix} 0 & \frac{1}{2}(g_{tt}+\Omega g_{\phi t})_{,x} & \frac{1}{2}(g_{tt}+\Omega g_{\phi t})_{,z} & 0 \\ \# & 0 & 0 & -\frac{1}{2}(g_{t\phi}+\Omega g_{\phi\phi})_{,x} \\ \# & \# & 0 & -\frac{1}{2}(g_{t\phi}+\Omega g_{\phi\phi})_{,z} \\ \# & \# & \# & 0 \end{pmatrix}. \qquad (4.3.1)$$

As the rotation tensor is antisymmetric the notation "#" is used to indicate $\omega_{\mu\nu} = -\omega_{\nu\mu}$. Components of the vorticity pseudo-vector are

$$\begin{aligned} \omega^t &= \frac{1}{2}\eta^{t\beta\nu\mu}u_\beta w_{\mu\nu} \quad , \\ &= \frac{1}{2}\eta^{t\phi\nu\mu}u_\phi\omega_{\mu\nu} \quad , \\ &= 0 \qquad\qquad\qquad\qquad \text{as } \omega_{xz} = 0 \quad . \end{aligned}$$

$$
\begin{aligned}
\omega^x &= \frac{1}{2}\eta^{x\beta\nu\mu}u_\beta w_{\mu\nu} \quad , \\
&= \frac{1}{2}\eta^{xt\nu\mu}u_t w_{\mu\nu} + \frac{1}{2}\eta^{x\phi\nu\mu}u_\phi w_{\mu\nu} \quad , \\
&= \eta^{xtz\phi}u_t w_{z\phi} + \eta^{x\phi tz}u_\phi w_{tz} \quad , \\
&= \frac{-A}{\sqrt{-g}}\left(u_t\frac{1}{2}(g_{t\phi}+\Omega g_{\phi\phi})_{,z} - u_\phi\frac{1}{2}(g_{tt}+\Omega g_{\phi t})_{,z}\right) \quad , \\
&= \frac{-A^2}{2\sqrt{-g}}\left((g_{tt}+\Omega g_{t\phi})(g_{t\phi}+\Omega g_{\phi\phi})_{,z} - (g_{t\phi}+\Omega g_{\phi\phi})(g_{tt}+\Omega g_{\phi t})_{,z}\right) \quad . \qquad (4.3.2) \\
\omega^z &= \frac{1}{2}\eta^{z\beta\nu\mu}u_\beta w_{\mu\nu} \quad , \\
&= \frac{1}{2}\eta^{zt\nu\mu}u_t w_{\mu\nu} + \frac{1}{2}\eta^{z\phi\nu\mu}u_\phi w_{\mu\nu} \quad , \\
&= \eta^{ztx\phi}u_t w_{x\phi} + \eta^{z\phi tx}u_\phi w_{tx} \quad , \\
&= \frac{-A}{\sqrt{-g}}\left(-u_t\frac{1}{2}(g_{t\phi}+\Omega g_{\phi\phi})_{,x} + u_\phi\frac{1}{2}(g_{tt}+\Omega g_{\phi t})_{,x}\right) \quad , \\
&= \frac{-A^2}{2\sqrt{-g}}\left(-(g_{tt}+\Omega g_{t\phi})(g_{t\phi}+\Omega g_{\phi\phi})_{,x} + (g_{t\phi}+\Omega g_{\phi\phi})(g_{tt}+\Omega g_{\phi t})_{,x}\right) \qquad (4.3.3) \\
\omega^\phi &= \frac{1}{2}\eta^{\phi\beta\nu\mu}u_\beta w_{\mu\nu} \quad , \\
&= \frac{1}{2}\eta^{\phi t\nu\mu}u_t \omega_{\mu\nu} \quad , \\
&= 0 \quad . \qquad\qquad\qquad \text{as } \omega_{xz} = 0
\end{aligned}
$$

It is always possible to make a rotation $\chi^\alpha = a^\alpha_\beta\,\chi^\beta$ in three space about the $\hat{\phi}$ axis that leaves the form of the line element unchanged but alligns the angular momentum w^μ with the z axis. The vanishing of ω^x requires that

$$
\begin{aligned}
(g_{tt}+\Omega g_{t\phi})(g_{t\phi}+\Omega g_{\phi\phi})_{,z} &- (g_{t\phi}+\Omega g_{\phi\phi})(g_{tt}+\Omega g_{\phi t})_{,z} = 0 \quad , \\
\frac{(g_{t\phi}+\Omega g_{\phi\phi})_{,z}}{g_{t\phi}+\Omega g_{\phi\phi}} &= \frac{(g_{tt}+\Omega g_{\phi t})_{,z}}{g_{tt}+\Omega g_{t\phi}}, \quad \text{If } g_{tt}+\Omega g_{\phi t} \neq 0 \text{ and } g_{t\phi}+\Omega g_{\phi\phi} \neq 0 \quad , \\
\frac{\partial \log(g_{t\phi}+\Omega g_{\phi\phi})}{\partial z} &= \frac{\partial \log(g_{tt}+\Omega g_{t\phi})}{\partial z} \quad , \\
\log(g_{t\phi}+\Omega g_{\phi\phi}) &= \log(g_{tt}+\Omega g_{t\phi}) + f(x) \quad ,
\end{aligned}
$$

$$g_{t\phi} + \Omega g_{\phi\phi} = F(x)(g_{tt} + \Omega g_{t\phi}) \qquad F(x) = \exp f(x) \quad ,$$
$$F(x) = \frac{g_{t\phi} + \Omega g_{\phi\phi}}{g_{tt} + \Omega g_{t\phi}} \quad . \tag{4.3.4}$$

The advantage of this is that if the axis of rotation is aligned in the $\hat{z}$ direction then g_{tt} can be expressed in terms of $g_{t\phi}, g_{\phi\phi}$ and the single variable function $F(x)$. In Newtonian physics ω^i represents the angular velocity of the fluid. In the flat spacetime limit ($u_\mu = \delta^0_\mu$but $u_{\beta,\mu} \neq 0$) of the vorticity vector is

$$\omega^i \approx \frac{1}{2}\eta^{i0kl}u_{k,l} = \frac{1}{2}\left(\frac{\partial u_l}{\partial x^k} - \frac{\partial u_k}{\partial x^l}\right) \quad .$$

This is the curl of the velocity vector in Newtonian mechanics,

$$\vec{\omega} = \frac{1}{2}\vec{\nabla} \times \vec{v} \quad .$$

4.4 Relativistic centrifugal force

Centrifugal force in Newtonian physics is the component of the net force in the direction perpendicular to its motion. It is called centrifugal as it forces trajectories change direction without affecting the speed. In the context of rigidly rotating fluids the centrifugal force is that which provides angular velocity to the fluid.

Though there is no concept of a gravitational force in general relativity it is possible to introduce one and compare the result of relativity with Newtonian physics. One of the major themes of this work is the comparison between relativistic points of view and a Newtonian ones. In order to make the comparison more complete it would help to introduce the notion of centrifugal force in a relativistic context. This can be done quite naturally, as is about to be shown.

The key difference between a Newtonian approach and one of Relativity is that of geometry. A Newtonian arguments are often is very coordinate dependent. Consider for example the Newtonian version of a rigidly rotating perfect fluid.

Assuming that pressure and density are related by an equation of state, $\varrho = \varrho(P)$. If surfaces of constant pressure and density are described by the equation $S(x, z) = 0$. The

net force, which is the sum of the force due to pressure dF_μ and gravity, dF_y provides a centrifuzal force which makes the fluid have circular motion.

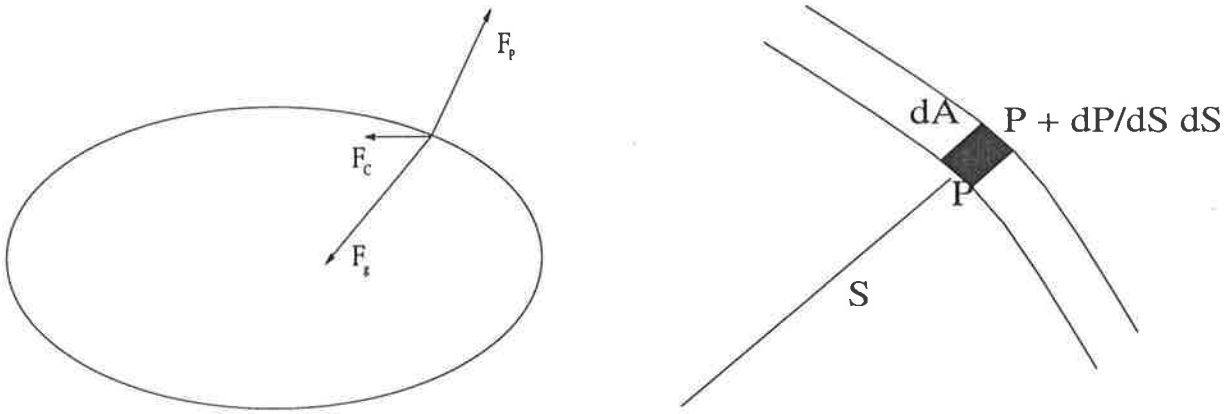

Figure 4.2: Centrifugal force

The surface of revolution is determined by equating the nett force with the centrifugal force.

$$d\vec{F}_p + d\vec{F}_g = -dm\Omega^2 x \quad .$$

The pressure component is

$$\begin{aligned} d\vec{F}_p &= \left(PdA - (P + \frac{dP}{dS}dS)dA \right) \hat{S} \quad , \\ &= -\frac{dP}{dS}dV\hat{S} \quad , \\ &= -\frac{dP}{dS}\frac{dm}{\varrho}\hat{S} \quad . \end{aligned} \tag{4.4.1}$$

The gravitational part dF_g has much more complicated to calculate. The evaluation of dF_g requires the integraing mass distribution over the shape of the star. This rather arduous tasks is the subject of a book by Chrandrasekhar [75] and will not discussed to much further here. Though the physics is rather simply the mathematics is not. Such solutions generally involve hyperbolic and elliptic functions.

In general relativity these methods are not applicable as there is no notion of force. All that can said is that fluid flows in a congruence of curves satisfying 4.2.16. Despite this, a natural relativistic generalization of centrifugal forces will be introduced.

The basic idea comes from the alignment of the vorticity vector in the $\hat{z}$ direction. As the vorticity vector only has components in the $\hat{z}$ direction our definiation of centrifugal force should have components in the $\hat{x}$ direction only. The relativistic generalization of forces should be of the form.

$$\vec{F_P} + \vec{F_g} = \vec{F_c} \quad .$$

To see how this can be done let us recall equation 4.2.16, which tells how to relate the rate of change in pressure to the acceleration,

$$\frac{-P_{,\mu}}{P+\varrho} = a_\mu \quad .$$

The plan is to manipulate this equation so that the centrifugal force depends only on x.

$$\begin{aligned}
\frac{-P_{,\mu}}{P+\varrho} &= \frac{-1}{2} g_{\mu\nu,\mu} u^\mu u^\nu \quad , \qquad \text{Aside 2: Theorem 5} \\
&= \frac{-1}{2} A^2 \left(g_{tt} + 2\Omega g_{t\phi} + \Omega^2 g_{\phi\phi} \right)_{,\mu} \quad , \\
&= -\frac{1}{2} A^2 \left(g_{tt} + \Omega g_{t\phi} + \Omega (g_{t\phi} + \Omega g_{\phi\phi}) \right)_{,\mu} \quad , \\
&= -\frac{1}{2} A^2 \left((g_{tt} + \Omega g_{t\phi}) (1 + \Omega F(x)) \right)_{,\mu} \quad .
\end{aligned}$$

As the fluid velocity is timelike $u_\mu u^\mu = -1$ which means that

$$\begin{aligned}
A^2 &= \frac{-1}{g_{tt} + 2\Omega g_{t\phi} + \Omega^2 g_{\phi\phi}} \\
&= (g_{tt} + \Omega g_{t\phi}) (1 + \Omega F(x)) \qquad (4.4.2)
\end{aligned}$$

so that

$$\begin{aligned}
\frac{-P_{,\mu}}{P+\varrho} &= -\frac{1}{2} \left[\frac{(g_{tt} + \Omega g_{t\phi})_{,\mu}}{g_{tt} + \Omega g_{t\phi}} + \frac{\Omega F(x)_{,\mu}}{1 + \Omega F(x)} \right] \quad , \\
\frac{-P_{,\mu}}{(P+\varrho)} &+ \frac{1}{2} \frac{(g_{tt} + \Omega g_{t\phi})_{,\mu}}{g_{tt} + \Omega g_{t\phi}} = -\frac{1}{2} \frac{\Omega F(x)_{,\mu}}{1 + \Omega F(x)} \quad , \qquad (4.4.3) \\
\vec{F}_p &+ \vec{F}_g = \vec{F}_c
\end{aligned}$$

In Newtonian physics the left hand side of the above equation would represent the sum of forces due to pressure and gravity. The right hand side would be the centrifugal force. In

relativity rotation effects are seen as $g_{t\Phi}$ terms which vanish in the Newtonian limit. In the Newtonian limit $u^t \approx 1, g_{t\phi} \approx 0, g_{\phi\phi} \approx x^2, g_{tt} \approx$ so that

$$F(x) \approx \Omega x^2 / g_{tt} \quad , \tag{4.4.4}$$

resulting in

$$d\vec{F_c} \approx -\Omega^2 x \hat{x} \quad .$$

as expected.

4.5 Conclusion

This chapter has developed a number of Theorems regarding the general properties of stationary axisymmetric spacetimes describing rigidly rotating perfect fluid interiors. After deriving the canonical form of axisymmetric spacetimes it was shown that if these spacetimes where to perfect fluid interiors then the four velocity is given by 4.2.12. The congruence of curves defined by this four velocity is expansionless. The shear was shown to vanish if and only if Ω is constant. Both the acceleration and rotation tensor where shown to have in a particularly simple form for shear-free perfect fluids. Evaluation of the rotation tensor made it possible to provide further simplification of the canonical form of the metric tensor by alligning the vorticity vector in the $\hat{z}$ direction.

Lastly the notion of a relativistic centrifugal force was introduced. Though nothing specifically was calculated with it. It was deemed to be a handy tool in the examination of the physical properties of stationary axisymmetric spacetimes. Relativistic centrifugal force as introduced naturally as a consequence of alligning the vorticity vector in the $\hat{z}$ direction. The result of this chapter still leave a large amount of room for further study. It is not clear whether the simplification of made by the spin allignment will eventually result in a reduction of Einstein's equations to such a stage that they are solvable.

Chapter 5

Introduction to chaos

5.1 Deterministic chaos

Most people have a common sense notion of what chaos means. To the lay person the adjective chaotic describes behaviour utterly without order or arrangement. When physicist and mathematicians speak of deterministic chaos they are describing behaviour which is governed by a set rules but appears to be anarchic. It is a physicist inherent belief that nature is governed by a set of laws which are well defined, "God does not play dice". Though this quote by Einstein was referring to quantum mechanics it is equally suited to chaotic dynamics. Reconciliation between the often chaotic behaviour nature and the deterministic laws which describe it comes from the aptly subject of deterministic chaos. The theory is that apparently random behaviour is described by a sometimes surprisingly simple rules.

Before continuing further a distinction needs to be made between deterministic and indeterminstic chaos. At each stage of evolution of deterministic systems all relevant variables are recorded and the dependence on each other accounted for. Deterministic chaos is often found in systems consisting of three or more bodies. A classic example of how an understanding of deterministic chaos can be used to account for previously inexplicable observations it is found in the asteroid belt.

The asteroid belt is a group of asteroids in orbit between Mars and Jupiter. Within the asteroid belt their are regions of high and low density. Low density regions are known as

Kirkwood gaps the high density one the Hilda group. Kirkwood gaps occur in regions where the ratio of the period for an asteroid moving in uniform circular motion to that of Jupiter is 2:1, 3:1, 4:1, 5:2 and 7:2. The Hilda group clump is in 3:2 resonance with Jupiter. Using a simplified model consisting of the Sun, Jupiter and one asteroid Wisdom [76] discovered that asteroids in 3:1 resonance with Jupiter exhibit chaotic behaviour. These unpredictable trajectories cross the orbit of Mars and eventually collide with it ensuring that no asteroid survives an extended length of time in 3:1 resonance with Jupiter. In a similar manner the other Kirkwood gaps understood once the gravitational effect of Mars is incorporated.

The existence of Hilda group is element which is common to many chaotic systems, i.e., order within chaos. Bands of order are punctuated by disorder and vice versa. A full understanding of chaos is the determination of what regions are stable and which are chaotic.

Indeterministic systems are those in which all relevant variables can not be measured with sufficient accuracy and/or the dependence of each other is inadequately determined. The uncertainty of long term weather prediction is something which most people have experienced and is often termed chaotic. On reason for which the weather is unpredictable is because it depends too many variables measured accurately or to know precisely how they effect each other.

This work explores only deterministic chaos as it is by far the more interesting. Deterministic chaos tells us that some systems which are well defined by a rigorous set of rules have outcomes can not be predicted! The consequence in physics and other disciplines is far reaching. Evidently it is vital to know what can and can not be predicted.

Having present an intuitive notion of what chaos is it is an opportune moment to give a more formal one. Following the work of C.J. Thompson [77] systems will be termed chaotic if and only if they having the following properties.

- Motion is deterministic and bounded, but mostly aperiodic and irregular.

- There is extreme sensitivity on initial conditions leading to unpredictability.

- This behaviour is dense in some set but includes a (possibly infinite) subset of initial conditions giving rise to periodic or ordered behaviour.

It has been known for a long time that rather simple mathematical functions can produce very complicated shapes (e.g. fractals) and behaviour that appears to be irregular. When working on the Hills reduced model of the three–body problem, Henri Poincaré in describing the Poincaré section states:

> One is struck with the complexity of this figure that I am not even attempting to draw. Nothing can give us a better idea of the complexity of the three-body problem.

Motion described by simple deterministic equations can appear to behave in a random or chaotic manner. The study of chaos is an attempt to find an underlying set of rules and theories to help us find some order in this chaos and to determine when and if a system changes from being regular and well behaved to being chaotic. Not until the 60's with the advent of high-speed computing was it possible to look more deeply into this phenomena. The resurgence of chaos theory came in 1963 when E. N. Lorenz [78] was using a computer to study a simplified climate model. He noticed that the relevant equations exhibited irregular behaviour and extreme sensitivity on initial conditions. Since then much analytic and computational work has been done on a wide variety of chaotic systems. Some of this chaos theory will be reviewed as it is essential to an understanding of this work.

5.2 Attractors and attractor basins

Systems starting with entirely different initial configurations may end up in the same final state. This final state is called the attractor and the initial values which finish at this attractor are the attractor basin. Consider a set of values x and a map f which maps a point x_i in x to a new point $f(x_i)$ The kth mapping of the initial point x_i is denototed $f^k(x_i)$.

F is an attractor for f if $f(F) = F$ and

$$\lim_{k\to\infty} f^k(x_i) - F = 0 \ \forall\, x \ \in \ V_F.$$

$k \to \infty$ for all x in an open set V_F containing F. The Set V_F is called the basin of the attraction of F.

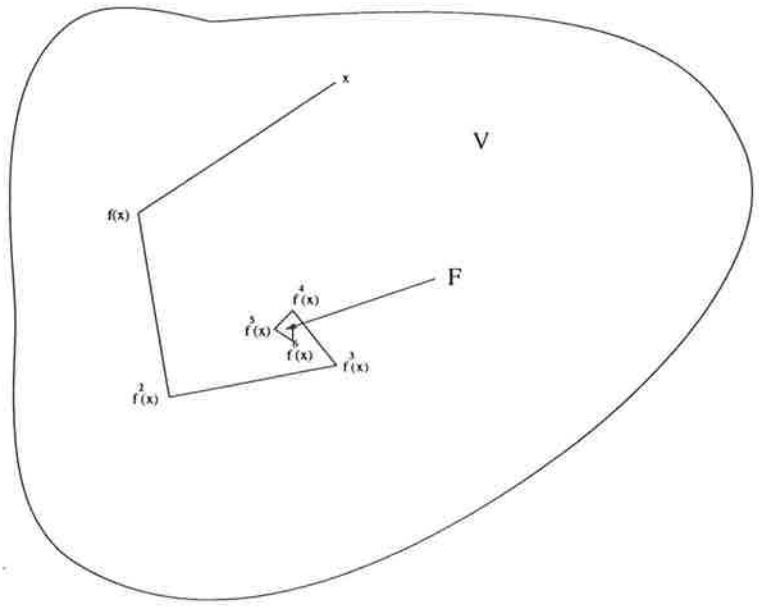

Figure 5.1: Attractors

Suppose $f(x) = \cos x$ repeatedly pressing the button on your calculator for any initial value of x between 0 and 2π you notice that the final result converges to $0.739\ldots$. In this case the attractor of f is $F = 0.739\ldots$ and the attractor basin all 0 to 2π. This happens if there is dissipation of energy or there is capture. An attractor may be one point of a set of points. If the attractor is a set of points and that set of points describes a fractal set it is known as a strange attractor. Fractals are discussed in the next section.

So far attractors and attractor basins have been described in a abstract manner. The description of dynamical systems is the evolution of phasespace values. A particle starts off with at some initial position and momentum and evolves in time according to the Hamiltonian describing the system. The language of chaos can be transcribed to Hamiltonian systems if x is considered the set of phasespace values and the map f as Hamilton's equations. Attractors exist in Hamiltonian systems if one or more of the phasespace values

converge to a particular point. Dissipation of energy is one reason this may occur capture is another. The subsequent chapter shows that relativistic dynamics leads to the capture trajectories which in Newtonian mechanics does not attractors. Therefore the chaotic behaviour of relativistic trajectories may be studied via examination the fractal nature of attractor basins.

5.3 Fractals

Once again from the work of C. H. Thomson [77] A set S is said to be a fractal if and only if it has the following key properties;

- S has some degree of self–similarity. i.e has some scale invariance.
- S has a fine structure on an arbitrarily small scale.
- S lacks smoothness and the boundary of S cannot be described by any simple analytic function.
- For any point on S there exists a ball of radius greater than zero in which lie an arbitrary large number of points at various distances also in S. All points on this ball do not lie in the set S.
- S can have a non-integer dimension.
- The fractal dimension of S (defined later) is usually greater than the topological dimension.

The last two items speak of the a non-integer dimension of the set S. The dimension is something which we intuitively assume to have an integer value. It is found that there exists definitions for dimension which have values 0, 1, 2 or 3 for dots, lines areas and volumes but non-integer dimensions for fractal. lead to the next question.

There are a number of ways to define the dimension of a fractal in the literature. The one that is used here is called the Hausdorff box, or the capacity dimension. There is a small technical difference between these two definitions. It is not important in most cases

and the reader is referred to [79] for further information. The Hausdorff Box dimension is used here because of its ease in computation and its common occurrence.

Definition of Hausdorff Box dimension:

Consider the bounded set S which is a subset of $\Re^n$. If $N_\epsilon(S)$ is the least number of cubes of length ϵ required to completely cover S then $N_\epsilon(S)$ increases according to

$$N_\epsilon(S) \propto \epsilon^{-d_B}. \tag{5.3.1}$$

where d_B is the Hausdorff box dimension of the set. Equivalently

$$d_B F = \lim_{\epsilon \to 0} \frac{\ln N_\epsilon(S)}{-\ln \epsilon}. \tag{5.3.2}$$

It can seen that this definition gives the expected topological results. For example if S is a single point then $N_\epsilon(S) = 1$ and ϵ is arbitrary hence from (5.3.2) $d_B = 0$ as expected. A line of length L can be divided up into segments ϵ of length L/N. In which case

$$\begin{aligned} d_B F &= \lim_{\epsilon \to 0} \frac{\ln N_\epsilon(S)}{-\ln \epsilon} \\ &= \lim_{\epsilon \to 0} \frac{\ln N_\epsilon(S)}{-\ln L + \ln N_\epsilon(S)} \\ &= 1 \end{aligned}$$

As in the limit $\epsilon \to 0$ $N_\epsilon(S) \to \infty$. Similarly for squares and cubes $N_\epsilon(S) = S/\epsilon^2$ and V/ϵ^3 hence $d_B = 2, 3$ respectively.

Using this definition one finds that many sets can have a non–integer dimension. Consider for example the Cantor Set. The Cantor Set is formed by taking a solid line and removing the middle third. Then from the remaining two thirds the middle third of each segment is removed and so on. Finally an infinite set of points known as the Cantor Set is generated.

It is possible to calculate the fractal dimension of this using equation (5.3.2). After each iteration the size of each cube (a cube in 1–d is a line) is 1/3 of the previous ones

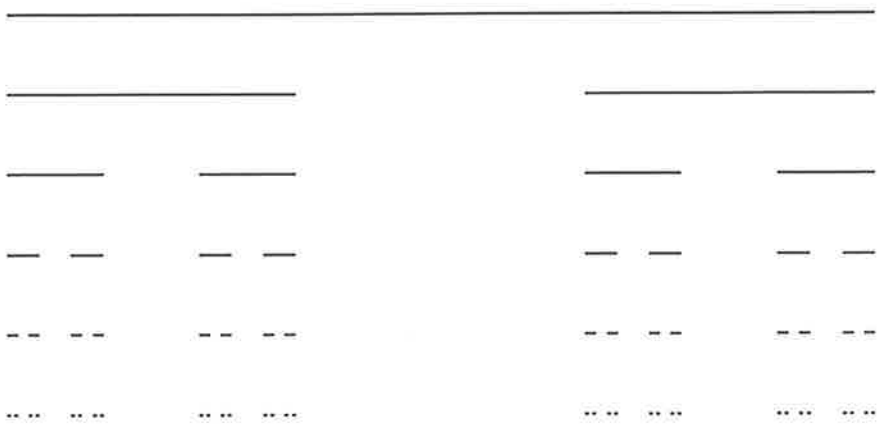

Figure 5.2: The Cantor Set

and the number of cubes is doubled. Hence after the $I'th$ iteration the number and size of cubes is.

$$N = 2^I \quad \epsilon = L(1/3)^I. \tag{5.3.3}$$

In the limit $I \to \infty$ $\epsilon \to 0$. Combing equation (5.3.3) in conjunction with equation (5.3.2) gives the result

$$\begin{aligned} d_B F &= \lim_{I\to\infty} \frac{I \ln 2}{I \ln (1/3) + \ln L} \\ &= \frac{\ln 2}{\ln 3} \\ &= 0.6309\ldots \end{aligned}$$

Notice here that the dimension is greater than zero but less than one. This seems to make sense because the set is more than a point but less than a line.

The popularity of fractal images on T-shirts or as posters probably stem from their beauty and infinite detail. Scientists are fascinated by them because this fine detail is generated by surprisingly simply algorithms. They are prime examples of how the complexity of nature can be governed by a set of simple rules. The ubiquitous Mandelbrot set is a fine example of this principle in action. Each complex value in this set is mapped to the next according to the following rule:

$$z_{n+1} = z_n^2 + c.$$

The initial condition is that $z_0 = 0$, c is the position in the complex plane for which the colour is determined. Black appears in Figure (5.3) if $z_{15} < 4$, white if $z_n > 4$ for $n \leq 15$.

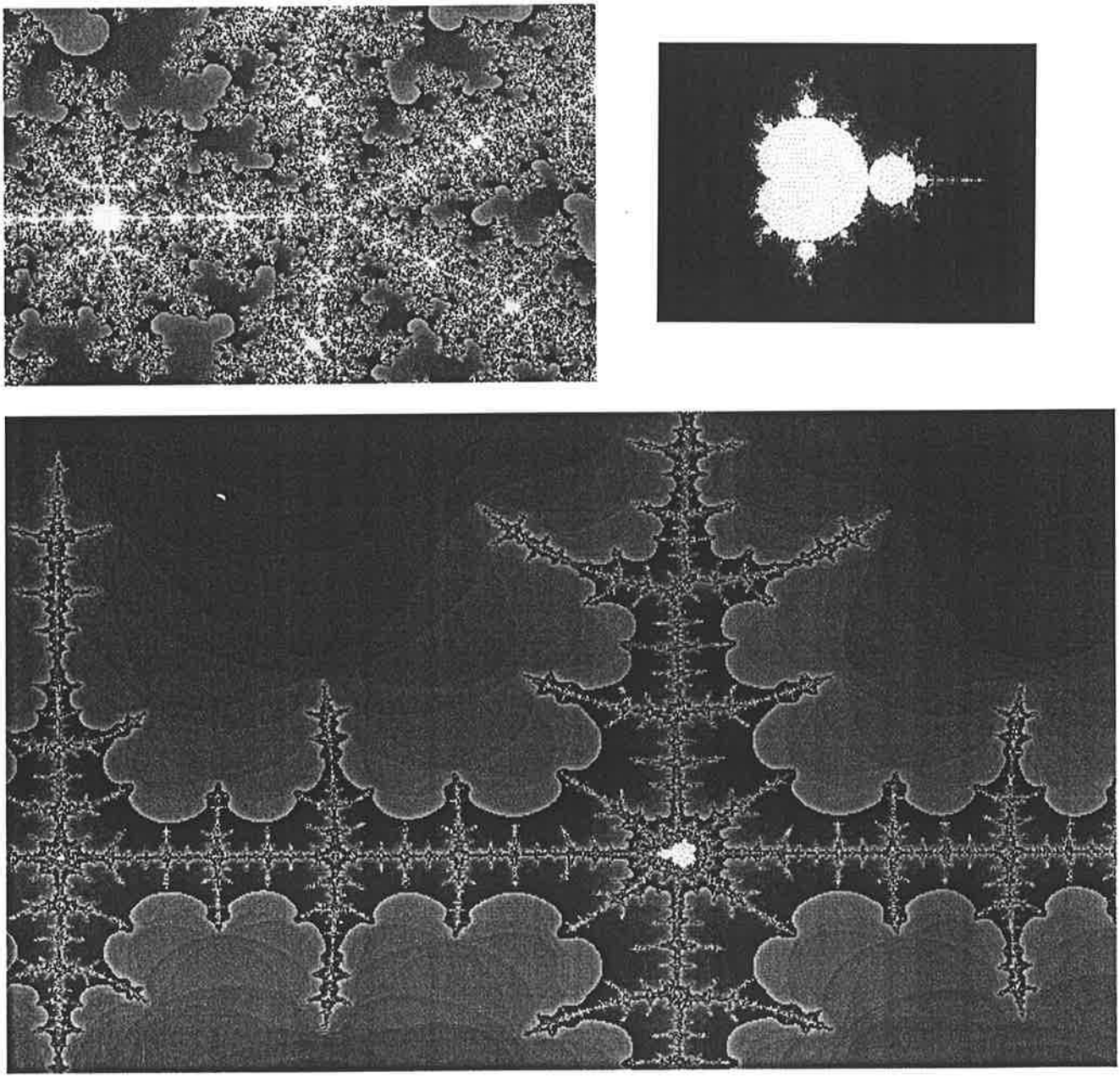

Figure 5.3: The Mandelbrot set

5.4 Lyapunov exponents

Chaotic systems are characteristically extremely sensitive to initial conditions. This sensitivity can be classified by drawing a ball around the initial data set and measuring changes to that ball as it evolves. The shape of the ball can change from being spherical to ellipsoidal and the volume encompassed by the ball may also vary. Sensitivity is determined by the rate at which each axis of the ellipsoid varies. Extremely sensitive systems (chaotic) are defined as those having exponential growth in ellipsoidal axis. Lyapunov exponents measure the growth of axis in the following way:
Consider a cure $\vec{x}(\tau)$ is defined in an N dimensional space by the N differential equations

$$\frac{dx^i}{d\tau} = f^i(\vec{x}). \tag{5.4.1}$$

If the curve $\vec{x}(\tau)$ is deviated by a small amount $\vec{\epsilon}$ perpendicular to the tangent of $\vec{x}$ then to first order its equation of motion is

$$\begin{aligned} \frac{d(x^i + \epsilon^i)}{d\tau} &= f^i(\vec{x}) + \sum_{k=1}^{N} \frac{\partial f^i(\vec{x})}{\partial x^k}\epsilon^k \\ \frac{d\epsilon^i}{d\tau} &= \sum_{k=1}^{N} \frac{\partial f^i(\vec{x})}{\partial x^k}\epsilon^k. \qquad \text{From 5.4.1} \end{aligned} \tag{5.4.2}$$

The Lyapuonv exponent λ in the k direction λ^k is difined as

$$\lambda^k = \lim_{t\to\infty} \frac{1}{t} \ln \left| \frac{\epsilon^k(\tau)}{\epsilon_0^k} \right|. \tag{5.4.3}$$

where ϵ_0^k is the value of $ep^k(\tau)$ when $\tau = 0$. If one or more Lyapunov exponent is zero the system is chaotic. Though the equations governing $\vec{x}(\tau)$ are known at each point on the curve it may not be possible to write know $\vec{x}(\tau)$ explicitly, especially if the system is chaotic. Determining the value of the Lyapunov exponents from 5.4.3 equation 5.4.1 require numerical integration if these equations can not be solved analytically.

For Hamiltonian systems $\vec{x}(\tau)$ describes the phasespace trajectories whose tangents $\vec{f}$ are given by Hamilton's equations. Louvilles theorem tells us that if the system is non-dissipative (no energy loss) then the phasespace volume of enclosed by the ellipsoid $\epsilon(\tau)$ is constant for all values of τ. Hence the resulting sum of Lyapunov exponents is zero for non-dissipative Hamiltonian systems.

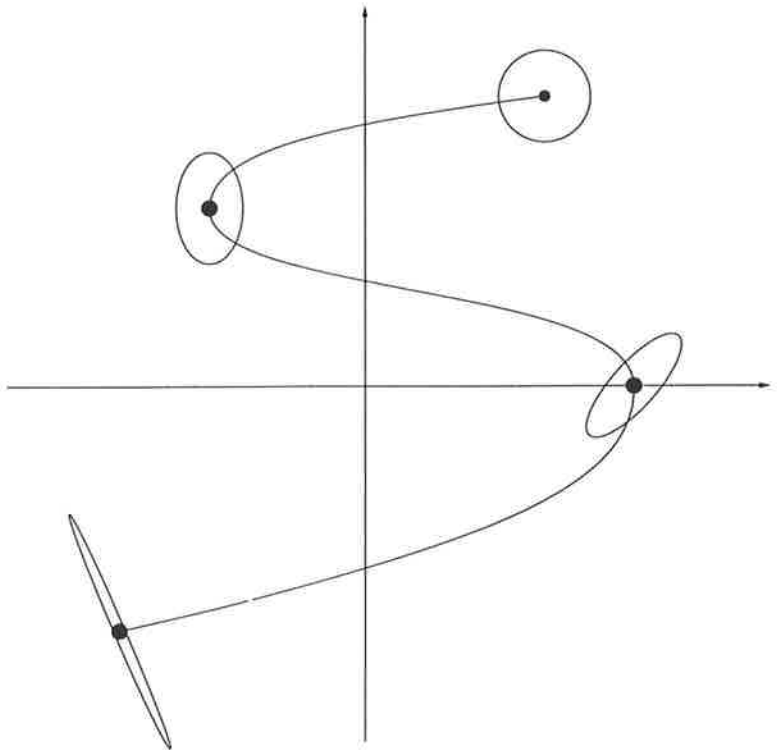

Figure 5.4: Lyapunov exponents

5.5 Chaos and computing

Descriptions of chaotic behaviour invariable mean that they defy analytic representations. Where it not for the impressive advancements of high speed computing choas theory probably never would have been developed. By their very nature the outcome of chaotic systems can only be modelled with numerically integration. It is not feasible to imagine that this can be adequately done by humans.

There is an appearant contradiction in using computers to studing chaos. It comes from the fact that all computer integration incorporates rounding errors. Even if these rounding errors are minimised it may drastically effect the outcome of a chaotic systems, as they are extremely sensitive to initial conditions. A rounding error, no matter how small will dramtically effect the outcome at some later stage. So even with the most powerful computers imaginable it is not possible to determine results with chaotic dynamics.

What is important to realise is that in chaotic studies it is not the final outcome

which is important, it is its predictability. If very small rounding errors lead to long term uncertainity then the system is chaotic. Studies of chaos are concentrated on the why and when systems are chaotic and when they regular, not the final outcome. This is a situation for which the computer is ideally suited.

Chapter 6

Chaos in special relativistic dynamics

6.1 Introduction

The classical three body problem has engaged physicists for over 200 years. In that time, though much progress has been made, solutions have only been found for a few special cases [80]. One such case is the Newtonian motion of an infinitesimal body subject to the $1/r$ potential of two fixed finite bodies. The problem considered in this chapter is the motion of an infinitesimal charged particle about two fixed charged particles described by a special relativistic Hamiltonian. To the best of the our knowledge it has not been studied previously. This is a three body problem with a difference. Trajectories of the test particles are markedly different from the Newtonian model. They behave in a chaotic manner though in Newtonian mechanics they do not [80]. Comprehensive studies have already been made for the more complicated gravitational analog of this problem. In these studies [3, 7] the motion of charged test particle about two fixed, charged black holes was considered. Herein, the fixed two centre problem is studied in the absence of gravitational interactions and comparisons are made between the two problems. Despite the very different spacetime geometry and global causal structure exhibited by the special and general relativistic cases, it is found that both systems have very similar chaotic behaviour.

A qualitative understanding of the two centres problem can be gained by considering the dynamics in terms of particle motion in an effective potential. In the Newtonian limit the

effective potential can be shown to be integrable. Relativistic corrections to the effective potential introduce nonlinearities which cause two qualitative changes in the dynamics. The first change allows trajectories to be captured by the central singularities - even if the trajectories have nonzero angular momentum. The second change in the dynamics comes from the relativistic corrections rendering the effective potential non-integrable. The study of this second effect will occupy the majority of this chapter. The phenomenon of relativistic capture means that the chaotic system we are studying here is an open one. Although we will be studying energetically bound trajectories, the dynamics can be consider as a form of chaotic scattering as the captured orbits are not bounded in phase space. Indeed, the capture phenomenon makes the dynamics similar to that seen in Hamiltonian exit systems .

The phenomenon of relativistic capture makes the dynamics difficult to study using standard indicators of chaos such as Lyapunov exponents and Poincare sections as they rely on the existence of long-lived periodic orbits [81]. When attracting regions of phase space exist, it has been suggested [3, 4] that the best way to study chaos is to examine the nature of the attractor basin boundary (ABB). Indeed there is a complementary relationship between these methods as Lyapunov exponents are best for studying trajectories which are quickly captured. An additional reason cause us to favor ABB's over Lyapunov exponents for relativistic systems, namely, Lyapunov exponents are not Lorentz invariant quantities, while the fractal dimension of the ABB's is. Another technique commonly used to chaos employs Poincare' sections. For open systems these are very difficult to generate as most trajectories quickly escape to various asymptotic regions of phase space. It is possible to generate Poincaré sections for trajectories near stable orbits, but these only account for trajectories forming a set of measure zero in phase space. Rather than struggling to find these rare orbits the quick capture of typical orbits was used to our advantage which allowed us to concentrate on generating plots of the basin boundaries. In section 6.4 the use of ABB's is argued more strongly in determining chaos.

Before launching into this problem, some indication is needed that it may be chaotic. The first signs of this came in [4] where the fractal nature of an ABB was shown for two small mass black holes (small relative to their separation in natural units). The small masses meant that for large regions the spacetime was approximately Minkowskian. While

the chaotic nature of the small mass case suggests that chaos might persist in the special relativistic analog, it is not conclusive. This is because the multi-black hole spacetime only truly recovers Minkowski spacetime when the black hole masses vanish. No matter how small a non-zero mass black hole might be, it always gives rise to a causal barrier at the horizon, leading to a distinct causal topology not shared by Minkowski space.

To examine the fixed two centre problem in a Minkowski metric, it is sufficient to consider a test particle with charge q and mass m. Choosing the charge to mass ratio so that $q/m \gg 1$ ensures that Coulomb interaction dominates gravity. Our special relativistic version of the fixed two centre problem has lead us into electrodynamics. This raises the issue of radiation. It is well known that accelerating charged particles radiate. Under what conditions, if any, can radiation effects be neglecited? For example, a classical hydrogen atom would collapse within a micro second due to radiation losses. In section 6.2 it is shown that it is always possible to select masses and charges so that radiation can be neglecited without loss of generality.

Having now established a motivation and suitable model for the special relativistic two centre problem, the outline for the rest of the chapter is as follows. Section 6.2 establishes the form of the Super-Hamiltonian used to describe the dynamics. Because a relativistic extension of a Newtonian problem is considered it is important to understand why the Newtonian model is integrable while the relativistic model is not. Using the Hamiltonian one is able to find a set of orbits that are exactly integrable, and hence do not exhibit chaos. This is done by obtaining Hamilton's principal function for these orbits. It is shown that this set of orbits includes small velocity Newtonian-type orbits. For weakly relativistic examples these orbits coexist in phase space with small regions of chaotic orbits.

The relativistic Hamiltonian is not generally separable using the method outlined in section 6.2. It is not even possible to use perturbative techniques since velocities can become ultra-relativistic, as occurs when particles get close to one or other of the charges.

Apart from non-integrability the relativistic Hamiltonian differs from the Newtonian one in that capture occurs for particles with non-zero angular momentum. Section 6.3 examines this phenomenon fully. A set of conditions is found for when capture occurs, leading us to examine the attractor basins. Capture conditions are used as a rough analytic

check of the computational integration routine.

The chaotic nature of the system becomes apparent when the attractor basins are studied. The attractor basin boundary (ABB) lies on a fractal set. Section 6.4 is devoted to the generation of ABB's, the calculation of their fractal dimension, and a scale parameter related to their location. An explanation is given as to why ABB's is chosen as a measure of chaos. Also in section 6.4 is an outline of the computational methods used and a description of how each image was generated.

The last section, section 6.5, is devoted to analysing the variations of ABB's with fundamental parameters. In this section how parameters, such as mass and charge, affect the chaotic nature of the system is discussed. Results are presented in graphic form. The conclusion made is that while the relativistic two centre problem is chaotic, the measures of chaos appear to vary in an orderly manner.

Finally section 6.6 develops a conclusion and outlines some suggested further work and extensions to the model.

6.2 Formalism

The introduction stated that the effects of radiation would be neglecited in this study. In this section it will be shown how this can be done without altering the fundamental nature of the system. The loss of energy due to radiation can be neglecited only if the typical rate of change in kinetic energy is very much greater than the power loss due to radiation. The power radiated by a relativistic particle of charge q and mass m is [82]

$$P = \frac{2q^2}{3}\gamma^6 \left[\dot{\mathbf{v}}^2 - (\mathbf{v} \times \dot{\mathbf{v}})^2\right] \quad , \tag{6.2.1}$$

where $\mathbf{v}$ is particle's velocity, γ the Lorentz boost factor, and the dot represents a derivative with respect to coordinate time. For a charged particle moving in a potential V

$$\dot{\mathbf{v}} = \frac{-q}{\gamma m}\left[\nabla V - \mathbf{v}(\mathbf{v} \cdot \nabla V)\right], \tag{6.2.2}$$

$$\dot{E} = m\dot{\gamma} = -q\mathbf{v} \cdot \nabla V. \tag{6.2.3}$$

The condition which ensures radiation reaction can be neglecited is

$$P \ll |\dot{E}| \,. \tag{6.2.4}$$

Using Eqs. (6.2.1), (6.2.2) and (6.2.3) the inequality in (6.2.4) can be written in terms of the divergence of the potential as

$$P = \frac{2q^4\gamma^2}{3m^2}\left[(\nabla V)^2 - (\mathbf{v}\cdot\nabla V)^2\right] \ll q|\mathbf{v}\cdot\nabla V|. \tag{6.2.5}$$

If the potential is due to two fixed equal charges, Q, separated by a distance a, i.e., a potential like Eq. (6.2.13) for $n = 2$, then Eq. (6.2.5) can be evaluated explicitly. In section 6.3 it is demonstrated that capture occurs for particles that are ultra-relativistic. Since the relativistic capture of particles is being studied an exmination of the ultra-relativistic limit ($\mathbf{v} \to 1$) of Eq. (6.2.5) is necessary. In this limit the result depends on the type of orbit examined. If the motion is a direct plunge, $\mathbf{v}$ is parallel to (∇V), then the γ^2 factor on the left hand side of Eq. (6.2.5) is cancelled and thus

$$\frac{q^3}{m^2}|\nabla V| \ll 1. \tag{6.2.6}$$

Taking a typical value for the gradient of the potential to be Q/a^2 the above condition can be written as

$$\mathcal{F}^2\frac{q}{Q} \ll 1, \tag{6.2.7}$$

with $\mathcal{F}$ defined as

$$\mathcal{F} = \frac{qQ}{ma}. \tag{6.2.8}$$

The scaled electrostatic energy, $\mathcal{F}$, in this way because it proves to be very useful for later calculations. If on the other hand the motion is orbital, close to circular, then $\mathbf{v}$ is perpendicular to (∇V) and the γ^2 persists. However, γ can be estiminated from viral theorem considerations to be approximatley by $\mathcal{F}$ in the ultra-relativistic limit. For orbits such as these Eq. (6.2.5) now is

$$\mathcal{F}^4\frac{q}{Q} \ll 1. \tag{6.2.9}$$

Eqs. (6.2.7) and (6.2.9) imply that radiation can be neglecited no matter how large $\mathcal{F}$ is , as long as q/Q sufficiently small.

It is worth noting that the factor of γ^2 difference between the direct plunge and circular orbit cases is directly related to the problems found in ring and linear colliders. Radiation loss is never a serious problem in linear colliders.

This means that for orbits which are captured relatively quickly, i.e., with a capture time of order $t_c = a/v$, the effect of radiation can be neglecited. Stated another way, with a careful choice of parameters, relativistic capture can dominate the capture due to radiation loss.

Having established a suitable model it is now possible to examine the dynamical properties of the system. The relativistic equations of motion for a non-radiating particle of charge q in an electromagnetic field can be obtained from the super Hamiltonian [82],

$$\mathcal{H} = \frac{1}{2}(P_\alpha - qA_\alpha)(P^\alpha - qA^\alpha), \tag{6.2.10}$$

in conjunction with Hamilton's equations,

$$\frac{dx^\alpha}{d\lambda} = \frac{\partial \mathcal{H}}{\partial P_\alpha} \quad \text{and} \quad \frac{dP_\alpha}{d\lambda} = -\frac{\partial \mathcal{H}}{\partial x^\alpha}. \tag{6.2.11}$$

Here, λ is an affine parameter which is related to the proper time by $\lambda = \tau/m$, where m is the mass of the test particle. The dynamic equations of motion represented here describe a continuous flow of phase space coordinates on a differential manifold. The first of Hamilton's equations relates the canonical momentum, P_α, to the mechanical momentum, p^α:

$$p^\alpha = mu^\alpha = P^\alpha - qA^\alpha. \tag{6.2.12}$$

Since a static electric field is considered the spatial components of the vector potential all vanish, $A_i = 0$. The field is generated by placing n fixed charges Q_i at positions (x_i, y_i, z_i) in space, so that $A_0 = V$ is given by

$$V = -\sum_{i=1}^{n} \frac{Q_i}{\sqrt{(x - x_i)^2 + (y - y_i)^2 + (z - z_i)^2}}. \tag{6.2.13}$$

For fields generated in this way Hamilton's equations can be written as,

$$\gamma = \frac{1}{\sqrt{1 - \dot{\mathbf{x}}}} \tag{6.2.14}$$

$$m\gamma = E - V \tag{6.2.15}$$

$$\dot{\mathbf{x}} = \frac{\boldsymbol{\pi}}{\sqrt{\boldsymbol{\pi}^2 + 1}} \tag{6.2.16}$$

$$\dot{\boldsymbol{\pi}} = -\frac{q}{m}\nabla V. \tag{6.2.17}$$

The dot on top of a vector refers to the derivative with respect to coordinate time and $\boldsymbol{\pi} = \mathbf{p}/m$. In most cases these equations cannot be solved analytically. Thus numerical integration appears to be the only viable option to calculate trajectories. However, if $n = 1$ or 2 some analytic results can be obtained. The case n=1 is the classic special relativistic scattering problem and has been throughly studied. A more interesting case occurs for $n = 2$. It is interesting because there is no chaos in the Newtonian version of the problem, nor for certain classes of orbits in the relativistic problem, but for other classes of orbits the system is chaotic. If two equal fixed charges Q are placed at (0,0,-a) and (0,0,a) then Eqs. (6.2.14) to (6.2.16) are unchanged by a rescaling of coordinates. By scaling the coordinates so that the fixed charges are at (0,0,-1) and (0,0,1) Eq. (6.2.17) may be written as

$$\dot{\boldsymbol{\pi}} = -\mathcal{F}\nabla V_0. \tag{6.2.18}$$

$\mathcal{F}$ is defined as before and V_0 is defined:

$$-V_0 = \frac{1}{\sqrt{x^2 + y^2 + (z-1)^2}} + \frac{1}{\sqrt{x^2 + y^2 + (z+1)^2}}. \tag{6.2.19}$$

The equations are written in this form so that all parameters that affect the field strength are combined into one scaling quantity, $\mathcal{F}$.

The Newtonian version of this problem has been solved by a number of authors, for example see [83]. The problem is solved by changing to prolate spheroidal coordinates,

$$x = \sinh\psi \sin\theta \cos\phi \quad y = \sinh\psi \sin\theta \sin\phi \quad z = \cosh\psi \cos\theta, \tag{6.2.20}$$

and using the Hamilton-Jacobi separation of variables (see Goldstein [84]). In relativity this method proves to be useful only for a certain class of orbits. In special relativity the super Hamiltonian written in these coordinates is

$$\mathcal{H} = 1/2\left[-\left(S_{,t} - \frac{2qQ\cosh\psi}{a\mathcal{Q}}\right)^2 + \frac{1}{\mathcal{Q}}\left(S_{,\psi}\right)^2 + \frac{1}{\mathcal{Q}}\left(S_{,\theta}\right)^2 + \frac{1}{\left(\sinh\psi\sin\theta\right)^2}\left(S_{,\phi}\right)^2\right] = -S_{,\lambda}\,, \tag{6.2.21}$$

where

$$\mathcal{Q} = \sinh^2\psi + \sin^2\theta \tag{6.2.22}$$

and S is Hamilton's Principal function. Since t, ϕ and λ are cyclic coordinates they each have a constant of the motion associated with them. The physical significance of these constants are clear. $E = -S_{,t}$ and $L = S_{,\phi}$ are the total energy and angular momentum of the test particle. The constant associated with λ comes from the fact that the rest mass is conserved. This can be seen explicitly in the following way,

$$-S_{,\lambda} = \mathcal{H} = \frac{1}{2}(-m^2\gamma^2 + \mathbf{p}^2) = -m^2/2\ . \tag{6.2.23}$$

The generating function S is said to be completely separable if it can be written in the form

$$S(\lambda, t, \psi, \theta, \phi) = S_\lambda(\lambda) + S_t(t) + S_\psi(\psi) + S_\theta(\theta) + S_\phi(\phi). \tag{6.2.24}$$

The separability of S in the super Hamiltonian is broken by the term

$$\left(\frac{2qQ\cosh\psi}{a\mathcal{Q}}\right)^2. \tag{6.2.25}$$

This is because any term with $\mathcal{Q}^2$ can not be separated into a sum of two functions involving θ and ψ only. However, if the term given in Eq. (6.2.25) is small compared to $4EqQ\cosh\psi/(a\mathcal{Q})$, i.e., if

$$\mathcal{F} \ll \left(\frac{\mathcal{Q}}{\cosh\psi}\right)\frac{E}{m} = \frac{\gamma\mathcal{Q}}{\cosh\psi}\ , \tag{6.2.26}$$

then the system becomes completely separable and

$$S(\lambda, t, \psi, \theta, \phi) = 1/2m^2\lambda - Et + L\phi + S_\theta(\theta) + S_\psi(\psi), \tag{6.2.27}$$

where

$$S_\psi(\psi) = \int \sqrt{E^2\sinh^2\psi - \frac{L^2}{\sinh^2\psi} + \frac{4EqQ^2\cosh\psi}{a} - m^2\sinh^2\psi + \alpha}\ d\psi \tag{6.2.28}$$

and

$$S_\theta(\theta) = \int \sqrt{E^2\sin^2\theta - \frac{L^2}{\sin^2\theta} + -m^2\sin^2\theta + \alpha}\ d\theta. \tag{6.2.29}$$

The fourth constant of motion, α, is

$$\alpha = E^2 \sinh^2\psi - \frac{4EqQ\cosh\psi}{a} - (S_{,\psi})^2 - \frac{L^2}{\sinh^2\psi} - m^2\sinh^2\psi \qquad (6.2.30)$$

$$= E^2\sin^2\theta - (S_{,\theta})^2 - \frac{L^2}{\sin^2\theta} - m^2\sinh^2\theta. \qquad (6.2.31)$$

Eqs. (6.2.28) and (6.2.29) can be used in conjunction with [84]

$$\beta_i = \frac{\partial S_{q_i}(q_i)}{\partial\alpha_i} \qquad (6.2.32)$$

to find explicit solutions involving time. The β_i's are the initial conditions, the q_i's refer to phase space co-ordinates as well as time, and the α_i's are constants of the motion associated with each coordinate. Such orbits are said to be integrable and hence not chaotic. The KAM [85][86][87] theorem states that if a small nonlinear perturbation is added to the Hamiltonian, regions of regular motion will continue to occur. This implies that if relativistic effects are small then there will exist some regions in phase space which do not have chaotic trajectories. The inequality in Eq.(6.2.26) gives a condition for the type of orbits that are integrable. As expecited, these include Newtonian type orbits where $\mathcal{Q}$ is large, i.e., the field is weak and $E \approx m$. If $\mathcal{Q}$ is large then ψ is large. For large ψ, $\mathcal{Q} \approx \sinh^2\psi$ and $\cosh\psi \approx \sinh\psi$. The inequality in Eq.(6.2.26) now becomes

$$\gamma_o \gg \frac{\mathcal{F}}{\sinh\psi}, \qquad (6.2.33)$$

where γ_o is the value of γ at time $t = 0$. Eq. (6.2.33) is satisfied for certain relativistic orbits as well as Newtonian ones. An example of an orbit which does not escape yet does not collapse is shown in Fig. 6.1. Fig. 6.1 was generated using a fourth-order adaptive step size Runge-Kutta routine [88]. In this figure $\mathcal{F} = 0.06$ and the motion appears to be periodic. This orbit is not typical of the type studied here. Collapse to a singularity does not occur hence radiation effects can not be neglecited as they are cumulative. For this reason orbits chosen to be studied are those in which the inequality in Eq. (6.2.26) is seldom obeyed. In the next section examines what happens when Eq. (6.2.26) is not satisfied. In the relativistic limit the equations of motion are not completely separable in prolate spheroidal coordinates. This does not prove that the system is non-integrable, but it does show that if the system is chaotic, the chaos is due solely to relativistic effects.

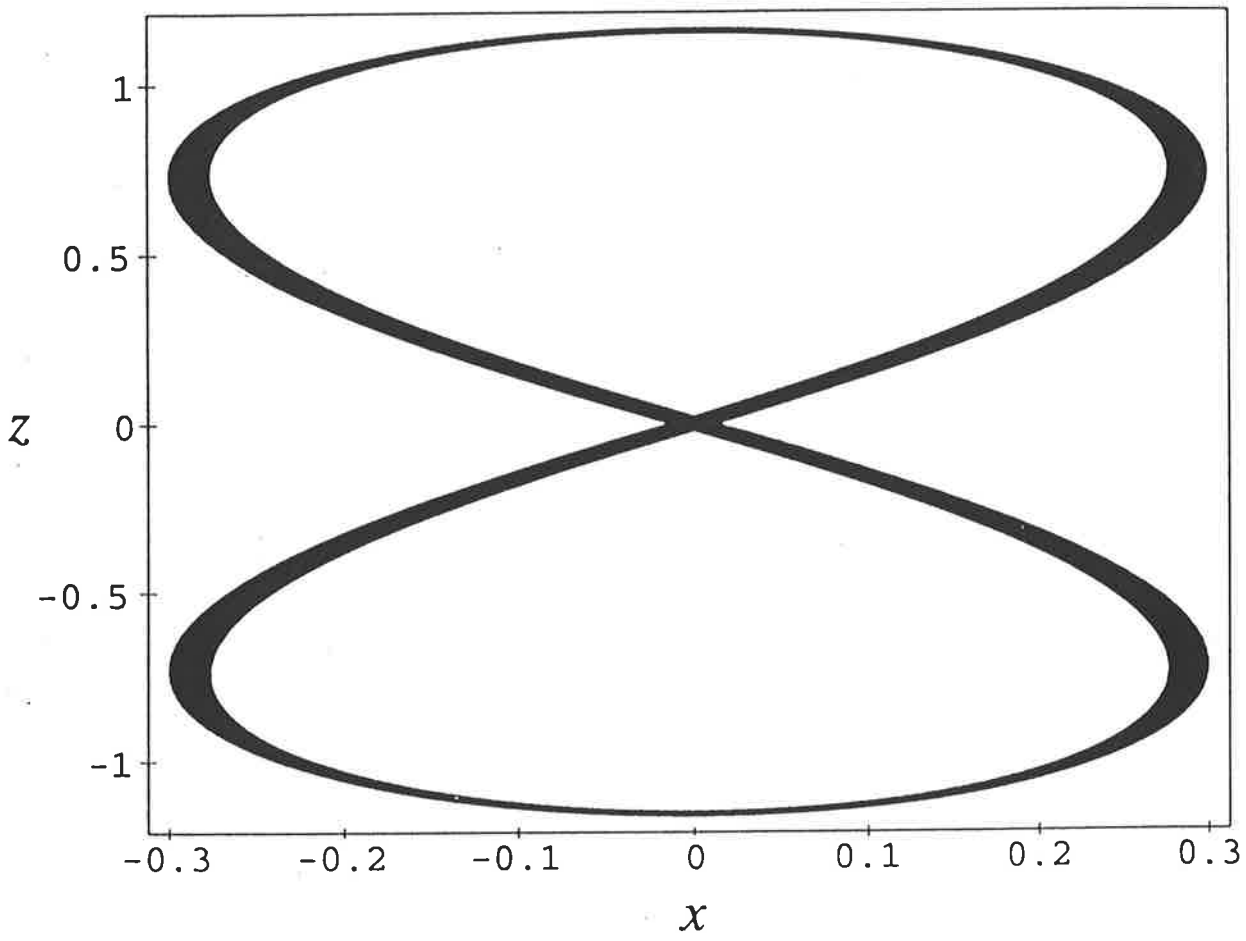

Figure 6.1: A trajectory with $\mathcal{F}0.03$ and initial conditions ($x = 4.5, y = 2.0,$ and $\pi = 0$).

6.3 Relativistic capture

In Newtonian mechanics, trajectories with non-zero angular momentum do not collapse into a singularity. In relativity, even trajectories with non-zero angular momentum can terminate at the central singularity. This effect can be easily demonstrated in the case of one fixed centre. The spherical symmetry in this case allows the motion to be modelled by a one-dimensional effective potential. The super Hamiltonian may be used to obtain the condition

$$m^2\left(\frac{dr}{d\tau}\right)^2 + V_{eff}^2 = E^2 \,. \tag{6.3.1}$$

Here τ is the proper time along the trajectory and the effective potential is given by

$$V_{eff}^2 = m^2 - \frac{2EqQ}{r} + \frac{L^2 - q^2Q^2}{r^2} \,. \tag{6.3.2}$$

In the Newtonian limit this reduces to

$$V_{Neff}^2 = m^2 - \frac{2mqQ}{r} + \frac{L^2}{r^2} \,. \tag{6.3.3}$$

Near $r = 0$ the Newtonian effective potential is always dominated by the repulsive angular momentum barrier L^2/r^2. For relativistic orbits the repulsive barrier only exists when $L > qQ$. Trajectories with $L < qQ$ can be captured.

It is worth noting that in the ultra relativistic limit the angle θ between the position and the momentum vectors is given near $r = 0$ by

$$\theta \approx \arcsin\frac{L}{qQ}. \tag{6.3.4}$$

This means that θ is constant, hence the trajectory is a spiral of finite length and therefore takes a finite time to be captured.

Fig. 6.2 was generated by following the trajectories of particles that start at the origin with various initial values of π_x and π_z. Trajectories that finish at (0,0,-a) are labelled black, those that finish at (0,0,a) are labelled white, and those that do not collapse to a singularity, within a finite time, are labelled grey. Fig. 6.2 is an 840×840 plot with $\mathcal{F} = 1$. The two most noticeable features of this figure, apart from its regions of complexity, is the escape of particles with a $\|\boldsymbol{\pi}\| \geq 2.8$ and the capture of particles with a $\pi_x \leq 1$. Both these results can be shown analytically.

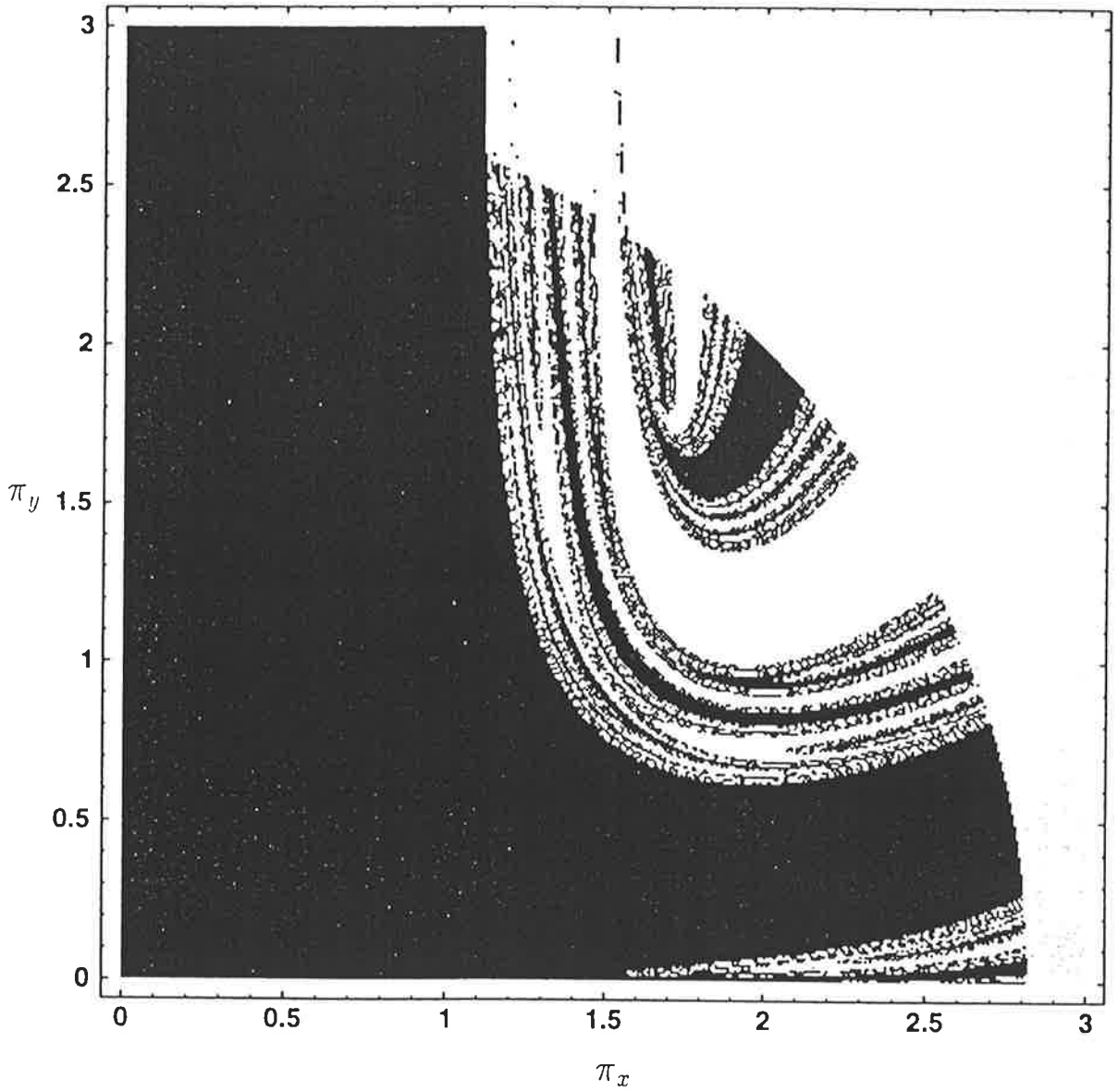

Figure 6.2: A section of attractor basins for $x = 0$ and $\mathcal{F} = 1$.

If a particle is set in motion at the origin, then in order for its motion to be bounded it must have an energy less than or equal to the rest mass of the particle. This implies that

$$\|\vec{\pi}\| \leq \sqrt{(2\mathcal{F}+1)^2 - 1} \tag{6.3.5}$$

For $\mathcal{F} = 1$ Eq. (6.3.5) tells us that escape occurs for $\|\vec{\pi}\| \geq \sqrt{8} \approx 2.8$. The capture of particles with $\pi_x \leq 1$ can be shown by considering the simpler case where the potential due to the second fixed charge is ignored. The justificatin of this comes from assuming that momentum in the z direction is unaffecited until the particle is so close to one charge that the other can be ignored. Using the condition $L < qQ$, in conjunction with the fact that $L = am\pi_x$ at the origin, the capture condition becomes

$$\pi_x \leq \mathcal{F}. \tag{6.3.6}$$

At this point note that capture occurs for similar conditions in general relativity. For a single, extremally charged black-hole the effective potential reads

$$V_{eff}^2 = \frac{1}{(1+M/r)^4}\left(m^2\left(1+\frac{M}{r}\right)^2 + \frac{L^2}{r^2}\right), \tag{6.3.7}$$

in isotropic coordinates [89], [90]. The potential has (6.3.7) a maximum at

$$r = \frac{L^2 - 2M^2m^2 - L\sqrt{L^2 - 4M^2m^2}}{2Mm^2}. \tag{6.3.8}$$

Particles with an energy which exceeds the maximum value of the potential barrier are subject to capture by the black hole. For ultra-relativistic particles the capture condition reads

$$L < 2\sqrt{4(E/m)^2 - 1}(Mm), \tag{6.3.9}$$

whilst for non-relativistic particles the condition becomes

$$L < \sqrt{2}\sqrt{2+\sqrt{13}}(Mm). \tag{6.3.10}$$

Termination of trajectories at a central singularity is a standard feature of relativistic dynamics, both special and general.

6.4 Fractal attractor basin boundaries

The capture of particles leads us to examine the nature of the attractor basin boundary. Studies of chaotic systems often focus on the determination of Lyapunov exponents as a measure of chaos [91]. The Lyapunov exponents λ_k in flat spacetime are defined by choosing a point x in phase space, at the centre of a ball of radius $\epsilon \ll 1$. After a time t the ball evolves into an ellipsoid with semi-axes $\epsilon_k(t)$, where k ranges from one to the dimension of the phase space. The Lyapunov exponents are:

$$\lambda_k(x) = \lim_{t\to\infty} \lim_{\epsilon\to 0} \ln \frac{\epsilon_k(t)}{\epsilon}, \tag{6.4.1}$$

assuming the limits exist. The λ_k are constant along a trajectory, and are often constant over larger regions of phase space such as the basin of an attractor. However there are problems with this approach. Firstly, the existence of a positive Lyapunov exponent is not enough to determine if a system is chaotic [77]. For example, the Newtonian version of the fixed two centre problem (which is not chaotic) has a set of positive Lyapunov exponents for orbits that are perpendicular to the z-axis. Secondly, the computation of Lyapunov exponents requires setting a finite time limit, thus inducing an error. If particles are captured too quickly this error is large.

In the general relativistic problem the topology of the ABB was used as a measure of chaos. A particularly appealing feature of this method in general relativity is that ABB's furnish a coordinate independent measure of chaos. While this is not an issue in special relativity, the ABB's continue to recommend themselves as a measure of chaos since they do not require long-lived orbits.

In chaotic systems the ABB will lie on a fractal set, while in non-chaotic systems they will not. Using this approach does not have the problems associated with finite time capture. In fact the faster the capture the better since it reduces computational time. To determine if the ABB lies on a fractal set measures the fractal dimension of the ABB. One of the distinguishing features of fractal sets is their non-integer fractal dimensions. This gives us an unambiguous way of determining the chaotic nature of the system.

If the y-axis is chosen so that it is perpendicular to the plane of motion, then the ABB's lie in a four dimensional phase space. Clearly, it is not possible to generate graphics

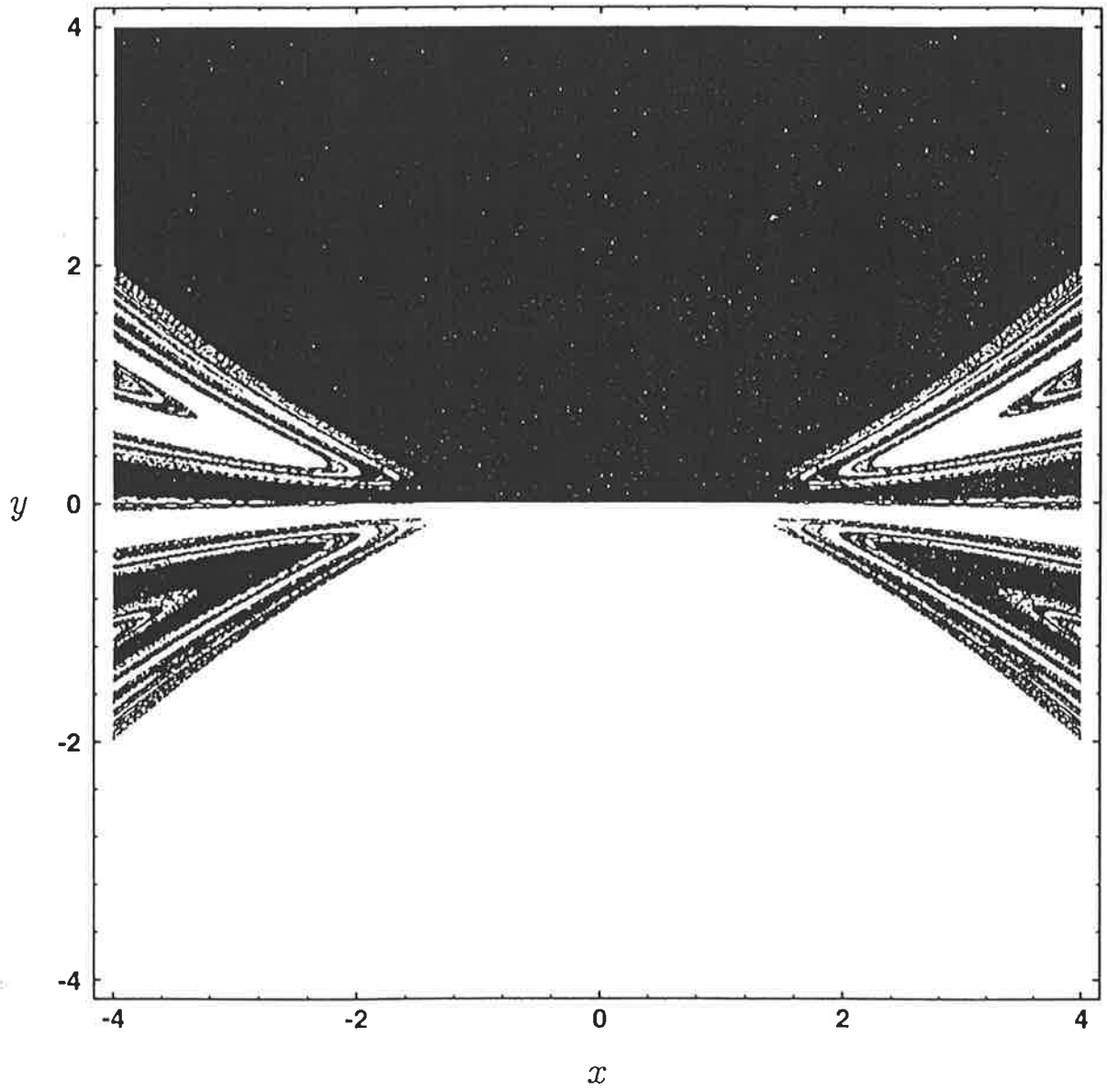

Figure 6.3: A section of attractor basins for $\pi = 0$ and $\mathcal{F} = 1$.

for these. A two dimensional slice of this phase space must be taken in order to generate tangible pictures. All the ABB's generated for this chapter are on a 840×840 grid, and are generated in the same manner as Fig. 6.2. Most of the phase space slices are done by setting the initial momentum to zero. This not only reduces computational time, by enabling most trajectories to be captured, but makes comparison with the general relativistic study easier.

The ABB for $\mathcal{F} = 1$ is shown in Fig. 6.3. Notice that it appears to have all the expected symmetries. One of the most fascinating features of this image is the large portion of the ABB that appears to have a fractal nature. Repeated magnification of this image, Figs. 6.4, 6.5, 6.6, reveals detailed structure on finer and finer scales. This is one of the properties that all fractals have in common. Punctuated between these regions of fractal phase space are regions which are distinctly non-fractal. This suggests that there are regions of stability within regions of chaos.

Having decided what slice of the ABB phase space to measure, the next step is to find the fractal dimension. There are a number of definitions of fractal dimensions in the literature. The one that is used here is called the box dimension [92]. It will be used because of its ease in computation and of its frequency in the literature.

Consider the bounded set F, which is a subset of R^n, then $N_\epsilon(F)$ is the least number of sets of cubes of length ϵ which completely covers the set F. By definition the box dimension for F is

$$\dim_{BF} = -\lim_{\epsilon \to 0} \frac{\ln N_\epsilon(F)}{\ln \epsilon}.$$

Because our set is not defined by any known iterative map it is not possible to find the dimension analytically. Consequently computational techniques are used. From Eq. (5.3.2) one sees that the negative gradient of $\ln N_\epsilon$ versus $\ln \epsilon$ gives us the box dimension.

The set to examined is the set of points which lie on the ABB in some region of phase space. To do this the whole region of interest is covered by a grid. Cubes of length ϵ are construcited from this grid. If a cube contains two more grid points that fall into different attractors then that cube lies on the ABB. Put more formally, each point x_i has an attractor associated with it A_{x_i}. A cube $B(x_0, \epsilon)$ of length ϵ and centred at x_o is said

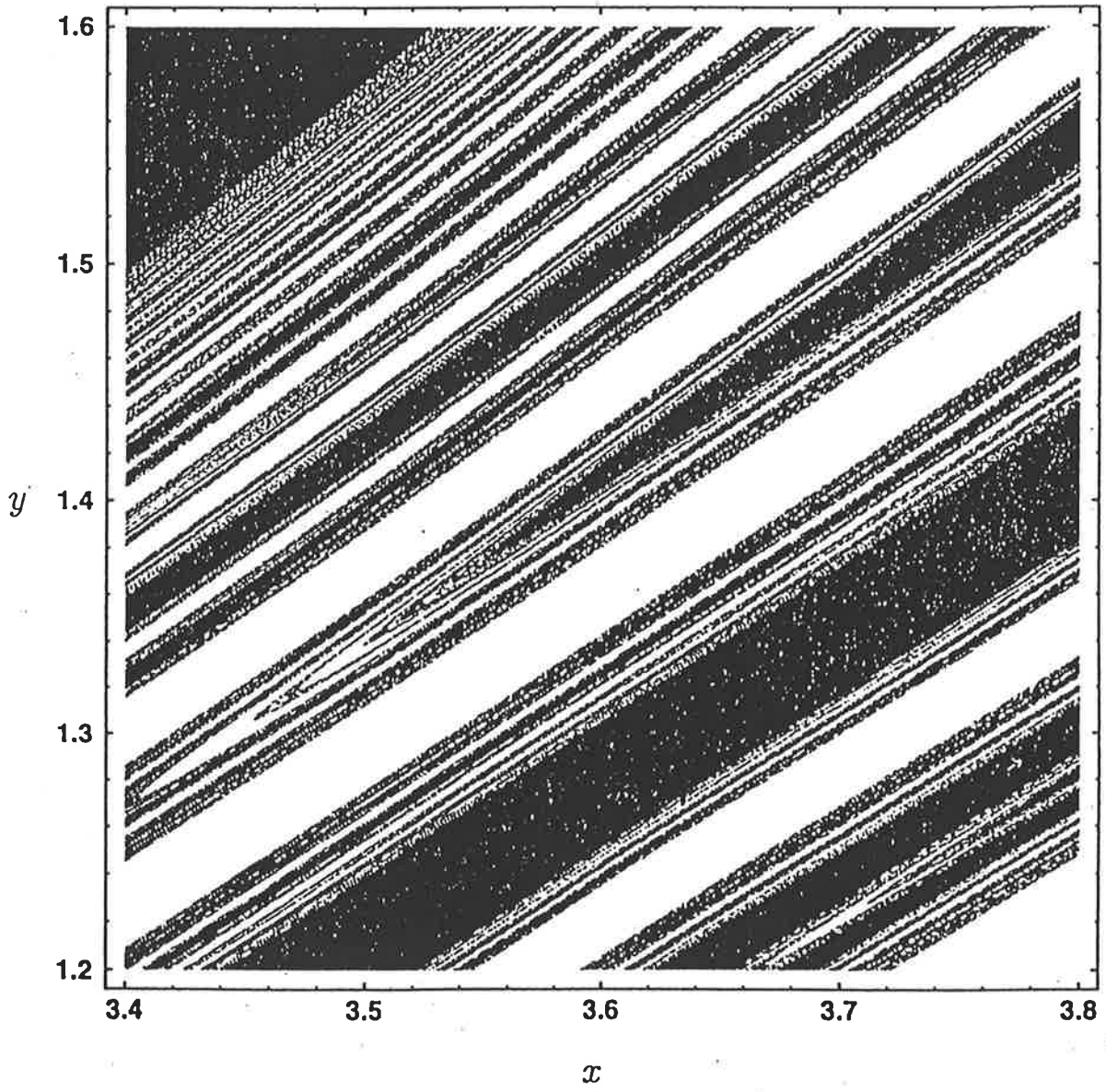

Figure 6.4: Magnification of Figure 3

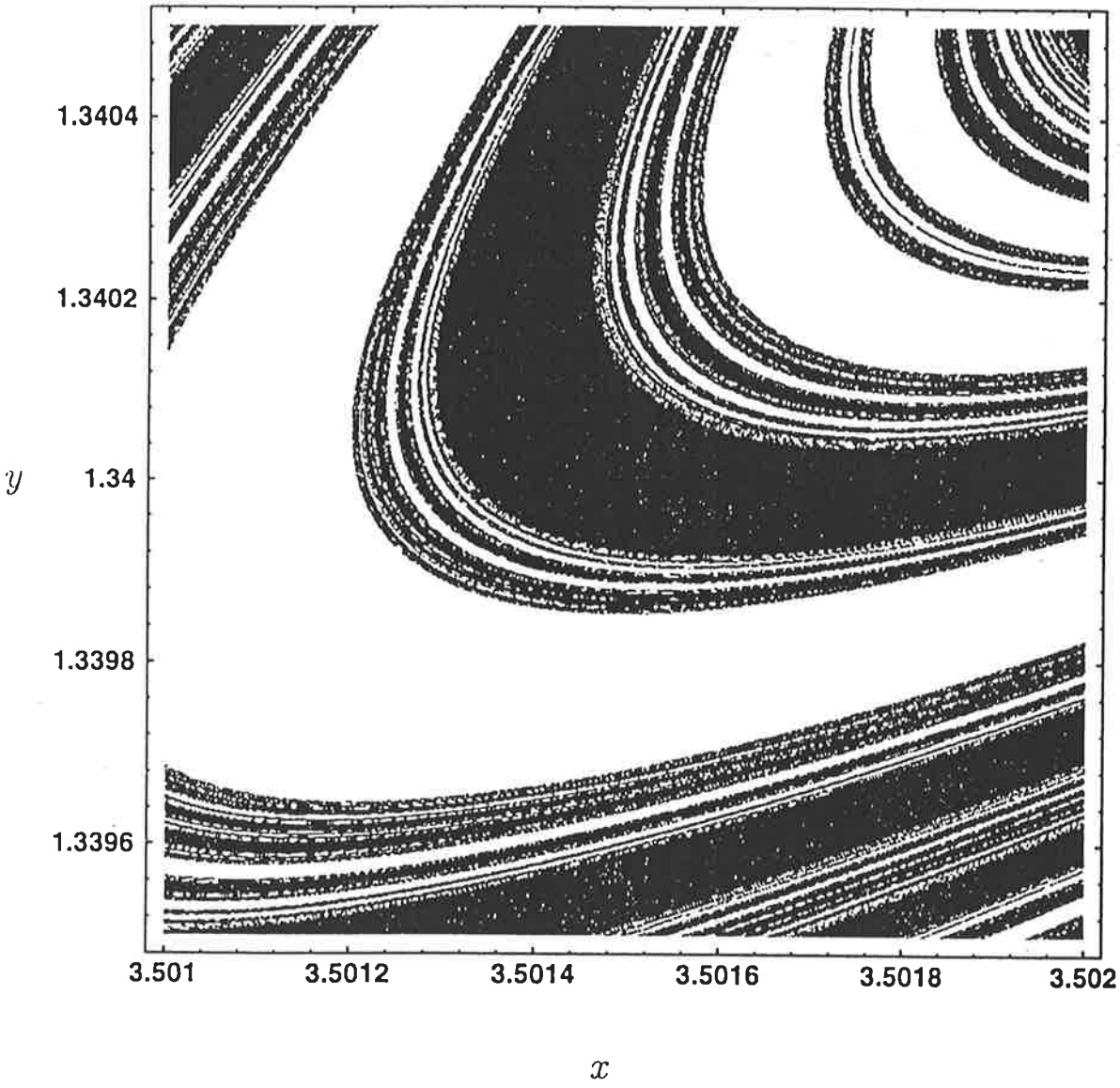

Figure 6.5: Magnification of Figure 4

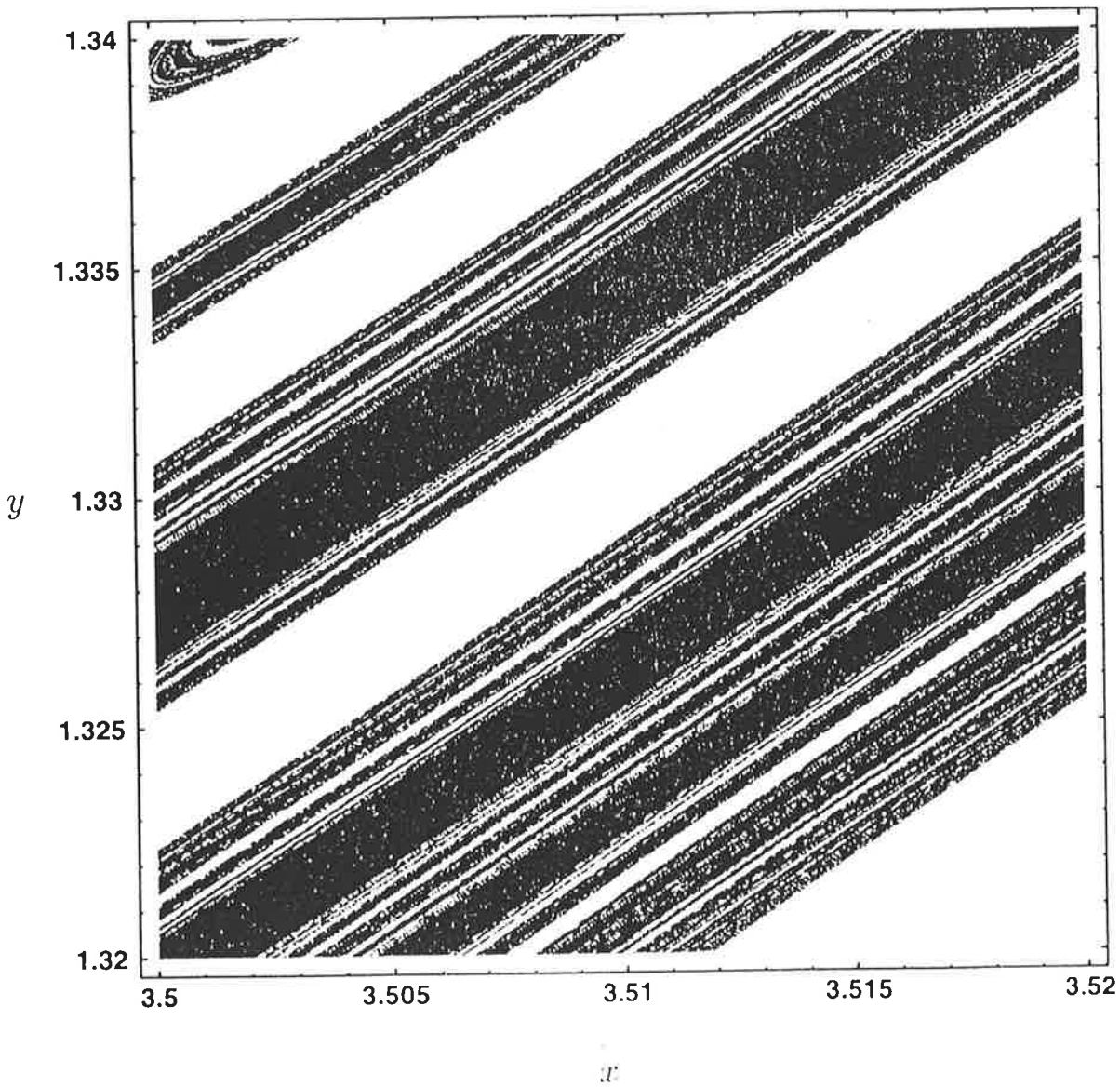

Figure 6.6: Magnification of Figure 5

to lie on the ABB if

$$\forall \epsilon > 0 \; \exists \; x_1, x_2 \; : \; \{x_1, x_2 \in B(x_0, \epsilon)\} \text{ and } \{x_1 \neq x_2, A_{x_1} \neq A_{x_2}\} \tag{6.4.2}$$

To find the limit in Eq. (5.3.2) the number of cubes N_ϵ of length ϵ that lie on the ABB are counted. This is repeated for as many values of ϵ as possible. Plotting $\ln N_\epsilon$ against $\ln \epsilon$ gives a straight line. The gradient of this line, which is the negative of the box dimension, is calculated using a chi-squared fit.

In order to maximise the accuracy in calculating the box dimension the greatest number of values for ϵ is needed. The implication being that the size of the grid should be chosen so that as many combinations of cubes as possible completely cover the phase space slice. Therefore, the attractor basin is divided into an 840×840 grid since 840 has 31 factors. This is the largest number of factors for any number below 1000, the number chosen as an upper limit due to program running time.

The box dimension for Fig. 6.7 was calculated in the manner described above. The result is shown in Fig. 6.8. This figure shows that most of the points do in fact lie on a straight line. This gives us confidence that these images are in fact true fractals and not just round off errors in the computer.

On closer inspection it can be seen that for large ϵ their seem to be to many cubes (a cube is a square in two dimensions) that lie on ABB. The reason for this is quite clear. If ϵ is too large, i.e., by dividing the phase space into four sections, then all the cubes will most likely contain both black and white. This means essentially that all cubes lie on the boundary, i.e., we have over counted.

A second and slightly more subtle complication occurs for small ϵ. From Eq. (5.3.2) it would seem that the smaller the value of ϵ the better. The problem comes about because the colour of a sub-cube is defined by only one point in that sub-cube. Imagine for example that that sub-cube lies on the boundary and is half filled with black and half with white. This would mean there was a 50/If our cube ϵ was made up of four such sub-cubes then there would be a 1/8 chance that this cube would not be counted as being on the boundary. If ϵ was made up of nine such sub-cubes then there is a $(1/2)^8$ chance that it will not be counted. For this reason their will be fewer counts than expecited for small ϵ.

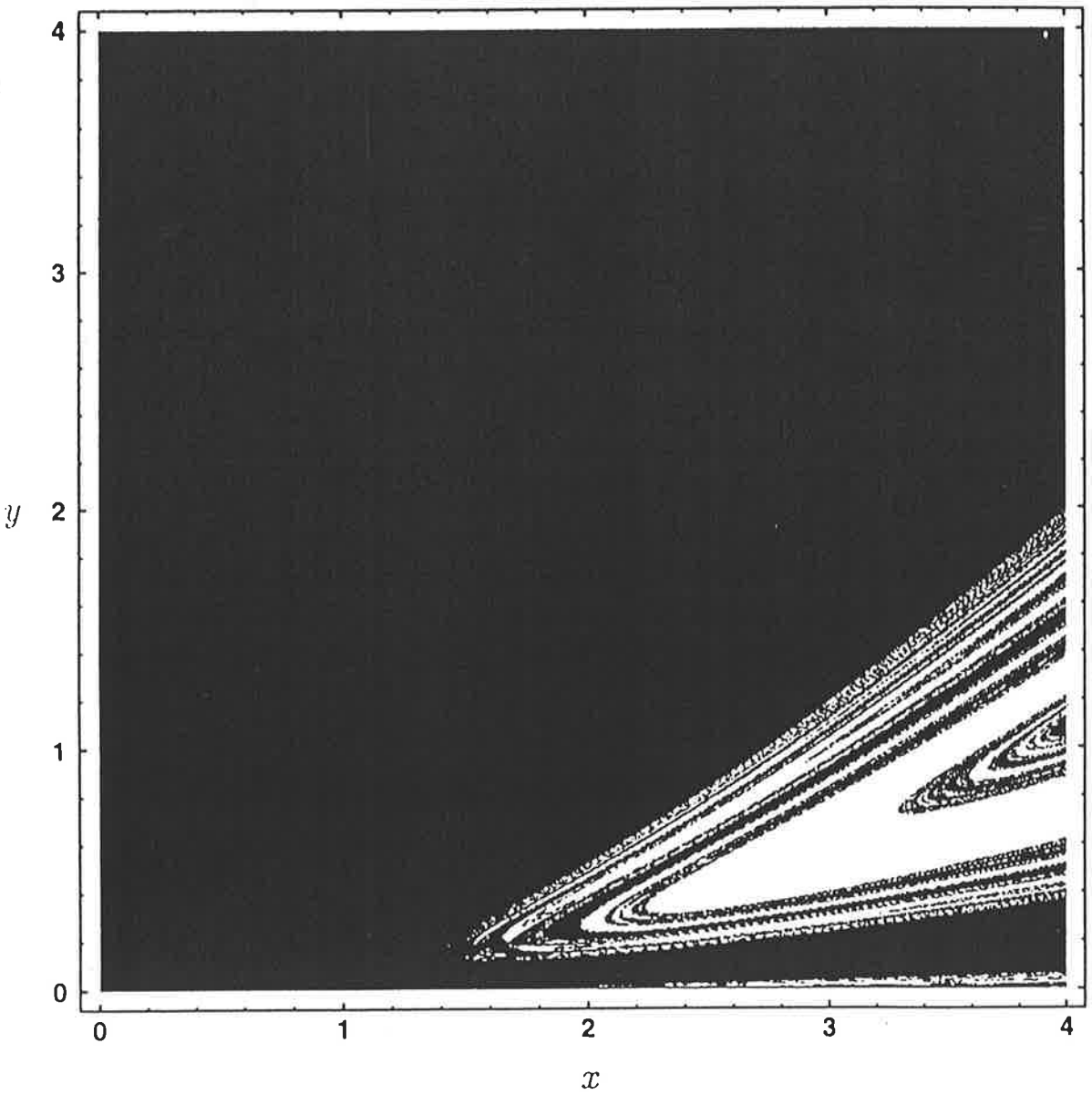

Figure 6.7: A subsection of the attractor basins boundary

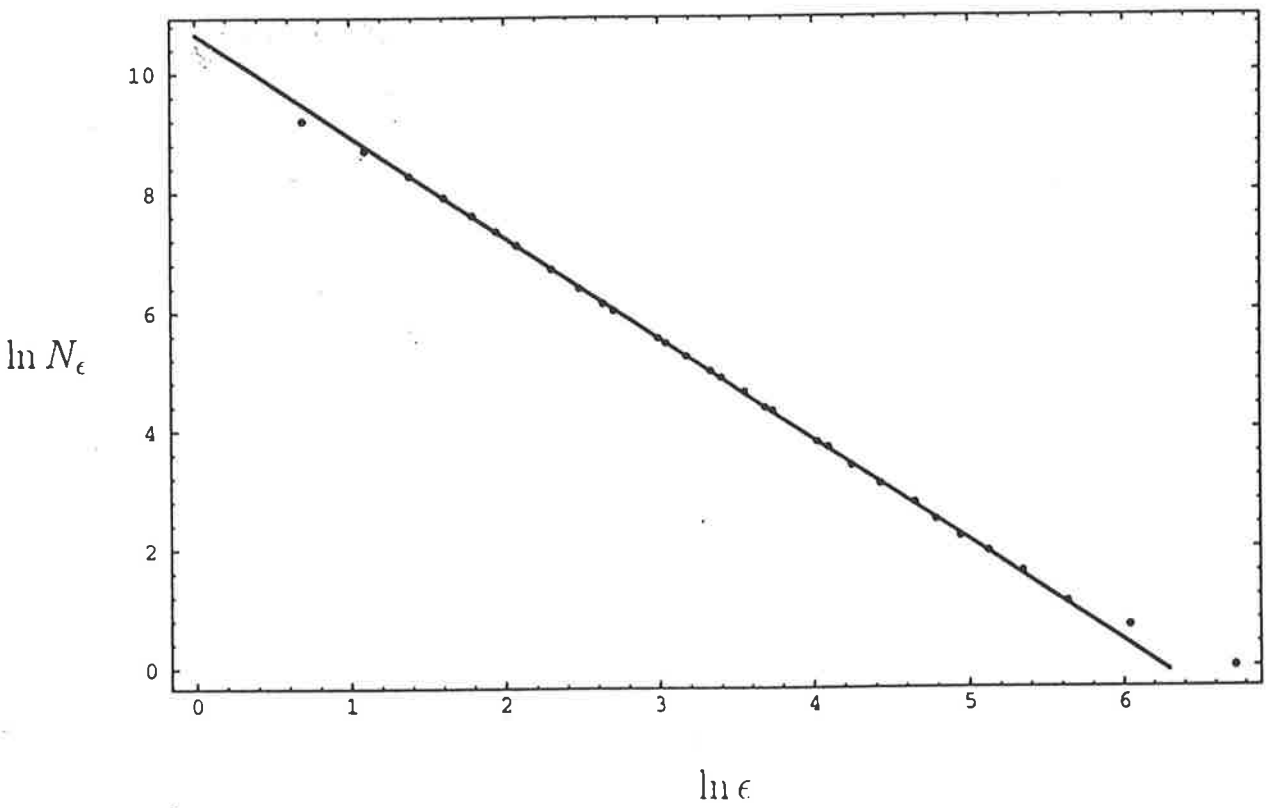

Figure 6.8: Calculation of box dimesion for $\mathcal{F} = 1$.

To eliminate both these errors the the first three and last six points of Fig. 6.8 are removed before determining the gradient. The result is that the fractal dimension of the ABB for Fig. 6.3 and hence Fig. 6.7 is $d_B = 1.75 \pm 0.01$.

6.5 Dependence of fractal structure on $\mathcal{F}$

Since the ABB is used as a measure of chaos in the system it is imparative to understand it depends on the field strength. It is of fundamental importance not only to determine whether or not a system is chaotic, but how the chaotic nature changes with the fundamental parameters. Figs. 6.9 to 6.12 show a major change of fractal structure in different regions and for different values of $\mathcal{F}$. The graphics make the differences explicitly apparent. To study this strong dependence on $\mathcal{F}$ it is adjusted then the box dimension is remeasured. However, the dimension for a given scaling parameter $\mathcal{F}$ varies depending on the portion of the attractor basin examined. For this reason the box dimension is measured within the same relative region each time. How the region is chosen is related to the scale point, described below. Apart from the box dimension there is also another measure of the onset of chaos in the system. For the purposes of this thesis it is called the scale point P. The scale point is the smallest value of x at which a particle with zero initial momentum does not fall into the nearest charge. This point represents the least lower bound of the fractal set. As such, it indicates that a set of unstable trajectories with non-zero measure exist beyond this point.

The scaling point leads naturally to deciding what region of phase space the box dimension is measured for. Somewhat arbitrarily, the box dimension for each $\mathcal{F}$ is measured in a square of phase space whose length is five times P. Each square is located so that the bottom left hand corner is at the origin.

Figs. 6.13 and 6.14 show how the dimension and scale point vary with $\log \mathcal{F}$. The error bars in Fig. 6.13 are the standard deviation of points from the line of best fit used to determined the gradient. In both cases it is clear that there exists a functional relationship between $\mathcal{F}$ and what is being measured. Determining this functional relationship is not trivial. Both plots show that for $\mathcal{F} \leq 20$ the fractal nature of the ABB changes quite

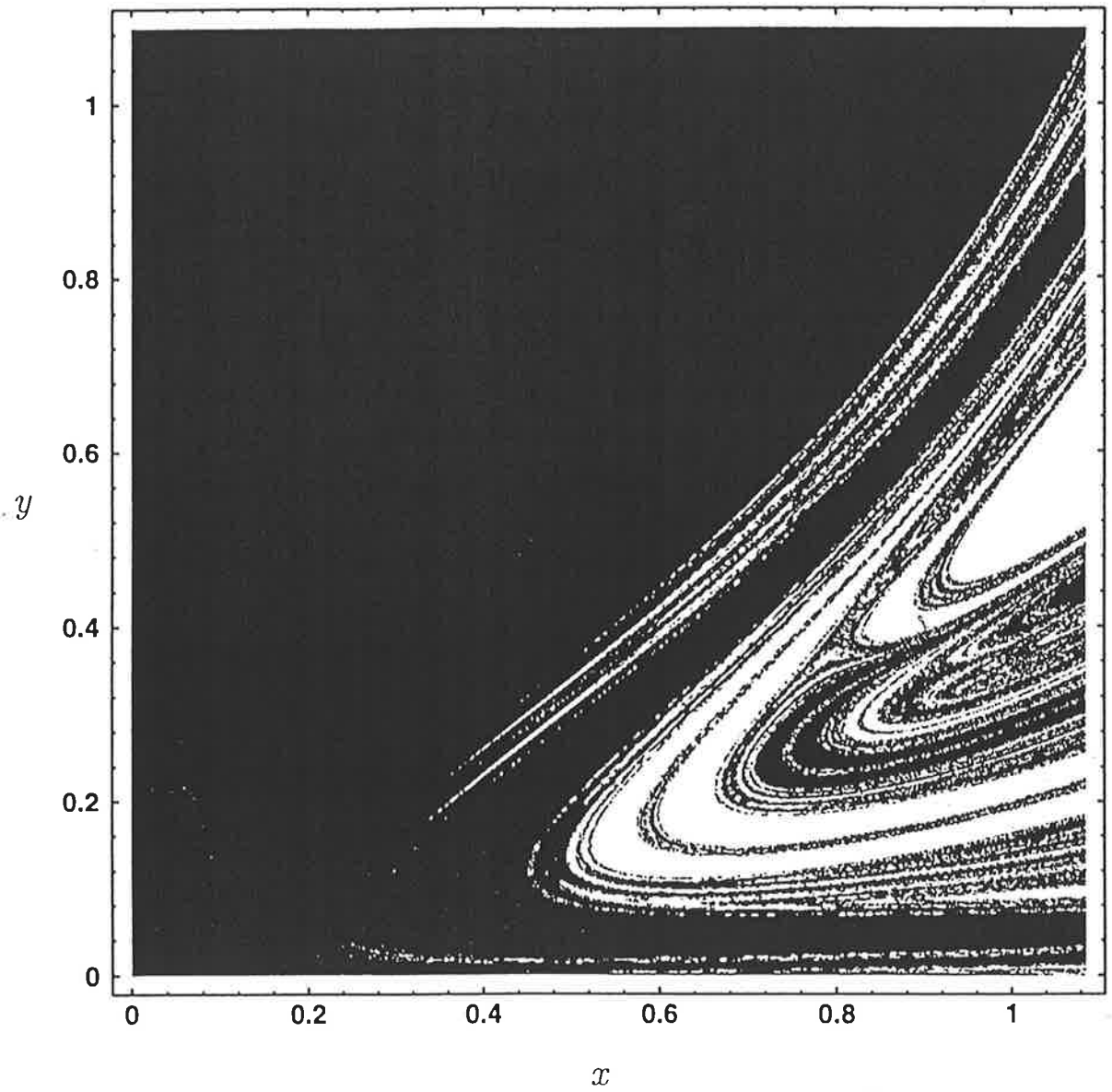

Figure 6.9: A section of attractor basins for π =0 and $\mathcal{F} = 0.03$

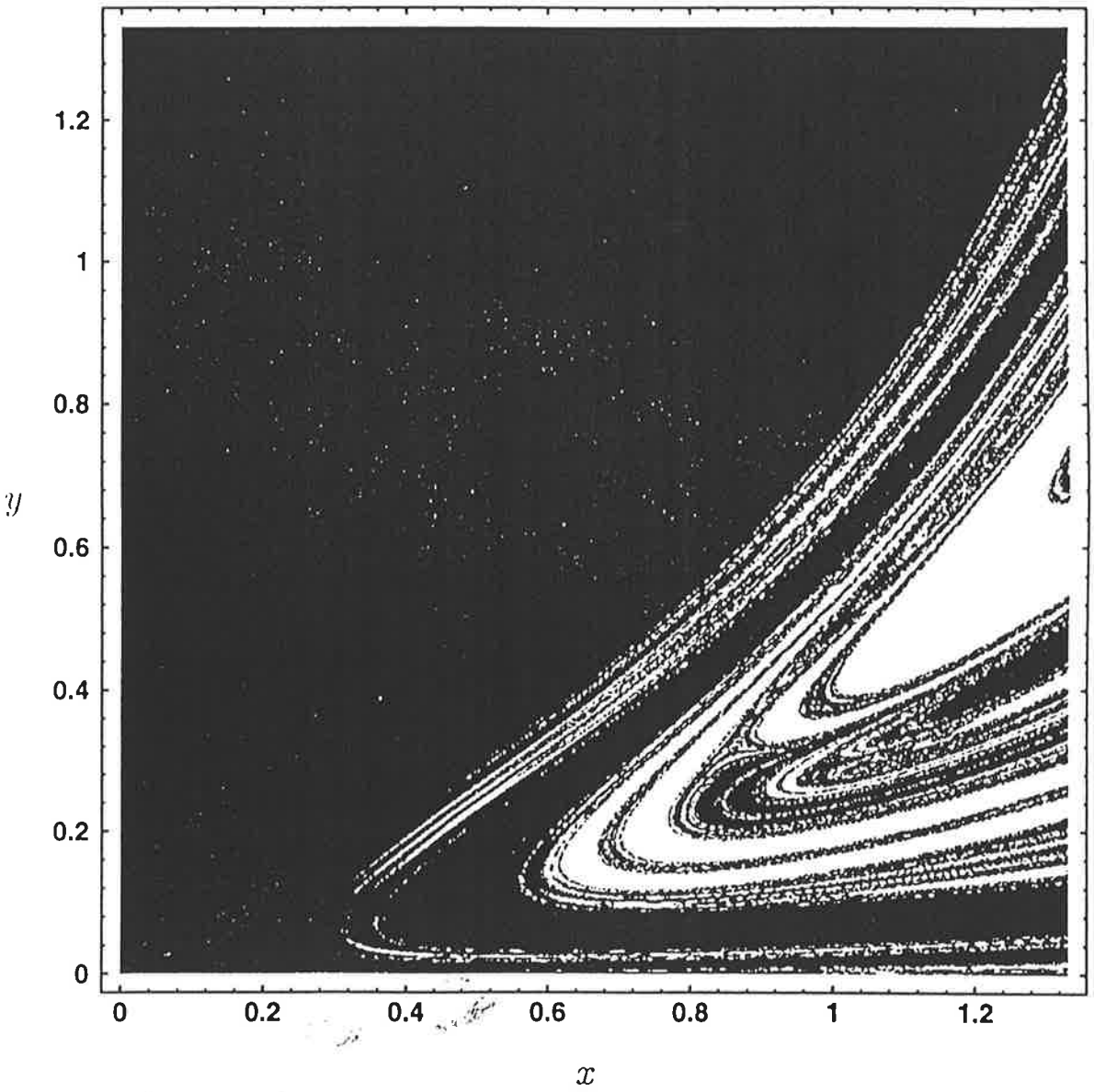

Figure 6.10: A section of attractor basins for π =0 and $\mathcal{F} = 0.05$

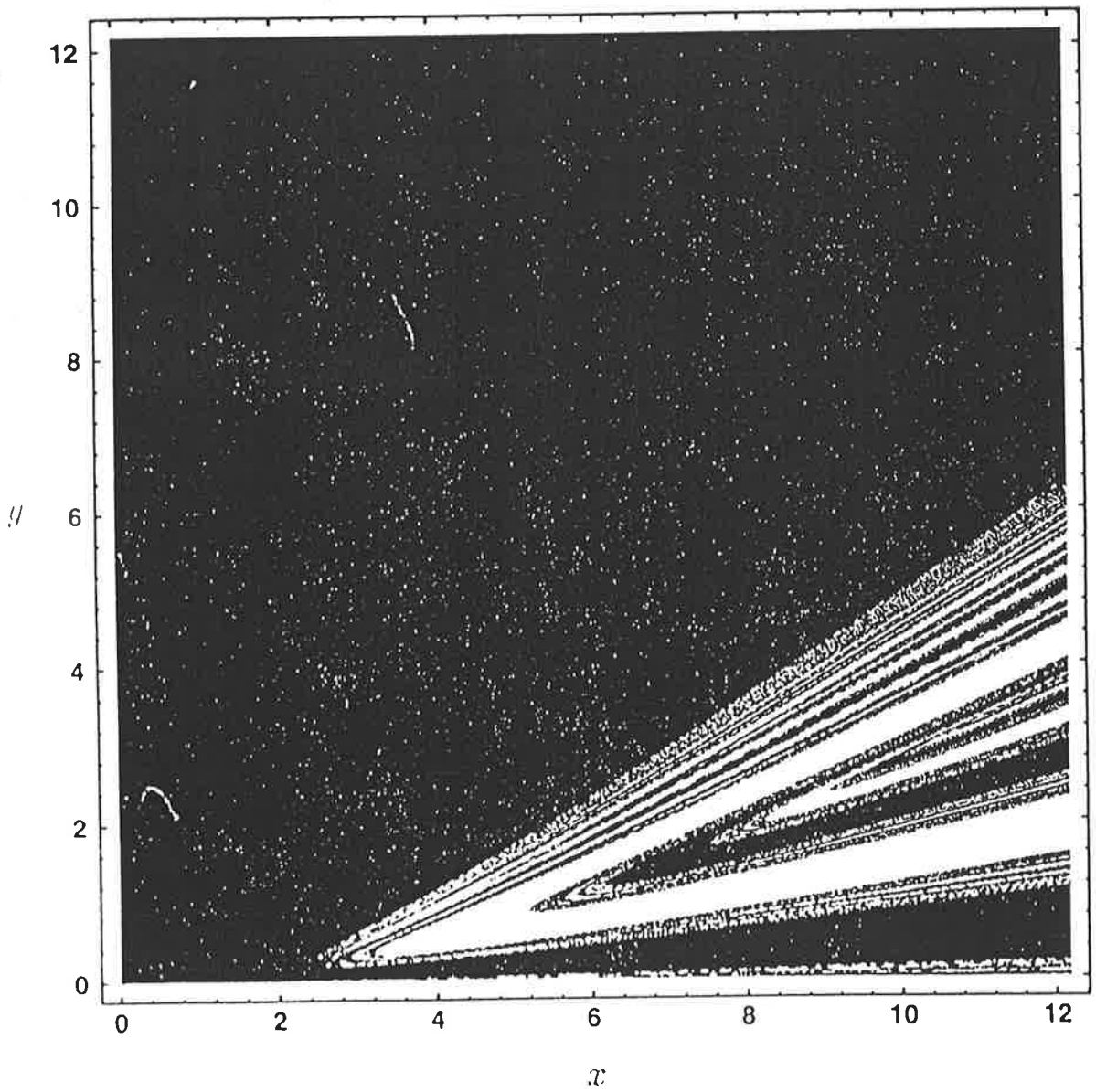

Figure 6.11: A section of attractor basins for π =0 and $\mathcal{F} = 3$

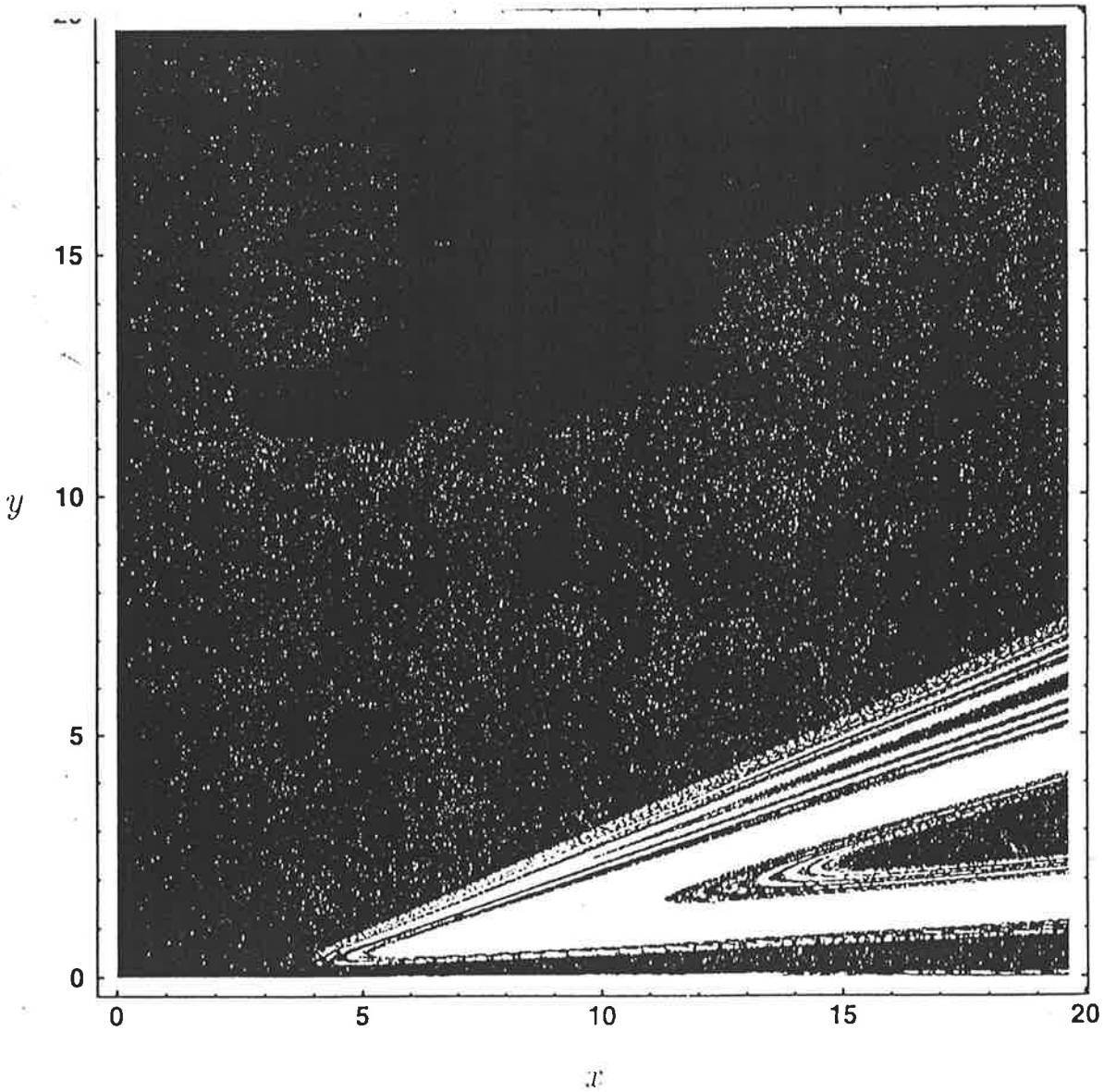

Figure 6.12: A section of attractor basins for π =0 and $\mathcal{F} = 50$

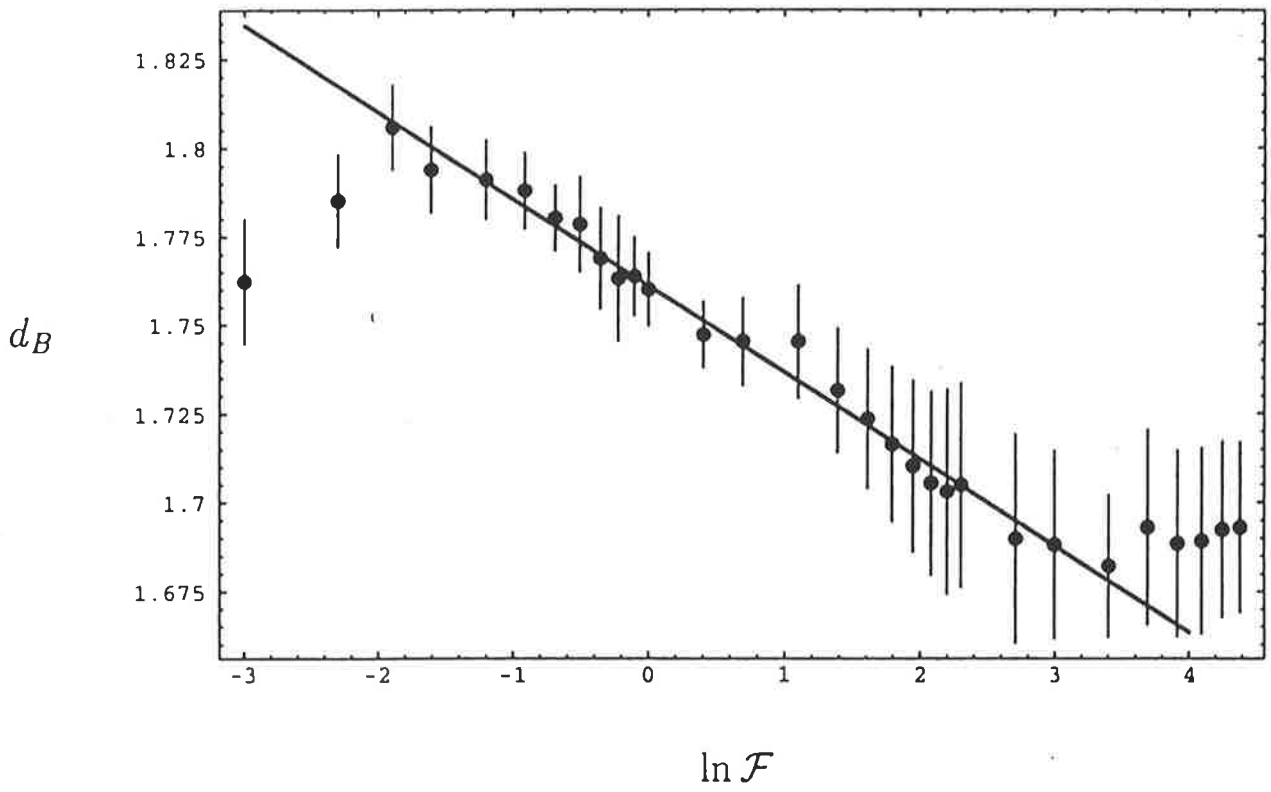

Figure 6.13: The effect of varyng $\mathcal{F}$ has on the box dimension.

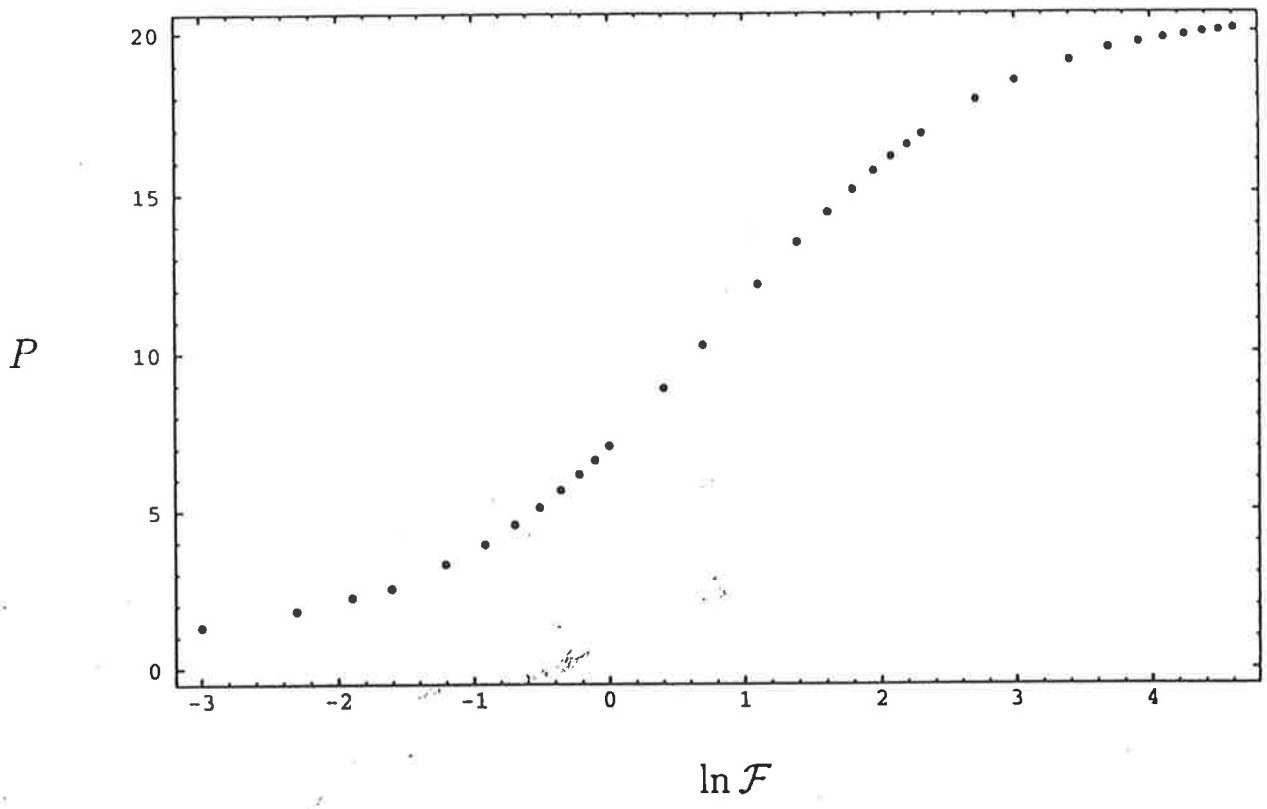

Figure 6.14: The effect of varyng $\mathcal{F}$ has on the scaling point

dramatically. In this region both the box dimension and scale point are both very sensitive to $\mathcal{F}$. For values of $\mathcal{F} \geq 20$ the scaling point and box dimension seem to approach a limit.

Fig. 6.13 can reasonably be fitted to a straight line for values of $\mathcal{F}$ between about 0.15 to 30. In this region the functional relationship between box dimension d_B and $\mathcal{F}$ is

$$d_B \approx 1.76 - 0.02 \log \mathcal{F}. \tag{6.5.1}$$

Fig. 6.14 on the other hand can not reasonably be fitted to a straight line for any significant range of $\mathcal{F}$ values. Its characiteristics resemble more of an arctan type function.

These results now complete the study of the relativistic fixed two centre problem. This work and the work on the general relativistic problem has shown that the fixed two centre problem is chaotic. In fact, the Newtonian limit is unique in that it is integrable. The chaotic nature of this system is nicely shown by the fractal nature of the ABB.

6.6 Conclusion and further work

This work has established that the simplest three body problem, motion with two fixed centres, is not integrable when special relativistic effects are taken into account. While this result has already been discovered in the context of general relativity [5], it is now realised that it is not due to any exotic behaviour caused by black holes. In particular, it should not be attributed to the non-linearity of the gravitational force. Chaos is present even when the potentials generated by the two centres obey the superposition principle. Clearly, it is the relativistic description of the kinematics, and not the loss of the superpostion principle, which renders the special and general relativistic two centres problem chaotic. To be specific, it is the nonlinear way in which the potential energy enters the relativistic Hamiltonian that renders the dynamics nonintegrable.

Our study can be summarised as follows. After establishing that radiation reaction could be neglecited, the Hamilton-Jacobi method was employed to discover under what conditions the system was integrable. The integrable cases were found to include Newtonian type orbits. For non-Newtonian orbits some properties unique to the relativistic Hamiltonian were found. One of these properties was the capture of particles with non-

zero angular momentum. This meant that relativistic particles could spiral into one of the charges within a finite time. As a consequence of this a study was done of the attractor basin boundaries. These ABB's turned out to be fractals and hence indicated that the system was chaotic. To study how the fractals changed with $\mathcal{F}$, both the scaling point and box dimension were examined.

Though this study is comprehensive, there is still further work that could be done. For example, radiation effects could be added. This would mean that orbits which are not ultra-relativistic will be captured due to loss of energy. Some other dissipative force such as a viscous drag could also be included. Lyapunov exponents could be calculated for orbits that do not terminate in a finite time. A possible connection between the dimension of the ABB and the magnitude of the Lyapunov exponents could also be investigated.

Chapter 7

Conclusion

7.1 Exact solutions to Einstein's field equations for stationary axisymmetric spacetimes.

The first part of this thesis addressed the problem of obtaining exact solutions to Einstein's field equations describing rotating perfect fluids. The way in which the topic was handled was the following:

- Understand how and why the Newman-Janis algorithm (NJA) is successful in generating exact solutions to Einstein's field equations.
- Establish whether the Newman-Janis algorithm can be used to obtain exact solutions of rotating perfect fluids. Below is a point summary of the technique to generate solutions without solving Einstein's equations explicitly.
- As the Newman-Janis algorithm is shown only to be successful in generating vacuum solutions, determining whether a simple generalization exists making it possible to generate non-vacuum solutions.
- The GNJA generates a class of metrics whose physical properties can not easily be evaluated. On the other hand it is a relatively simple task to determine which of them can be matched smoothly to the Kerr metric. It therefore makes sense to evaluate conditions under which metrics can be joined smoothly to the Kerr metric on static axisymmetric hyperesurfaces.

- As the GNJA generates solutions whose physical properties can not be easily calculated it is important to establish that at least in the static limit they describe perfect fluids.

Having only got partial solutions by applying the GNJA the next chapter took the more general approach of developing theorems for stationary axisymmetric spacetimes representing rigidly rotating perfect fluids. Once again a point form summary of the procedure is given.

- Write the canonical form of stationary axisymmetric metrics.
- Prove that if the metric represents a perfect fluid then that fluid has a four velocity given by $U^\alpha = A(\delta^\alpha_t + \Omega\delta^\alpha_\phi)$.
- Prove that the fluid is shear-free if and only if Ω is a constant.
- Calculate the vorticity vector ω^α and make a rotation so that the only non-zero component of ω^α is in the $\hat{z}$ direction.
- The alignment of the ω^α in the $\hat{z}$ direction provides a relationship between $g_{tt}, g_{t\phi}, g_{\phi\phi}$ and an arbitrary function $F(x)$. This can be used to simplify the canonical form of the metric further.
- Alignmet of the vorticity vector can be used to provide a generalization of the Newtonian concept of centrifugal force.

7.1.1 An explanation of the Newman-Janis algorithm.

To find exact solutions the idea was to apply the Newman-Janis algorithm (NJA) to non-rotating perfect fluid "seed" metric and generate rotating perfect fluids. The notion that this might be possible comes from the success of the NJA in generating rotating blackhole solutions from non-rotating ones. Herrea and Jiménez have used the NJA to generate stationary axisymmetric metric tensors from static spherically symmetric ones [27]. The solution found by Herrea and Jiménez is which can be joined smoothly to the Kerr metric. The solution obtained by Herrea and Jiménez can only be considered partially successful

as it does not remove any of the ambiguities stemming from the original formulation. Another shortcoming of the Herrea and Jiménez solution is that in the static limit ($a \to 0$) the pressure is anisotropic, $P_r \neq P_\theta$.

Part of the problem associated with the NJA is the uncertainty of why it actually works. Chapter 2 sets out the NJA as a specific (perhaps overly) five step procedure. This process ensures that all ambiguity present in the original derivation is removed. It was shown in chapter 2 that the NJA produces a stationary metric containing only two arbitrary single variable functions, $j(r)$ and $k(r)$. Results of chapter 2 concluded that no perfect fluid metrics could generated by the NJA, except the trivial case of $P = \varrho = 0$, and that the only algebraically special metric generated by the NJA, with a vanishing Ricci tensor is the Kerr-Newman metric.

It could be argued that the requirement the fluid be perfect, in the sense of having isotropic pressure, should be relaxed, as it places too large a constraint on the metric. From a physical point of view (as opposed to mathematical) to justify the consideration of non-isotropic pressures one would need to successfully argue that the random motion of the gas particles had a preferred direction. For solids, such as graphite, the directional nature thermal motion is observed and understood. Graphite forms large connected planar surfaces, which slide smoothly parallel to each other, but do not move so freely in directions perpendicular to planar surfaces. It is therefore important to consider anisotropic pressures as well. The most stringent limit on the NJA is not placed by the the isotropic pressure condition, but the vanishing of $G^{r\theta}$. This condition requires that $k(r) = r^2 + a^2\cos^2\theta$. A consequence of this is that $\exp\Phi = \exp -\lambda$. In the static limit ($a = 0$) the only metric with $\exp\Phi = \exp -\lambda$ which are perfect fluids and have the equations of state $P = \varrho$. Solutions of this type have a speed of sound equal to the speed of light, and as such should not be considered as physically sensible.

7.1.2 Generalizing the Newman-Janis algorithm.

Relaxing one of the conditions on the NJA, namely that $1/r \to 1/\tilde{r}$, provides a generalization of the NJA (GNJA). The advantage of this generalization is that rotating perfect fluids may be generated. The disadvantage is that the metric becomes one for which exact

solutions pertaining to rotating perfect fluids are difficult to find. Chapter 3 shows that the GJNA generates metrics which can be matched smoothly to the Kerr metric and represent perfect fluids in the static limit. It still remains to be seen whether or not metrics generated by the GNJA are perfect fluids in the non-static limit. The full physical properties of the "trial" solution generated by this procedure could only be explored in the static limit. The static limit of these solutions were found to be perfect fluids and "physically reasonable". The term "physically reasonable" refers to the fact that, the strong and weak energy conditions are obeyed, both P and ϱ are monotonically decreasing functions of the radial coordinate r, Pressure and density are related by and equation of state. Though the trial solution did have infinite pressure and density at the centre it was not considered grounds for being dismissed as unphysical as the total mass and energy remained finite.

A whole class of metrics generated by the generalized Newman-Janis algorithm is waiting to be explored the hope is that one day it may be used to obtain a perfect fluid solutions to the Kerr metric.

7.1.3 Canonical form of stationary axisymmetric rigidly rotating perfect fluids.

Some theorems were developed in chapter 4 regarding the metric properties of rigidly rotating perfect fluids. In particular it was proven that stationary axisymmetric spacetimes written in canonical coordinates $x^\alpha = \{t, x, z, \phi\}$ have a four velocity given by $u^\alpha = A(x,z)\left(\delta^\alpha_t + \Omega(x,z)\delta^\alpha_\phi\right)$ and are shear-free if and only if Ω is a constant. It was further shown in this chapter that the canonical form of (SAS) metrics can be simplified further if an angular rotation is made so the fluids vorticity vector is defined in the $\hat{z}$ direction.

Defining the vorticity vector to be in line with the $\hat{z}$ axis lead naturally to the formulation of a relativistic version of centrifugal force. Though this result was not used in the context of obtaining interior solutions to axisymmetric perfect fluids it was pointed out that is helpful in the comparison between Newtonian results and relativistic ones.

7.2 The onset of chaos in the Hill's reduced model

Part 2 of the thesis dealt with a completely different aspect of relativity, namely the chaotic nature of relativistic dynamics. The question posed was whether or not the known chaotic nature of geodesics in the relativistic fixed two centre problem is due to the non-linear nature of general relativity or the kinematic properties relativistic mechanics. The way in which the chaotic nature of special relativity was examined is as follows:

- Propose a model in which chaos is known not to occur in the Newtonian physics, known to occur and general relativity and which is not studied in special relativity.
- Determine what features of the special relativistic Hamiltonian differ from the Newtonian one.
- To establish whether the system is chaotic numerically integrate trajectories in the non-Newtonian region.
- Measure the chaotic nature of the system by evaluating fractal nature of the attractor basin boundaries.
- Try to understand how the chaotic nature of the system varies with the fundamental parameters, such as, magnitude of charges, separation of charges, masses of particles.

The model chosen for the study of chaos in special relativity in this thesis was the special relativistic version of the fixed two centre problem. This model was chosen as it is ideal for addressing the question that part 2 of the thesis was concerned with, whether chaos in general relativity was due to the non-linear nature of general relativity. The fixed two centre problem (or Hill's reduced model) has the advantage of being one of the few three body problems in Newtonian mechanics which is exactly solvable. What is special about the Hill's reduced model is that the Newtonian Hamiltonian is separable in prolate spheroidal coordinates. In both special and general relativity the seperability no longer occurs which suggests, but does not prove, that the system may be chaotic.

As capture occurs for a large number of phasespace trajectories in the relativistic (both special and general) fixed two centre problem the system has attractor basins associated

with it. Chaos in attractor systems can be determined by examining the nature of the attractor basin boundaries. For Hamiltonians in which the attractor basin boundary lies on a fractal set the system is chaotic. It was for precisely this reason that the chaotic nature of the Hill's reduced model was investigated via the use of fractal attractor basis boundaries. The fractal nature was examined by determining the Hausdoff box dimension of the attractor basin boundary sets. Hausdoff box dimension was calculated by dividing the attractor basin boundary set into N_ϵ cubes of size ϵ and evaluating

$$-\lim_{\epsilon \to 0} \frac{\ln N_\epsilon}{\ln \epsilon}$$

Variation of box dimension d_B with the electro-static potential scale parameter $\mathcal{F}$ and the onset of chaos scale parameter P were investigated. It was found that a comparatively simply analytic relationship exists between the box dimension and each of the parameters P and $\mathcal{F}$. The reason for this the existence of this relationship is not known.

7.3 Axisymmetric spacetimes

The conclusion drawn from the studies of parts one and two is that the properties of relativistic stationary axisymmetric spacetimes are quite different from what is found in Newtonian physics. It is clear that more exact results are required in general relativity if we are ever to fully appreciate what all its consequences are. What both of the two parts of this thesis do is point how inadequate a Newtonian approach to relativity often is. It is a disappointing fact that while Newtonian physics often provides inadequate or even wrong explanations to physical phenomenon, it is so much easier to calculate with. It is precisely the lack of exact solutions in general relativity that motivated the work of part 1. Until such time as exact solutions are found describing the interior geometry of rotating stars it is impossible to conclude what further results, counter to our Newtonian intuitive will occur.

Fortunately in the modern era the popularity and ease of use of computer algebra programs mean that the acquisition of exact solutions is made a lot easier. It is no longer necessary for a physicist to grind through the pages of algebra in order to obtain the Einstein's tensor from the metric tensor. The thereoms of chapter 4 relied very heavily

on the use of algebraic computation in order to attain the results. Theit is some object to computational proofs because they can not reasonable be check by human beings. The answer to this is that is why they are so useful, their is simple on other way to do thereoms of this kind. It is hoped that the work of Part 1 will eventually be used to an exact solutions to either the Kerr interior or the interior of a rigidity rotating perfect fluid.

Computers also make it possible to examine functions for which exact solutions can not be found. Studies of chaos emphasize how essential computers are to the modern physicist. It is impossible to conceive how the conclusions of part 2 could have been made without computational integration. The results of part 2 illustrate once again that relativistic effects lead to results which are completely absent in the Newtonian limit. The onset of chaos of relativistic systems is an area which requires further exploration. The results of this work demonstrate that relativistic kinematics is enough to introduce chaos into an otherwise integrable system. The results of this still need to be fully realized but it is now appropriate that chaos is not simply due to the non-linear nature of general relativity.

A

APPENDIX ON ISRAEL BOUNDARY CONDITIONS

The problem of matching two separate space-times on a common surface is a well explored area of general relativity. A large number of papers exist on the subject, and now an algebraic programme [66] is available to speed up calculations. However Israel's original paper [94] still remains a definitive work on the subject. Although the formalism was originally developed to examine the motion of expanding bubbles in the universe it has applications that range far wider. This appendix esstential follows the same lines as introductory section of [95]. Consider two spacetime manifolds M^+ and M^- seperated by a hypersurface Σ. For any spacetime dependent quantity X one must specify the region of space-time in which it is to be calculated. The notation X^+ means that the quantity X is calculated in the exterior space-time geometry M^+. The notation $X^+ \mid_s$ signifies that the value X is calculated in M^+ and evaluated at the surface. Lastly $[X] \equiv X^+ \mid_s - X^- \mid_s$ measures the jump discontinuity in the value of X as calculated by the two metrics and evaluated at the surface. Two spacetimes are said to match smoothly both the first and second fundamental forms are continous on the hypersurface Σ.

A.1 First junction condition

Let $\{x^\mu\}^+ \left(\{x^\mu\}^-\right)$ be an arbitrary coordinate system in the $M^+ (M^-)$ region (the greek indices take four values and numerate components of four-dimentional tensors while latin

indices take three values and numerate components of the three-dimentinal tensors of the hyperspaceΣ), and $\{\xi^i\}$ be an arbitrary coordinate system on Σ. The metric $g^+_{\mu\nu}$ $\left(g^-_{\mu\nu}\right)$ determines the geometry on the M^+ (M^-) region :

$$\begin{aligned} ds^2 &= g^{\pm}_{\mu\nu} dx^\mu dx^\nu \\ &= \epsilon dn^2 + {}^3g_{ij}\xi^i\xi^j. \end{aligned} \tag{A.1.1}$$

Where ϵ is defined as being -1 for timelike surfaces $+1$ spacelike hypersurfaces and for null hypersurfaces $\epsilon = 0$. The first junction conditon is the coninuous matching of $g^+_{\mu\nu}$ and $g^-_{\mu\nu}$ on Σ. We shall call such a procedure the first junction. Let the equation of the hypersurface found in the coordinates x^+ be $F^+(x^+) = 0$, while in the coordinates x^- let it be $F^-(x^-) = 0$. Introduce new coordinates $(n, \xi^i)^\pm$ in such a way that the surfaces $n^\pm = 0$ coincide with the surfaces $F^\pm(x^\pm) = 0$, respectively. Since there are four arbitrary functions of coordinate transformations in each region, it is possible reduce the metric to the form

$$\begin{aligned} ds^{+2} &= \epsilon\, dn^{+2} + {}^3g^+_{ij}\left(\xi^+, n^+\right) d\xi^{+i}\, d\xi^{+j} \quad , \\ ds^{-2} &= \epsilon\, dn^{-2} + {}^3g^-_{ij}\left(\xi^-, n^-\right) d\xi^{-i}\, d\xi^{-j} \quad , \end{aligned} \tag{A.1.2}$$

where ${}^3g^\pm_{ij}$ are functions of $F^\pm$. The condition of the first junction will be satisfied if there exist on the junction surface $n = 0$ a transformation of coordinates $\xi^+ = \xi^+(\xi^-)$ such that

$${}^3g^+_{ij}\left(\xi^+, 0\right) = {}^3g^-_{ij}\left(\xi^-, 0\right) \frac{\partial\xi^{-k}}{\partial\xi^{+i}} \frac{\partial\xi^{-l}}{\partial\xi^{+j}} \quad . \tag{A.1.3}$$

After the first junction is carried out one can write the metric on the whole manifold in the form

$$ds^2 = \epsilon\, dn^2 + {}^3g_{ij}(\xi, n)\, d\xi^i\, d\xi^j \quad . \tag{A.1.4}$$

Such coordinates are known as Gaussian normal coordinates. Since $n = 0$ is the equation of the hypersurface Σ to be found, the interval

$$dl^2 = {}^3g_{ij}(\xi, 0)\, d\xi^i\, d\xi^j \quad , \tag{A.1.5}$$

determines the geometry on Σ. In what follows, the explicit expression for the coordinate $n = n(x^\mu)$ will not be necessary for us, though Gaussian coordinates shall be used. All

that is required is the direction of the normal vector $N_\gamma^\pm$. The normal vector is given by the

$$N_\gamma^\pm = \frac{\partial F^\pm}{\sqrt{\partial_\gamma F^\pm \partial^\gamma F^\pm}} \quad . \tag{A.1.6}$$

A slicing of the manifold by the surfaces $n = const.$ leads to a corresponding decomposition of both vectors and tensors. A vector A^μ is decomposed naturally giving the normal component A^n and the tangential components A^i. Similarly decomposition can take place for all tensors. For example, a four dimensional second-rank tensor $Q_{\mu\nu}$ has 16 components it is decomposed as a one component scalar Q^{nn}, two three component three-vectors Q_i^n and Q_n^i, and a nine componet three tensor Q_{ij}. If a vector A_μ is given in arbitrary coordinates $\{x^\mu\}$ then

$$A^n = \frac{\partial n}{\partial x^\mu} A^\mu = n_{,\mu} A^\mu \quad , \tag{A.1.7}$$

$$A_n = \epsilon A^n, \qquad A_i = \frac{\partial x^\mu}{\partial x^i} A_\mu \quad . \tag{A.1.8}$$

Similiarly for second rank tensors $Q_{\mu\nu}$

$$Q^{nn} = n_{,\mu}\, n_{,\nu}\, Q^{\mu\nu} \quad , \tag{A.1.9}$$

$$Q_n^n = \epsilon Q^{nn}, \quad Q_{nn} = Q^{nn} \quad , \tag{A.1.10}$$

$$Q_i^n = n_{,\mu} \frac{\partial x^\nu}{\partial x^i} Q_\nu^\mu, \quad Q_n^j = n^\nu \frac{\partial \xi^j}{\partial x^\nu} Q_\nu^\mu \quad , \tag{A.1.11}$$

$$Q_{ij} = \frac{\partial x^\mu}{\partial \xi^i} \frac{\partial x^\nu}{\partial \xi^j} Q_{\mu\nu} \quad . \tag{A.1.12}$$

Note that the above-written expression for A^n allows one to choose the sign of the normal. We shall call the normal the outer one if the normal vector $n_{,\alpha}$ has the direction from M^- to M^+. Then, choosing the surfaces $n = const.$ in such a way that the values $n < 0$ correspond to M^- $(n > 0 for M^+)$ one finds that the contravariant components of a unit outer normal vector should be

$$n^n = 1, n^i = 0, n_i = 0, n_n = \epsilon.$$

Hence $N_\mu = \epsilon n_{,\mu}$.

A.2 Second junction condition

In the Gaussian system of coordinates,, $y^\nu = \{n, \xi^i\}$ components of the Christoffel symbols containing two or three indices n are equal to zero. Components not containing indices n at all are regular, since the three dimensional geometry of the surface Σ is by assumption well defined. Thus, only those connection coefficients which contain just one index n, namely,

$$\Gamma^n_{ij} = -\frac{1}{2}\epsilon\, {}^3g_{ij,n} \quad \text{and} \quad \Gamma^i_{jn} = -\frac{1}{2}\, {}^3g^{il}\, {}^3g_{lj,n} \quad , \tag{A.2.1}$$

may be discontinuous at crossing Σ. The quantity $Kij \equiv -N_{i;j} = \epsilon\, \Gamma^n_{ij}$ is called the extrinsic curvature tensor or second fundamental form of the surface Σ. Since the quantity $N_{\mu;\nu}$ is a tensor, one can find it an arbitrary convenient system of coordinates $\{x^\mu\}$; then K_{ij} can be found using the formula

$$K_{ij} = -\frac{\partial x^\alpha}{\partial \xi^i}\frac{\partial x^\beta}{\partial \xi^j} N_{\alpha;\beta} \quad . \tag{A.2.2}$$

The extrinsic curvature measures the rate of change of the normal vector as it moves along the boundary surface. It is given explicitly by the expression

$$\begin{aligned} K_{ij} &= \frac{\partial x^\mu}{\partial \xi^i}\frac{\partial x^\nu}{\partial \xi^j} n_{\mu;\nu} \\ &= \frac{\partial x^\mu}{\partial \xi^i}\frac{\partial x^\nu}{\partial \xi^j}\left(n_{\mu,\nu} - \Gamma^\gamma_{\mu\nu}\right). \end{aligned}$$

This formula can be simplified further by noting that

$$\frac{\partial x^\mu}{\partial \xi^i}\frac{\partial x^\nu}{\partial \xi^j} n_{\mu,\nu} = \frac{\partial x^\mu}{\partial \xi^i}\frac{\partial x^\nu}{\partial \xi^j}\frac{\partial N_\mu}{\partial x^\nu} \tag{A.2.3}$$

$$= \frac{\partial x^\mu}{\partial \xi^i}\frac{\partial N_\mu}{\partial \xi^j} \tag{A.2.4}$$

$$= \frac{\partial}{\partial x^j}\left(N_\mu \frac{\partial x^\alpha}{\partial \xi^1}\right) - N_\mu \frac{\partial^2 x^\mu}{\partial \xi^i \partial \xi^j}. \tag{A.2.5}$$

As the surface coordinates are ξ^i vectors tangential to the surface are given by

$$e^\mu_i = \frac{\partial x^\mu}{\partial \xi^i}.$$

Tangential vectors and normal vectors have a zero product so

$$N_\mu \frac{\partial x^\alpha}{\partial \xi^\imath} = 0$$

hence

$$K_{ij} = -n_\gamma \left(\frac{\partial^2 x^\gamma}{\partial \zeta^i \partial \zeta^j} + \Gamma^\gamma_{\alpha\beta} \frac{\partial x^\alpha}{\partial \zeta^i} \frac{\partial x^\beta}{\partial \zeta^j} \right), \tag{A.2.6}$$

The extrinsic curvature is particularly useful in examining the distribution of energy along the hypersurface seperating the two spacetimes. Two spacetimes manifolds are said to match continously on a hypersurface if on that surface the energy momentum tensor is continous. The Einstein tensor can be calculated in terms of the extrinsic curvature using equations A.1.7-A.1.8 and A.1.9-A.1.10. The $\binom{i}{n}$ and $\binom{n}{n}$ components of the Einstein tensor are

$$-\epsilon \left(K^j_{i|j} - K^l_{l|i} \right) = G^n_i, \tag{A.2.7}$$

$$-\frac{1}{2}\,{}^3R - \frac{1}{2}\epsilon K^i_j \left(K^j_i - \delta^j_i K^l_l \right) = G^n_n, \tag{A.2.8}$$

where ${}^3R$ is the three curvature of the hypersurface Σ and the vertical bar $|$ denotes the covariant derivative with respect to ${}^3g_{ij}$. As Σ is a regular hypersurface the the $\binom{i}{j}$ components of the Einstein tensor on Σ are the same whether they are calculated in the $\mathcal{M}^+$ manifold or $\mathcal{M}^-$. The jump discontinuity in the Einstein tensor is subtracting the value calculated in the $\mathcal{M}^-$ evaluated at the surface from Einstein tensor calculated in $\mathcal{M}^+$ evalutated at the surface

$$-\epsilon \left(\left[K^j_{i|j} \right] - \left[K^l_{l|i} \right] \right) = \left[G^n_i \right], \tag{A.2.9}$$

$$-\frac{1}{2}\epsilon \left(\left[K^i_j K^j_i \right] - \left[K^i_i K^l_l \right] \right) = \left[G^n_n \right] \tag{A.2.10}$$

$$\left[K^j_i \right] \equiv K^{j+}_i - K^{j-}_i \tag{A.2.11}$$

The continuity of the normal componets of the Einstein tensor are ensured if

$$[K_{ij}] = 0. \tag{A.2.12}$$

B

APPENDIX ON NEWMAN-PENROSE FORMALISM

The Newman-Penrose (NP) formalism is a particularly useful technique for examining the spacetime properties of the vacuum. It has also been made use of in chapters (3)-(4) in order to generate non-vacuum spacetimes.

At each point in the spacetime a tetrad is introduced, $Z_a^\mu = (l^\mu, n^\mu, m^\mu, \overline{m}^\mu)$. Two of these vectors l^μ and n^μ are real and null,

$$l_\mu l^\mu = n_\mu n^\mu = 0 \quad , \tag{B.0.13}$$

obeying the further condition

$$n_\mu l^\mu = 1 \quad . \tag{B.0.14}$$

The other two tetrads m^μ and $\overline{m}^\mu$ are complex null vectors

$$m_\mu m^\mu = \overline{m}_\mu \overline{m}^\mu = 0 \quad , \tag{B.0.15}$$

where $\overline{m}_\mu$ the complex conjugate of m_μ and with the normalization condition

$$m_\mu \overline{m}^\mu = -1 \quad , \tag{B.0.16}$$

The orthonormalization conditions Eq. (B.0.13)-(B.0.16) imply that the metric tensor for the spacetime is expressable as :

$$
\begin{aligned}
g_{\mu\nu} &= l_\mu n_\nu + l_\nu n_\mu - m_\mu \overline{m}_\nu - m_\nu \overline{m}_\mu \qquad \text{(B.0.17)} \\
&= \eta^{ab} Z_{a\mu} Z_{b\nu} \quad ,
\end{aligned}
$$

where

$$
\eta^{ab} = \begin{pmatrix} 0 & 1 & 0 & 0 \\ 1 & 0 & 0 & 0 \\ 0 & 0 & 0 & -1 \\ 0 & 0 & -1 & 0 \end{pmatrix} \quad . \qquad \text{(B.0.18)}
$$

Note that Eq. (B.0.18) implies that

$$
\delta^\nu_\mu = l_\mu n^\nu + n_\mu l^\nu - m_\mu \overline{m}^\nu - \overline{m}_\mu m^\nu \quad . \qquad \text{(B.0.19)}
$$

The above expression allows us to generate the tetrad components of a tensor from its coordinate components. For example :

$$
\begin{aligned}
\xi^\nu &= \delta^\nu_\mu \xi^\mu \\
&= (l_\mu \xi^\mu)\, n^\nu + (n_\mu \xi^\mu)\, l^\nu - (m_\mu \xi^\mu)\, \overline{m}^\nu - (\overline{m}_\mu \xi^\mu)\, m^\nu \quad . \qquad \text{(B.0.20)}
\end{aligned}
$$

In the NP formalism the 32 independent real Christoffel symbols $\Gamma^\alpha_{\beta\gamma}$ are replaced by 16 linearly independent complex spin coefficients $\alpha, \beta, \epsilon, \chi, \lambda, \mu, \nu, \pi, \rho, \sigma, \tau$.

It is convenient in the NP formalism to regard a general Lorentz transformation of the basis $(l^\mu, n^\mu, m^\mu, \overline{m}^\mu)$ as being comprised of the following three classes of rotations :

- **I. Rotations about l :**

$$
\begin{aligned}
l^\mu &\rightarrow l^\mu \quad , \\
m^\mu &\rightarrow m^\mu + a\, l^\mu \quad , \\
\overline{m}^\mu &\rightarrow \overline{m}^\mu + \overline{a}\, l^\mu \quad , \\
n^\mu &\rightarrow n^\mu + \overline{a}\, m^\mu + a\, \overline{m}^\mu + a\, \overline{a}\, l^\mu \quad , \qquad \text{(B.0.21)}
\end{aligned}
$$

where "a" is a complex number.

• **II. Rotations about n :**

$$\begin{aligned} n^\mu &\rightarrow n^\mu \quad , \\ m^\mu &\rightarrow m^\mu + b\, n^\mu \quad , \\ \overline{m}^\mu &\rightarrow \overline{m}^\mu + \overline{b}^\mu\, n \quad , \\ l^\mu &\rightarrow l^\mu + \overline{b}\, m^\mu + b\, \overline{m}^\mu + b\, \overline{b}\, n^\mu \quad , b\epsilon | C \end{aligned} \tag{B.0.22}$$

where "b" is a complex number.

• **III. A boost in the $l^\mu - n^\mu$ plane and a rotation $m^\mu - \overline{m}^\mu$ plane :**

$$\begin{aligned} l^\mu &\rightarrow A^{-1}\, l^\mu \quad , \\ n^\mu &\rightarrow A\, n^\mu \quad , \\ \overline{m}^\mu &\rightarrow e^{-i\theta}\, \overline{m}^\mu \quad , \\ m^\mu &\rightarrow e^{i\theta}\, m^\mu \quad , \end{aligned} \tag{B.0.23}$$

both A and θ are real.

One of the most useful applications of the NP formalism is the classification of the Weyl tensor. The 10 linearly independent real components of the Weyl tensor $C_{\alpha\beta\mu\nu}$ are expressed as 5 linearly independent complex quantities :

$$\begin{aligned} \Psi_0 &= -C_{\alpha\beta\mu\nu}\, l^\alpha\, m^\beta\, l^\mu\, m^\nu \quad , \\ \Psi_1 &= -C_{\alpha\beta\mu\nu}\, l^\alpha\, n^\beta\, l^\mu\, m^\nu \quad , \\ \Psi_2 &= -C_{\alpha\beta\mu\nu}\, \overline{m}^\alpha\, n^\beta\, l^\mu\, m^\nu \quad , \\ \Psi_3 &= -C_{\alpha\beta\mu\nu}\, \overline{m}^\alpha\, n^\beta\, l^\mu\, n^\nu \quad , \\ \Psi_4 &= -C_{\alpha\beta\mu\nu}\, \overline{m}^\alpha\, n^\beta\, \overline{m}^\mu\, n^\nu \quad . \end{aligned} \tag{B.0.24}$$

Under Class-I transformations :

$$\begin{aligned} \Psi_0 &\rightarrow \Psi_0 \quad , \\ \Psi_1 &\rightarrow \Psi_1 + \overline{a}\, \Psi_0 \quad , \\ \Psi_2 &\rightarrow \Psi_2 + 2\, \overline{a}\, \_Psi1 + \overline{a}^2\, \Psi_0 \quad , \\ \Psi_3 &\rightarrow \Psi_3 + 3\, \overline{a}\, \Psi_2 + 3\, \overline{a}^2\, \Psi_1 + \overline{a}^3\, \Psi_0 \quad , \\ \Psi_4 &\rightarrow \Psi_4 + 4\, \overline{a}\, \Psi_3 + 6\, \overline{a}^2\, \Psi_2 + 4\, \overline{a}^3\, \Psi_1 + \overline{a}^4\, \Psi_0 \quad . \end{aligned} \tag{B.0.25}$$

Under transformations of Class-II :

$$\begin{aligned}
\Psi_0 &\rightarrow \Psi_0 + 4\,b\,\Psi_1 + 6\,b^2\,\Psi_2 + 4\,b^3\,\Psi_3 + b^4\,\Psi_4 \quad , \\
\Psi_1 &\rightarrow \Psi_1 + 3\,b\,\Psi_2 + 3\,b^2\,\Psi_3 + b^3\,\Psi_4 \quad , \\
\Psi_2 &\rightarrow \Psi_2 + 2\,b\,\Psi_3 + b^2\,\Psi_4 \quad , \\
\Psi_3 &\rightarrow \Psi_3 + b\,\Psi_4 \\
\Psi_4 &\rightarrow \Psi_4 \quad .
\end{aligned} \tag{B.0.26}$$

Let us assume that $\Psi_4 \neq 0$, as long as the spacetime is not flat a rotation of Class-I can always be made so that this is true. Clearly it is alsoes possible to make a rotation of Class-II so that $\Psi_0 = 0$ if b is a root of the following equation

$$\phi_0 + 4b\phi_1 + 6b^2\phi_2 + 4b^3\phi_3 + b^4\phi_4 = 0 \quad . \tag{B.0.27}$$

The four roots of Eq. B.0.27 correspond to new directions of l^μ, namely, $l^\mu + \bar{b}\,m^\mu + b\,\overline{m}^\mu + b\,\bar{b}n^\mu$, known as the "*principal null directions*". If one or more of the roots coincide the spacetime is algebraically special. The classification of the roots (b_1, b_2, b_3, b_4) of Eq. B.0.27 leads to Petrov classification.

- **Petrov type I :** All four roots are distinct.

- **Petrov type II :** Two roots are the same and the other two are different, $b_1 = b_2, b_3, b_4$.

- **Petrov type D :** There are two pairs of roots $b_1 = b_2$ and $b_3 = b_4$. This means that a rotation of Class-II makes Ψ_0 and Ψ_1 vanish simultaneously, while a rotation of Class-I will also makes Ψ_3 and Ψ_4 vanish simultaneously. Hence if $\Psi_0 = \Psi_1 = 0$ the simultaneous vanishing of Ψ_3 and Ψ_4 by class I rotations can be expressed as :

$$\begin{aligned}
\Psi_3 &\rightarrow \Psi_3 + 3\,\bar{a}\,\Psi_2 = 0 \quad , \\
\Psi_4 &\rightarrow \Psi_4 + 4\,\bar{a}\,\Psi_3 + 6\,\bar{a}^2\,\Psi_2 = 0 \quad ,
\end{aligned} \tag{B.0.28}$$

eliminating $\overline{a}$,

$$\phi_2\phi_4 - \frac{2}{3}\phi^2 = 0 \quad . \tag{B.0.29}$$

- **Petrov type III :** Three roots coincide $b_1 = b_2 = b_3$, b_4

- **Petrov type N :** All four roots coincide $b_1 = b_2 = b_3 = b_4$

Bibliography

[1] S.M.Scott and P.Szekeres *G. R. & G.***18**, 571 (1986).

[2] $http://www.ssl.msfc.nasa.gov/newhome/headlines/ast06nov97_1.htm.$

[3] C.P. Dettmann, N.E. Frankel and N.J. Cornish, *Phys. Rev. D* **50**, R618 (1994).

[4] C.P. Dettmann, N.E. Frankel and N.J. Cornish, *Fractals* **3**, 161 (1995).

[5] G. Contopoulos, *Proc. R. Soc. London A* **431**, 183 (1990).

[6] G. Contopoulos, *Proc. R. Soc. London A* **435**, 551 (1991).

[7] G. Contopoulos and H. Papadaki, *Celest. Mech. Dyn. Astron.* **55**, 47 (1993).

[8] D.C.Robinson, *Phys. Rev. Lett.* **34**, 905 (1975).

[9] B.Carter, *Phys. Rev. Lett.* **26**, 331 (1972).

[10] S. Chandrasekhar, *The Mathematical Theory of Black Holes*, (Oxford University Press, Oxford, 1983).

[11] R. P. Kerr, *Phys. Rev. Lett.* **11**, 237 (1963).

[12] F. J. Ernst, *Phys. Rev.* **167**, 1175 (1968).

[13] F. J. Ernst, *Phys. Rev.* **168**, 1415 (1968).

[14] J. Martin and J. M. M. Senovilla, *J. Math. Phys* **27**, 265 (1986).

[15] A. H. Taub, *Ann. Phys* **134**, 326 (1981).

[16] C.F. Sopuerta, preprint gr-qc/9801103 (1998).

[17] F. Martin-Pascual and J. M. M. Senovilla, *J. Math. Phys.* **29**,37 (1986).

[18] J. M. M. Senovilla and C. F. Sopuerta, *Class. Quantum Grav.* **11**, 2073 (1994).

[19] E. T. Newman and A. I. Janis, *J. Math. Phys.* **6**, 915 (1965).

[20] E. T. Newman, E. Couch, K. Chinnapared, A. Exton, A. Prakash and R. Torrence, *J. Math. Phys.* **6**, 918 (1965).

[21] M. M. Schiffer, R. J. Adler, J. Mark and C. Sheffield, *J. Math. Phys.* **14**, 52 (1973).

[22] E. T. Newman, *J. Math. Phys.* **14**, 102 (1973).

[23] E. T. Newman, *J. Math. Phys.* **14**, 774 (1973).

[24] M. Gürses and F. Gürsey, *J. Math. Phys.* **16**, 2385 (1975).

[25] M. Demianski and E. T. Newman, *Serie. des Sciences Math., Astr. et Phys. - vol XIV*, 653 (1966).

[26] M. Demianski, *Phys. Lett.* **42A**, 157 (1972).

[27] L. Herrera and Jiménez, *J. Math. Phys.* **23**, 2339 (1982).

[28] S. P. Drake and P. Szekeres, to be submitted, "An explanationof the Newman-Janis algorithm".

[29] A.Tomimatsu and H.Sato, *Phys.Rev.Lett.* **29**, 1344 (1972).

[30] J.N. Islam, *Classical general relativity : proceedings of the conference on classical (non-quantum) general relativity,City University*, (Proc. Cambridge University Press, London, 1983).

[31] M.Mars and J.M.M.Senovilla, preprint gr-qc/9806094 (1998).

[32] R. Geroch, *J. Math. Phys.* **12**, 918 (1971).

[33] R. Geroch, *J. Math. Phys.* **13**, 394 (1971).

[34] J. Winicour, *J. Math. Phys.* **16**, 1806 (1975).

[35] V.Stockum, *Proc.Roy.Soc.* **A57**, 135 (1937).

[36] G. Neugebauer and R. Meinel, *Phys. Rev. Lett.* **73**, 2166 (1994).

[37] A.Krasinski, preprint gr-qc/9705078 (1997).

[38] A.Krasinski, preprint gr-qc/9705010 (1997).

[39] A.Krasinski, preprint gr-qc/9707021 (1997).

[40] V. H. Hamity, *Phys. Lett.* **56A**, 77 (1976).

[41] Meinel, preprint gr-qc/9703077 (1997).

[42] J.M.Cohen, *J.Math.Phys.* **8**, 1477 (1967).

[43] G. Magli, *J. Math. Phys.* **36**, 5877 (1995).

[44] G. Magli, *Gen. Rel. Grav.* **25**, 1277 (1993).

[45] N. Stergioulas, preprint gr-qc/9805012 (1998).

[46] S.L.Shapiro and S.A.Teukolsky, *Ap.J.* **298**, 34 (1985).

[47] E.M.Butterworth, Ap.J. **204**, 561 (1976).

[48] E.M.Butterworth and J.R.Ipser, *Ap.J.* **204**, 200 (1976).

[49] J.M.Bardeen and R.V.Wagoner, Ap.J. **180**, 359 (1971).

[50] T.Nozawa, N.Stergioulas,E.Gourgoulhon and Y.Eriguchi, preprint gr-qc/9804048 (1998).

[51] J.B.Hartle and K.S.Thorne, *Ap.J.* **153**, 807 (1968).

[52] A.K.Schenk, S.L.Shapiro and S.A.Teukolsky, preprint gr-qc/9801056 (1998).

[53] A.J.Kalnaj, *Ap.J.* **175**, 63 (1972).

[54] S. P. Drake, C. P. Dettmann, N. E. Frankel and N. J. Cornish, *Phys. Rev. D* **53**, 1351 (1996).

[55] E.T.Whittaker, *A Treatise on the Analytical Dynamics of Particles and Rigid Bodies*, (Cambridge University Press, London, 1970).

[56] M.P. Strand and W. P. Reinhardt, *J. Chem. Phys* **70**, 3812 (1979).

[57] D. McManus, *Class. Quant. Grav.* **8**, 863 (1991).

[58] A. Kransinski, *Ann. Phys.* **112**, 22 (1978).

[59] D. Kramer, H. Stephani, E. Herlt and M. MacCullum, *Exact Solutions of the Einstein's field equations*, (Cambridge University Press, Cambridge, 1980).

[60] E.J. Flaherty, *Hermitian and Kählerian geometry in relativity*, Lecture notes in Physics **46**, (Springer-Verlag, Berlin 1976).

[61] E. T. Newman and R. Penrose, *J. Math. Phys.* **3**, 566 (1962).

[62] S. W. Hawking and W. Israel, *General Relativity:An Einstein Century Survey*, (Cambridge University Press, Cambridge, 1979).

[63] C. W. Misner, K. S. Thorne and J. A. Wheeler, *Gravitation* (W.H. Freeman and Co., San Francisco, 1973).

[64] R. H. Boyer, *Proc. Camb. Phil. Soc.* **61**, 527 (1965).

[65] J. R. Oppenheimer and G. Volkov, *Phys. Rev.* **55**, 374 (1939).

[66] P. Musgrave and K. Lake, preprint gr-qc/9510052 (1995).

[67] H.H. Soleng, preprint gr-qc/9502035 (1995).

[68] M. Wyman, *Phys. Rev.* **75**, 1930 (1948).

[69] G. M. Murphy, *Ordinary Differential Equations and Their Solutions*, (D. Van Nostrand, Princeton, New Jersey, 1960).

[70] T. Lewis, *Proc. Roy. Soc. London A* **136**, 176 (1932).

[71] A. Papapetrou, *C. R. Acad. Sci. (Paris)* **257**, 2797 (1963).

[72] A. Papapetrou, *Ann. Inst. H. Poincaré* **A4**, 83 (1966).

[73] F. De Felice and C. J. S. Clarke, *Relativity on Curved Manifolds* (Cambridge University Press, Cambridge, 1990).

[74] L. P. Einsenhart, *Riemannian Geometry*, (Princeton Universtity Press, Princeton, 1960).

[75] S. Chandrasekhar, *Ellipsoidal figures of Equilibrium*, (Yale Univ. Press, New Haven, 1969).

[76] J. Wisdom, *Icarus* **72**, 241 (1987).

[77] C.J. Thompson, *Lecture Notes on Dynamical Systems and Chaos*, (University of Melbourne, Melbourne, 1992).

[78] Lorenz E.N., *J. Atmos. Sci.* **20**, 130 (1963).

[79] H. Essex and M.A.H. Nerenberg, *Am.J.Phys* **58**, 986 (1990).

[80] M. C. Gutzwiller, *Chaos in Classical and Quantum Mechanics*, (Springer-Verlag, New York, 1990).

[81] G. Benettin, L. Galfani, and J. M. Strelcyn, *Phys. Rev. A* **14**, 2338 (1976).

[82] J.D. Jackson, *Classical Electrodynamics*, (Wiley, New York, 1975).

[83] C.L. Charlier, *Die Mechanik des Himmels*, (von Veit, Leipzig, 1902).

[84] H. Goldstein, *Classical Mechanics*, (Addison-Wesley, Reading, 1980).

[85] A.N. Kolomogorov, *Proc. Int. Conf. Math.* **1** , 315 (1957).

[86] V. I. Arnold, *Russ. Math. Surv.* **18(5)**, 9 (1973).

[87] J. K. Moser, *Nachr. Akad. Wiss., Gottingen, Math. Phys, Kl* **2**, 1 (1962).

[88] W.H. Press et al., *Numerical Recipes in C*, (Cambridge University Press, Cambridge, 1992).

[89] S.Weinberg, *Gravitation and Cosmology: principles and applications of the general theory of relativity*, (Wiley, New York, 1972).

[90] A. Papapetrou, *Proc. Roy. Irish Acad.* **A51**, 191(1947).

[91] I. Shimada and T Nagashima, *Prog. Theor. Phys.* **61**, 1605 (1979).

[92] K. Falconer, *Fractal Geometry; Mathematical Foundationsand Applications*, (Wiley, Chichester, 1990).

[93] S. P. Drake and R. Turolla, *Class. Quantum Grav.* **14**, 1883 (1997).

[94] W. Israel, *Nuovo Cim.* **44B**, 1, (1966).

[95] V. A. Berezin and V. A. Kuzmin, *Phys. Rev.* **D36**, 2919 (1987).

PUBLICATIONS

1 - S. P. Drake and P. Szekeres, gr-qc/9807001
"An explanationof the Newman-Janis algorithm".

2 - S. P. Drake, C. P. Dettmann, N. E. Frankel and N. J. Cornish,
Phys. Rev. D **53**, 1351 (1996).

3 - S. P. Drake and R. Turolla, *Class. Quantum Grav.* **14**, 1883 (1997).